CHAPTER 7.
INSTRUMENTATION AND CONTROL

7. INSTRUMENTATION AND CONTROL

THE CONTROL SYSTEM FOR THE SLC

7.1 INTRODUCTION

The control of the SLC presents special problems. First, the SLC requires the coordinated operation of several major subsystems, one of them being the existing linac, which has already had a computer control system for some time. Second, the control precision needed for the components of the SLC is at least an order of magnitude more stringent than that needed for previous machines. For these reasons, it was decided that a new control system was needed to deal with all components of the SLC in a uniform way, with enough power to run large simulation and modelling programs, and that the new system should replace the existing linac system.

Since the different parts of the SLC will come into operation at different times, during which it is necessary to keep the linac in operation for filling PEP and SPEAR and to provide test and experimental beams, the new system has been installed progressively and it has been necessary to operate the linac with a mixed system. The first ten sectors of the linac were successfully converted to the new system for the "10 sector tests," and at the time of writing the remainder of the linac is being converted.

Although the SLC is made up of subsystems that perform very different functions, the subsystems are largely made up of the same types of components (magnets, power supplies, beam position monitors, vacuum apparatus, and so forth). Thus it is possible to take a common approach to the control hardware for all the subsystems, and take care of the difference in the software applications programs.

7.2 THE COMPUTER SYSTEM

The SLC control system uses a centralized computer system with distributed intelligence to monitor and control the machine. The logical topology is a star network with a Host machine coordinating approximately 50 slave microprocessor clusters distributed around the various parts of the SLC. The task organization for the microclusters is geographical rather than functional; each cluster controls all functions for a given area rather than one function for a larger area. The system employs a hierarchical distribution of intelligence. Where possible, first level processing of signals is performed by the Input/Output modules themselves. The microclusters perform the conversion to and from engineering units and execute standard algorithms in response to commands from the Host computer. The Host machine determines the operational configuration of the accelerator, maintains a centralized database, generates periodic checking and error reporting, and handles all operator interface functions such as display formatting and command transmission.

Because of the design of the software system based on shared data structures and the planned widespread use of modelling in the control algorithms, the computer system contains a single large central computer to control the slave processors. The control computer is at present a DEC VAX 11/780, with 6 Mbytes of main memory and 2 disks, running the VMS operating system. A second VAX 11/780 configuration is used for program development and as back-up for the control system VAX. When only a single machine is operational, it can access the user disk of the other machine via a switchable memory controller. The VAX was chosen because of extensive hardware and software support already existing at SLAC. If the Host computer becomes overloaded when all systems of the SLC are in operation, it will be upgraded to a more powerful processor, such as the long expected next generation of the VAX. Additional Host computers cannot easily be used to increase processing power as the system has not been designed to have multiple masters.

Each slave processor consists of a Multibus crate containing a single-board microcomputer using the Intel 8086 microprocessor, a memory board and other

modules as shown in Figure 7.2.1 and Table 7.2.1, forming a "microcluster." The VAX communicates with the slave processors using one channel of the cable system described in Section 7.5.1. Another channel is used by the program development VAX to communicate with separate microclusters driving test and emulation equipment. Some of the hardware and the message transfer protocol for this system (SLCNET) were specially developed for this project, and a brief description is given below.

Table 7.2.1 List of Multibus Modules Used in the SLC

	Typical Cluster Configuration
SBC1	Intel 86/30 Single-board Computer
	Memory Board 512 kBytes
MBCD	Multibus CAMAC Driver
SDMM	SLCNET Data Modem
	(Made up of FSK modem and SDLC controller)
PRIM	Pattern Receiver Interrupt Module
	Multibus Modules for a COW
SBC2	Intel 86/12A Single-board Computer
	Memory Board 256 kBytes
SDMM	SLCNET Data Modem
	Touchpanel Interface Board
	4-Channel Knob Interface
	Matrox RGB Graphics Board — 512 × 512 × 1
	Matrox RGB Graphics Board — 512 × 512 × 4

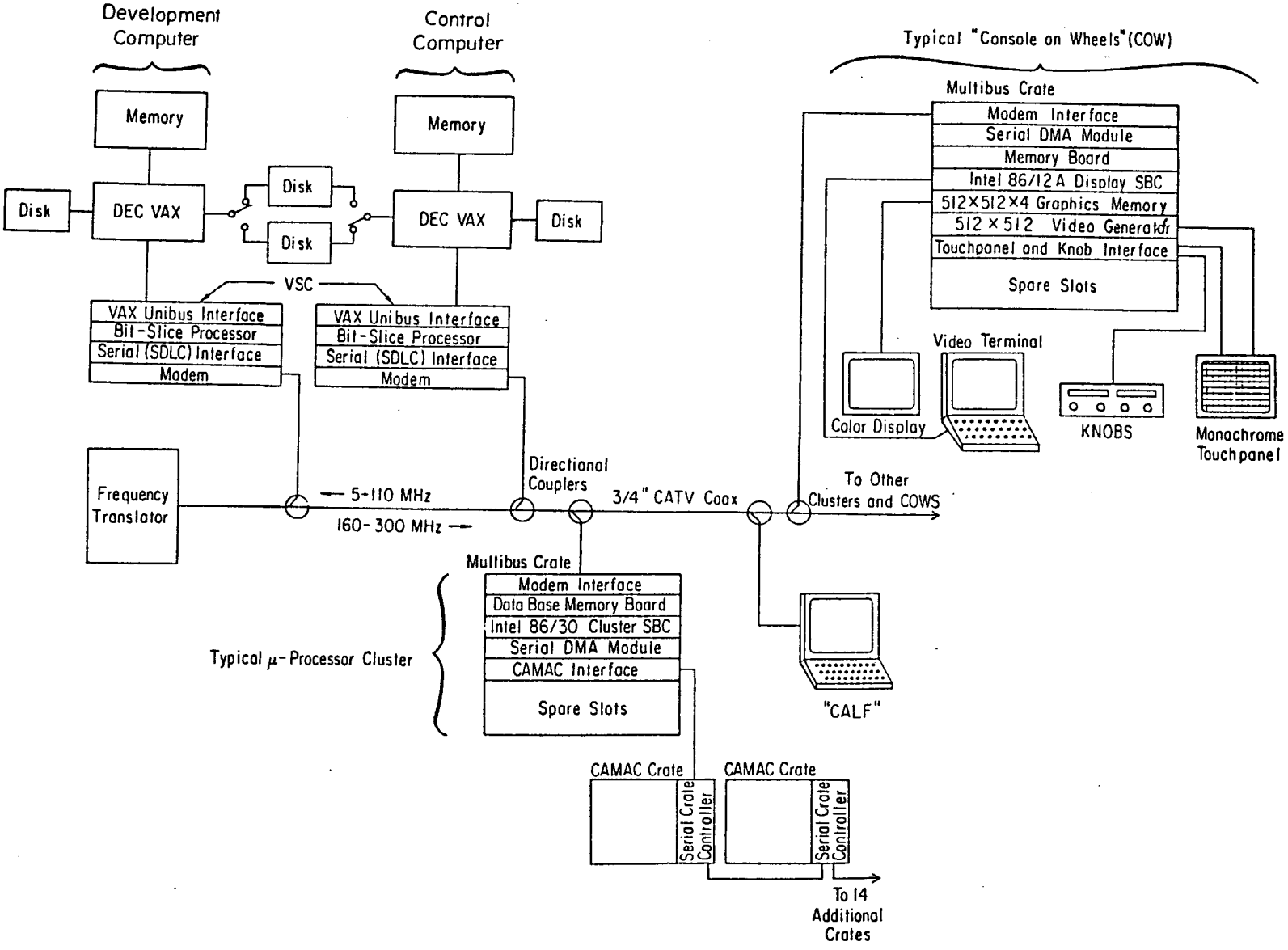

Figure 7.2.1 Main Components of SLC Control System.

7.2.1 Microprocessor Clusters

The Intel Multibus architecture was chosen for the microprocessor clusters, which require a bus capable of supporting multiple masters. This provides support for an arbitrary number of single-board computers which can communicate with each other through the use of shared memory and interrupts. At present only a single processor card is used in each crate. This is the Intel 86/30 single board computer, containing an 8086 with an 8087 floating point coprocessor and 256 Kbytes of on-board memory. This is supplemented by a separate memory board with 512 Kbytes of RAM. The iRMX multitasking operating system is used, and the software organization is described in Section 7.4.4. In addition to the modem and SLCNET controller, and a CAMAC driver, the crate also houses a Pattern Receiver Interrupt Module (PRIM). This module produces Multibus interrupts from external signals such as those of the Timing System (see Section 7.3).

7.2.2 Interface to the Equipment

The microprocessor clusters are connected to the SLC equipment through crates and modules conforming to the CAMAC specification. The optional upper backplane in the CAMAC crates is used to distribute timing signals (see Section 7.3). A number of CAMAC crates are driven from each multibus crate. The Multibus CAMAC Driver (MBCD) is a DMA device that directly executes lists of CAMAC commands from the Multibus address space, and passes the information to the CAMAC crates via a high-speed serial link, running at 5 Mbit/sec, using serial crate controllers developed at SLAC. Up to 16 crates can be driven from one controller.

The CAMAC modules used in the SLC control system are a mixture of commercially available modules and those developed at SLAC. Some of the latter include microprocessors, such as in the Smart Analog Monitor (SAM), to provide ranging, polarity selection and self calibration and in the Parallel Input/Output Processor (PIOP), which is used to provide the requirements for klystron and

modulator control. A description of the principal modules is given in Table 7.2.2.2, and a summary of the devices to be interfaced is given in Table 7.2.2.1.

For further details of the Control System hardware, see the SLC Hardware Manual. (Ref.1)

Table 7.2.2.1

POSITRON RETURN LINE

CRATES	POWER SUPPLIES	VACUUM	PROTECTION	DIAGNOSTICS	OTHER
MULTIBUS SECTOR 1 2 SECTOR 20 2 4 CAMAC SECTOR 1 4 SECTOR 20 4 SECT. 2–19 8 16	LARGE SUPPLIES 8 TRIM, STEERING 365 PULSED 3	VALVES – FAST 3 VALVES – SLOW 16 PUMPS 38 GAUGES 38	PPS DOORS 1 MPS ION CHAMBERS 4	BEAM POSITION MON. 156 SPECTRUM MON. 2 TEMPERATURE MON. 16 TOROIDS 12 WHEEL READOUT 1 PROF. MON. 32	
DAMPING RING					
MULTIBUS DR. ALCOVE 3 CAMAC DR. ALCOVE 12	LARGE P.S. 28 TRIM, STEERING 160 PULSED 2	VALVES – SLOW 4 PUMPS 6 FAST SWITCHES 12 CLEARING FIELD ELECTRODES 27 PAIRS	PPS GATES 6 MPS KLIXONS FLOW SWITCHES SCRAPER 1	BEAM POSITION MON. LTR 19 " " " RING 26 " " " RTL 21 SPECTRUM MON. 1 FARADAY CUP 1 SYNCHROTRON LIGHT MON. 1 TUNE MON. 1 TOROIDS/GAP 1 PROF. MON. 1	
ARCS					
MULTIBUS–IR6 SUPPORT BLDG. 1 IR12 " " 1 SECTOR 30 " " 1 F.F. " " 2 5 CAMAC–IR6 SUPPORT BLDG. 3 IR12 " " 3 SECTOR 30 " " 3 F.F. 6 TUNNEL ALCOVES (1 PER 300') 26 41	LARGE SUPPLIES 20 TRIM, STEERING 104 MOVING MAGNET 1000	VALVES 4 / ARC PUMPS 22 / ARC GUAGES 4 / ARC FAST SWITCHES 8 / ARC	PPS GATES 4 HATCHES 6 BEAM CONT. TOROIDS (PAIRS/ARC) 5 MPS ION CHAMBERS 4 FINDING FOILS 4 COLLIMATORS (4 JAWS) 10	BEAM POSITION MON. 500X, 500Y PROFILE MON. 5	
FINAL FOCUS					
MULTIBUS–F.F. SUPPORT BLDG. 1 CAMAC – " " 5 COW – " " 1	LARGE SUPPLIES 30 TRIM, STEERING 104 PULSED 4	VALVES – FAST – 4 VALVES – SLOW – 8 PUMPS – 40 GUAGES – 8 FAST SWITCHES – 8	PPS GATES 4 RADIATION MON. 2 BEAM CONT. TOROID PAIRS 6 MPS ION CHAMBERS 20 SCRAPERS 4 DUMP MON. 1 COLLIMATORS 2	BEAM POSITION MON. 64 SPECTRUM MON. 2 EMITTANCE MON. 2 COLLISION PT BPM F/B 1 PROFILE MON. 2	
LINAC AND CID INJECTOR					
MULTIBUS 32 CAMAC 160	LARGE SUPPLIES 1/SECTOR SMALL SUPPLIES 24/SECTOR	EXISTING SYSTEM	PPS, BEAM CONT., MPS } EXISTING LINAC SYSTEM	BEAM POSITION MON. 8/SECTOR SPECTRUM MON. 3 PROFILE MON. 10	MOD/KLY 8/SECTOR TEMPERATURE MON. 16/SECTOR GENERAL STATUS 100/SECTOR GENERAL ANALOG 12/SECTOR GENERAL CONTROL 30/SECTOR

Table 7.2.2.2

MODULE USE (acronym)	SOURCE	≈ NO. OF MODULES IN SYSTEM	DESCRIPTION	USE
Serial Crate Controller (SCC)	SLAC	250	Serves as a CAMAC Crate Controller. Interfaces to a host computer via 2 RS-422 level signals on a twisted pair cable. The bit data rate is 5 MHz. Sixteen controllers may be run from a single daisy-chained cable at distances in excess of 1000 feet with repeaters.	Used as the Standard SLC Crate Controller
Crate Verifier	SLAC	250	Contains command line spy register, independent function read and write register, LAM testing registers, and supply voltage and local temperature measurements (single width).	Used to verify proper crate and crate controller operation and aid in problem diagnosis.
Smart Analog Monitor (SAM)	Transiac Corp. or Standard Engineering Inc.	325	Provides 32 differential channels of micro-processor controlled digitization. Ranging, polarity selection, and self-calibration are fully automatic. All data is stored in a local memory and can be read asynchronously with the digitizing process. Auto ranging accommodates full-scale inputs ranging from 10 mV to 10.24 V and digitizes the signal with a resolution of 14 bits.	Temperature monitoring of LINAC waveguide. Monitoring of "multichannel small" power supplies. Monitoring of miscellaneous analog reference signals.

MODULE NAME (acronym)	SOURCE	≈ NO. OF MODULES IN SYSTEM	DESCRIPTION	USE
Transiac DAC	Transiac Corp.	275	Provides 16 channels of analog output with a full scale range of ± 10V and a resolution of 16 bits and a basic accuracy of .01%	Used to control multi-channel "small" power supplies and miscellaneous devices.
Isolated Digital Input Module (IDIM)	SLAC	200	Contains 32 optically isolated non-latching digital input channels	Used for reading miscellaneous digital status information.
Isolated Digital Output Module (IDOM)	SLAC	100	Contains 32 channels of open-collector opto-isolated digital output. Each channel may be be programmed to latch its output data or to pulse high or low for a prescribed time period.	Used for controlling digital devices such as power supply on/off, etc.
Pulsed Power Output Module (PPOM)	SLAC	75	Provides a minus 24 volt output pulse with a nominal duration of 1/4 second, to any one of 32 channels.	Primarily used to replace the "remote control system" in the Linac.
Power Supply Controller (PSC)	SLAC	175	Provides a 14 bit analog output, a 14 bit analog input port, digital input status bits, and 2 pulsed and 4 latched digital output bits.	Primarily used to control and monitor "large" power supplies.
Programmable Delay Unit (PDU)	SLAC	175	Contains 16 channels of of programmable pulse delay. Delay resolution is 8.4 ns and the delay is adjustable to 2.7 ms. The module is driven at its front panel by a 476 MHz square wave with a missing pulse serving as the "start delay" fiducial.	Used to time modules and devices such as BPMs, PAUs, PIOPs, etc., which must be synchronized to the beam.

Table 7.2.2.2 Continued

MODULE NAME (acronym)	SOURCE	≈ NO. OF MODULES IN SYSTEM	DESCRIPTION	USE
Single Timing Buffer (STB)	SLAC	175	Contains buffers to supply the 16 PDU channels to external destinations. Also contains a high-speed timer to measure delay of any channel for diagnostic purposes.	Used in conjunction with a PDU to verify its correct operation and to buffer its pulses.
Programmable Synchronization Unit (PSU)	SLAC	5	Provides a chain of "N" NIM level pulses of width W at pulse period of P after a delay D, where N, W, P and D are programmable in the module. The module is driven at its front panel by a 476 MHz square wave with a missing pulse serving as the "start delay" fiducial.	Used to synchronize devices to the Damping Ring beam.
Programmable Width Unit (PWU)	SLAC	10	Receives 8 delayed triggers from the CAMAC upper backplane and provides output pulses with a programmed duration.	Used in applications where programmed duration synchronization or gated pulses are required, such as gun triggers.
Vernier Delay Unit (VDU)	SLAC	5	Provides 2 channels of Vernier delay for timing signals. The delay resolution is 1 ns and the range is 10.5 ns.	Used in applications when the 8.2 ns resolution of the PDU is not sufficient.

Table 7.2.2.2 Continued

MODULE NAME (acronym)	SOURCE	≈ NO. OF MODULES IN SYSTEM	DESCRIPTION	USE
Cable Access Transmitter (CAT)	SLAC	5	Transmits a 2 Mb SDLC bit stream on the CATV cable. Sixteen bit parallel data may be supplied from the CAMAC backplane or from a front panel connector. Can be set to transmit on any of 5 CATV channels.	See CAR usage below.
Cable Access Receiver (CAR)	SLAC	100	Demodulates a 2 Mb SDLC serial bit stream from the CATV cable and converts it to 16 bit parallel data words. These pass through a FIFO buffer and can be read from the CAMAC backplane or from a front panel connector. It can be set to receive on any one of 5 CATV channels.	Used in specialized point-to-point digital communications applications, in the Beam Pattern System where one CAT transmits beam related information to approximately 100 CARs which receive the information simultaneously.
Video Cable Access Module (VCAM)	Coherent Systems Inc.	25	Can be programmed to accept one of eight video (TV camera) inputs and place it on one of five possible CATV channels. The images may then be observed anywhere in the system using standard television receivers.	Used to multiplex TV camera signals to operator control stations.

Table 7.2.2.2 Continued

MODULE NAME (acronym)	SOURCE	≈ NO. OF MODULES IN SYSTEM	DESCRIPTION	USE
Parallel I/O Processor (PIOP)	SLAC	250	Contains an Intel 8088 processor which supports both RAM and EPROM memory. Has a general purpose interface to the CAMAC backplane and contains a front panel I/O port that supports a differential driver/ receiver version of the 8088 I/O bus. It is designed to be used with special purpose "heads" which provide an interface to a device.	Primary use to date has centered on the klystron control for the LINAC. (see section 7.2.5.1)
Beam Position Monitor (BPM)	SLAC	400	Provides 12 bits of resolution and 8 bits of attenuation control as well as a self-calculation mode to digitize fast (1 ns) bipolar pulses	Digitizes signals derived from beam position monitor striplines.
Beam Position Multiplexer (SP10T)	SLAC	325	Provides a single pole 10 throw (SP10T) switch for fast (1 ns) bipolar signals.	Used to multiplex Beam position monitor signals into BPM modules.
Pulsed Amplitude Unit (PAU)	SLAC	25	Provides 32 "time-multiplexed" channels of pre-programmed analog amplitude. Receives timing information from CAMAC auxiliary backplanes and pattern information from CAMAC backplane.	Used for the control of devices such as pulsed magnets and phase shifters which must change state at the accelerator pulse rate.

Table 7.2.2.2 Continued

MODULE NAME (acronym)	SOURCE	≈ NO. OF MODULES IN SYSTEM	DESCRIPTION	USE
Toroid Charge Monitor (TCM)	SLAC	15	Digitizes a signal generated by charge passing through a toriod with a nominal 1% accuracy.	Used to digitize beam current intensities.

7.2.3 SLCNET

SLCNET is a broadband local area network for communication between the Host and remote microclusters, using half duplex SDLC and RF modems to utilize one 6 MHz channel of the CATV cable system. The initial instantaneous transmission rate is 1 Mb per second, limited by the SDLC hardware. The RF modems have a bandwidth of 2 Mb per second, and modems that could transmit at 5 Mb per second in the 6 MHz channel are potentially available. SLCNET Release 1 will operate at the present SDLC limit of 1 Mb per second, and the average throughput will be determined by software overheads. The basic SLCNET architecture has the potential to exceed 2 Mb per second throughput with long buffers.

The Host machine supports a VAX SLCNET Channel (VSC) which is a lineal descendant of the VAX CAMAC Channel. The VSC is a high speed (AMD 2903, 2910) bit slice microprocessor, 16 bits wide, with a Unibus buffered data path interface and a parallel-to-SDLC FIFO-buffered interface. The remote microclusters use Computrol SDLC Multibus interfaces with custom firmware replacing the vendor code.

The protocol allows only the Host to initiate any communication, and the remote may transmit only in response to the Host, obviating the need for collision detection and recovery. In the idle state, the VSC polls each remote in turn (POLL message), receiving a negative acknowledgment (null RPOLL) indicating that the remote is alive and well but has no traffic for the Host. This POLL-RPOLL interchange is expected to take about 200 microseconds (though at present it takes about 800 microseconds), so that 50 remotes can be polled in 10 milliseconds. Conversely, the mean time for the VSC to find a remote with a positive acknowledgment (non-null RPOLL) is 5 milliseconds.

The basic protocols support synchronized and unsynchronized reads and writes of buffers up to 8192 bytes. In addition, other protocols support interrupt and broadcast functions as well as bootstrap downloading procedures for the re-

motes. These protocols are described in detail in the SLCNET manual (Ref. 2) and the software higher level protocols are described in Section 7.4.3.1 below.

7.2.4 The Operator Interface

The SLC system is designed to allow the use of multiple independent control consoles. In normal operation, the SLC should be controlled by operators in the Main Control Center (MCC), but for commissioning and development of parts of the SLC, control from positions local to these parts as required. In addition, control and monitoring of individual pieces of equipment is required for maintenance purposes, both local to the equipment and in central maintenance areas.

To deal with these requirements, consoles have been developed that can be located anywhere that a connection to the broadband communications cable (see Section 7.5.1) can be made.

These consoles are of two types: one with a full compliment of interface hardware,which has been given the name COW (Console on Wheels) because it is, in principle, transportable and a smaller, portable unit called a CALF, which can provide a subset of the COW functions at a small fraction of the cost.

A COW has two major interaction devices; an 8×8 button touch panel and 8 general-purpose slew knobs together with three display devices; a four-color graphics display, a video monitor and an Ann Arbor Ambassador terminal.

Each COW has a Multibus crate housing a single board microcomputer and other modules to interface to the interaction devices, to generate graphic displays and to communicate with the VAX through SLCNET. The standard modules are defined in Table 7.2.1.

Initially, four COWs will be situated in the Main Control Center (MCC), one in the Damping Ring control room, one in the CID gun control room and one near the collision point.

A CALF consists of an Ann Arbor Ambassador terminal with a Sytek modem

which allows it to be connected to the CATV system to communicate with the VAX. The software in the VAX allows the terminal to emulate a display screen and touch panel, and most operations that can be performed using a COW can also be performed using a CALF. Full graphics displays cannot, of course, be shown in the same way on a CALF, but some graphics capability can be provided by adding an Ann Arbor Graphics Master Unit.

7.2.5 Special Purpose Hardware

In addition to the general purpose multibus and CAMAC modules described above, there are some special purpose hardware modules for particular systems.

7.2.5.1 RF Control: The SLC imposes severe requirements upon the reliability and stability of the linac accelerating system, the main active components of which are the 31 sector-subbooster klystrons and some 246 high power klystrons presently delivering 36 MW pulsed power at 2856 MHz, but soon to be replaced by newly-developed 50 MW klystrons. In order to meet the SLC design luminosity, the pulse to pulse fluctuations of RF phase and power at the output of each klystron must be contained within tight limits which are as small as 0.5 degrees of phase jitter and 0.1% of amplitude jitter for the low energy sections of the accelerator.

In order to meet the requirements and provide the necessary interface to the SLC control system, two new systems have been designed to replace parts of the old system which is described in the SLAC Blue Book.[4]

These are:

- The Modulator Klystron support system, which is designed to provide the necessary means to operate a klystron station in the gallery through the SLC control system, and
- The Phase and Amplitude detection system, which constitutes the primary diagnostic tool both for the purpose of phasing the klystrons and of detecting the phase and amplitude stability of their output RF pulses.

Figure 7.2.1 shows a schematic layout of the hardware configuration. Both the phase and amplitude detector (PAD) and the modulator-klystron support unit (MKSU) share the same controller, the parallel input/output processor (PIOP), which is a single unit CAMAC module containing an Intel 8088 microprocessor. The PIOP was designed to be the local real time processor for the klystron station. (See Table 7.2.2)

A klystron station contains the following components:

- The RF driver unit (IPHIA), which consists of the original mechanical phase-shifter equipped with a new stepping-motor actuator, the high power PIN-diode attenuator capable of handling 2 KW of pulsed RF power at 2856 MHz and the original isolators.
- The new version of the modulator which delivers high voltage and current pulses to the klystron.
- The klystron tube with its electromagnet and regulating power supply, the waveguides and accelerating structures.
- The SLED cavities with their motor actuated needle tuners.

The MKSU contains all the electronic devices necessary to interface the above mentioned equipment to the PIOP and the SLC controls system. It controls the RF drive level to the klystron by means of a digitally controlled current source driving the attenuator over a 20 dB range, and the klystron phase by means of the stepping motor driving the phase shifter with a resolution of 0.25 degrees/step. It also controls the SLED cavity tuner position by means of switches acting on a dc motor, and the klystron electromagnet current by means of a D/A converter.

It is responsible for the acquisition of status and fault information from both the modulator and klystron as well as for monitoring analog parameters, some of which need to be sampled pulse-to-pulse, such as the klystron output power, input power, beam voltage and beam current, while others vary relatively slowly such as the klystron body temperature, the electromagnet current, etc. The

MKSU also triggers the klystron modulator by amplification of the trigger pulse delivered by the PDU (see Section 7.3) through the PIOP, and extends the data bus from the PIOP to the phase and amplitude detector.

The phase and amplitude detector provides a measurement of the phase difference between the pulsed RF signal derived from the klystron RF output and the cw signal derived from the phase reference line at 2856 MHz to an accuracy of 0.1 degree. The main components of the phase and amplitude detector system are the RF detector head and the signal processor board. The RF detector head is a stripline circuit board containing a large-signal detector diode for linear amplitude detection, a double balanced mixer used as a phase detector, a varactor-diode linear phase shifter electronically controlled to null the output of the phase detector, and a $\pm 90°$s wobbler phase shifter used to eliminate the offset error at the mixer output.

The signal processor board is an electronics board which conditions the pulsed phase and amplitude detected signals by means of amplifiers and filters, tracks the level of each input signal and holds it when the trigger is pulsed. It performs the analog multiplexing of the two sampled signals and of the dc signals conveying the temperature and power supply voltage levels of the detector, digitizes the multiplexed analog signals by a 12 bit A/D converter, and stores the digital data in a local buffer memory. It provides the analog signal to bias the phase shifter in the RF head so that the phase detector output is nulled. This analog voltage is also multiplexed and digitized in the processor board. Lastly, it provides the square wave to bias the wobbler phase shifter alternatively to $\pm 90°$ at successive pulses.

The processor board and RF detector head are packaged together in the same temperature-stabilized enclosure. Together with their power supply they are housed in a 5 inch rack-mounted chassis located next to the klystron to minimize the cable length.

7.2.5.2 Beam Position Monitors: The monitoring of the beam trajectory

along the Linac and around the two Collider arms requires a large number of position detectors. A typical position monitor station consists of four striplines connected to coaxial feedthroughs mounted at 90 degree intervals around the vacuum chamber. A pair of opposite polarity sharp pulses (about 1 kV) are produced in each stripline electrode as the beam passes. The spacing between the pulses is determined by the length of the electrode which varies from about 4 cm to 30 cm in different parts of the machine.

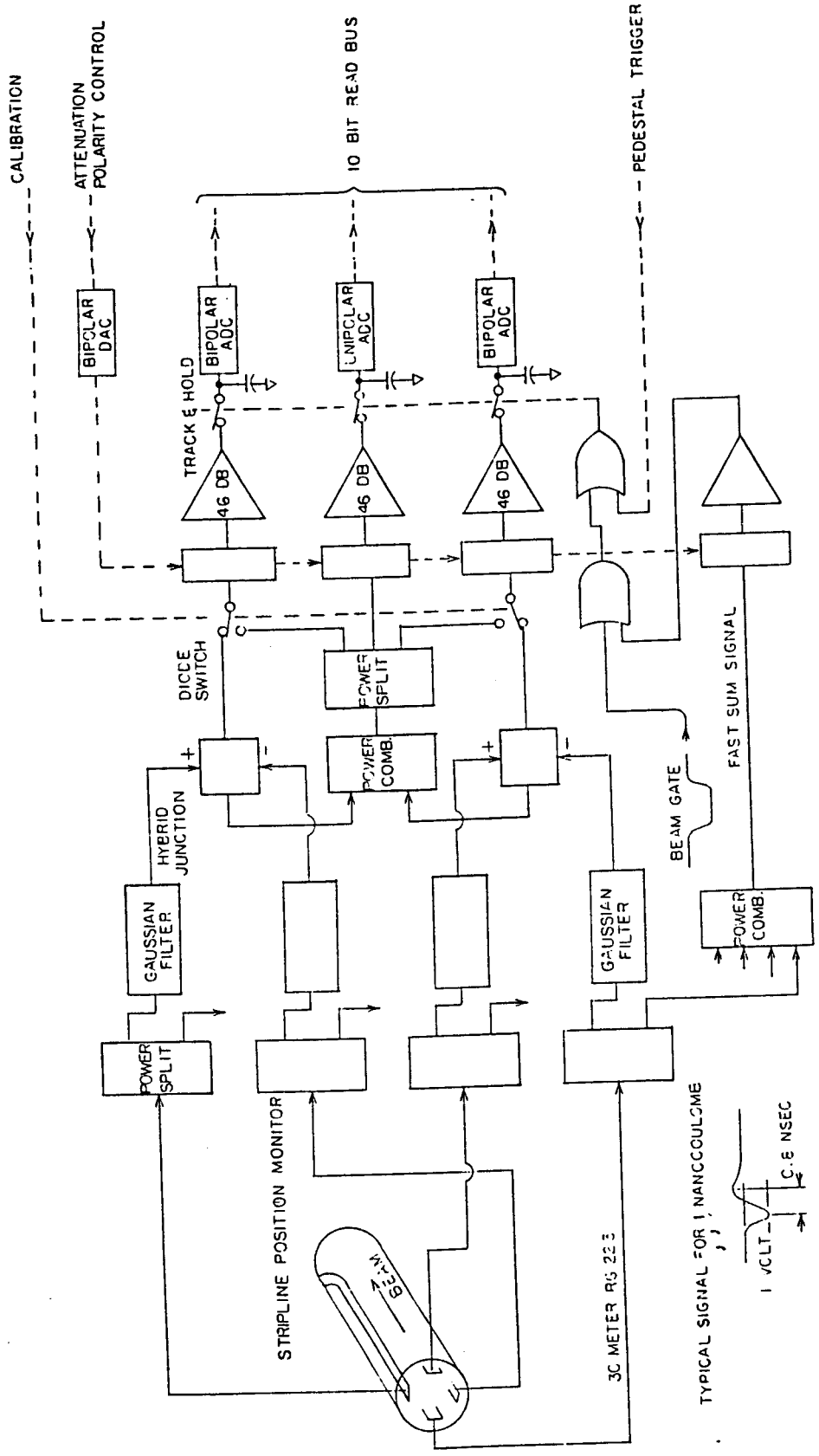
CALIBRATION
ATTENUATION
POLARITY CONTROL
10 BIT READ BUS
PEDESTAL TRIGGER
BIPOLAR DAC
BIPOLAR ADC
UNIPOLAR ADC
BIPOLAR ADC
TRACK & HOLD
46 DB
46 DB
46 DB
DICCE SWITCH
POWER SPLIT
POWER COMB.
HYBRID JUNCTION
GAUSSIAN FILTER
GAUSSIAN FILTER
BEAM GATE
FAST SUM SIGNAL
POWER COMB.
POWER SPLIT
STRIPLINE POSITION MONITOR
BEAM
30 METER RG 223
TYPICAL SIGNAL FOR 1 NANOCOULOMB
1 VOLT
6 NSEC

Figure 7.2.5.2

The four detected impulses will be "smoothed" with a length of ordinary cable and will then be processed in a conventional manner (Figure 7.2.5.2). The complete processing of each set of four signals will be completed in less than 5 milliseconds (which is shorter than the interpulse period), using low cost analog-to-digital converters. The data will be stored locally, then delivered upon command to the data acquisition system for calculation of the bunch position. In the linac, each set of four electrodes has its own processing electronics but, due to cost considerations, the damping ring and arc electrode sets are multiplexed approximately ten sets for each processing unit.

Given two signals, $V1$ and $V2$, obtained from opposite electrodes mounted on a beam pipe of radius R, the beam position in the direction defined by the two electrodes is simply given by $R(V1-V2)/(V1+V2)$. For the linac chamber, $R =$ 10 mm; thus a measurement of $V1$ and $V2$ to 0.5% will permit a beam position detection to 0.05 mm. In the Collider arcs, R is even smaller, so the tolerance on the measurement of $V1$ and $V2$ can be somewhat relaxed to obtain a precision of 0.1 mm. During tune-up and initial orbit corrections, digital averaging of data can be used to yield an even finer beam position measurement.

The BPMs are gated and processed in response to a command broadcast by the Master Pattern Generator (see Section 7.3). The microclusters cause the generation of gates in response to one command and then process the data in response to a second command. They reduce the data to transverse positions in millimeters and asynchronously transmit the data to the requesting process using the Message service.

There are other beam measurement devices, such as toroids and profile monitors, placed at strategic points along the SLC machine. Provisions have been made to control and display the signals from these devices as required.

7.2.5.3 Arc Magnet Moving System: Some 950 SLC arc magnets need remote position control for the purpose of orbit correction. Horizontal and vertical positioning mechanisms will be installed alternately on the magnet supports.

The moving mechanism consists of a shaft and a cam in the form of an off-center cylinder which displaces the magnet support when rotated. The magnet displacement range is $\pm$ 1 mm and the required position resolution is 10 μm. The shaft is rotated by a stepping motor through a planetary gear of ratio 108:1 and the cam rotation angle is measured by means of a rotary potentiometer.

The control hardware for the moving magnets system is located in each of the 26 arc alcoves.

A stepping motor controller, in a single width CAMAC module, controls 48 stepping motors by means of 12 motor driver cards housed in a Eurocard chassis. Each driver card supplies current pulses to four stepping motors from an 8A, 15V power supply.

Two analog acquisition CAMAC modules (SAMs) are used to read back the cursor voltage of the potentiometers and the bias voltage, the ratio of which is proportional to position.

7.3 THE TIMING SYSTEM

The SLC timing system provides accurately timed triggering pulses for devices such as klystrons and kicker magnets, and gates for diagnostic devices such as toroids and beam position monitors. It will provide these pulses on a beam by beam basis, thus allowing interlaced operation. Typically a given device has two timing system information paths leading to it. One of these paths carries accurate time information and another carries a digital code identifying the upcoming beams (the beam code). Thus the system can be broken into two subsystems in which these two types of data are created, broadcast, distributed and received.

Accurate time information is derived from the 476 MHz linac master oscillator located at Sector 0. Phase stability requirements placed on the 2.8 GHz klystron drive derived from the 476 MHz determine the maximum allowable phase drift in this source. Interbeam periods must be chosen so that external synchronization constraints (damping rings, PEP, SPEAR and power line AC) are satisfied. For SLC operation beam time triggers need only be locked to the power line and the damping ring. This is done by measuring the interval between the zero-crossings of a reference signal derived directly from the incoming high voltage 3-phase power-line in units of the damping ring rotation period (119 MHz). This measurement is done at Sector 30 near the master substation. The result of the measurement is transmitted to the Sector 0 area on the communication line where it is used to determine the upcoming interbeam periods. This system allows for pulse to pulse phase adjustments with respect to the power line. Present experience with high power beams at repetition rates greater than 60 Hz indicate that this will be needed for SLC operation.

Additional constraints on the beamtime triggers come from the need to use either straight-through beams (nondamping ring) or damped beams to fill SPEAR and PEP. This is done by comparing the PEP or SPEAR rotation RF with the LINAC 476 MHz at Sector 30 and transmitting the data to Sector 0 where it is processed and used to determine upcoming beam times. Alternatively, if

damped beams are needed for storage ring fills, the damping ring RF is frequency-modulated by the required amount so that the extracted beam is synchronized with one of the storage rings. Frequency- modulation is needed since PEP and SPEAR do not use harmonically-related radio frequencies.

A beamtime trigger is produced by the microcomputer in the Sector 0 area about 1 ms before actual beam time. It triggers a pulser which produces a single 2.1 ns pulse which is phase-locked to the 476 MHz. This pulse is combined with the 476 MHz master oscillator signal.

Distribution of this composite timing signal is done using the temperature-stabilized main drive line. In each sector (as well as main control and the damping rings) the signal is coupled out and processed by divide-by-4 units which produce four independent 119 MHz signals, with the fiducial superimposed as a missing pulse. These then drive 16-channel programmable 19-bit countdown units housed in CAMAC modules. The outputs of each countdown unit (known as a PDU) are distributed (along with the 119 MHz) on the printed-circuit-board transmission-line upper backplane of the CAMAC crate. The 119 MHz signal will also be distributed to the arc support buildings and the final focus on high quality cable.

The PDU is where the two data paths (timing and beam code) meet. The beam code is selected and broadcast by a dedicated microcluster called the Master Pattern Generator (MPG) about a millisecond before the fiducial signal is put on the Main Drive Line. The beam code is broadcast on a dedicated subchannel of the CATV cable and is demodulated and received on the Pattern Receiver Interrupt Module (PRIM) in each microcluster about 50 microseconds after transmission by the MPG. Upon receipt of the beam code, the PRIM interrupts the micro to execute a routine to load timing data into a set of PDUs.

The beam code is broadcast as a two byte message. The first byte is the actual code and the second is a command byte used to specify other synchronous activities for the system. Thus 256 different beams can be selected by the beam

code. These beams are specified by a set of Beam Matrices stored in the micro memory or in the PDU itself (Version II). Each row of the Beam Matrix corresponds to a particular beam code, and the elements of each row are the PDU timings that correspond to a particular beam. Specifically each row contains the data describing whether or not a particular klystron will produce a null, accelerate, or standby pulse for a given beam. Slow changes to a beam, for example changing a klystron from accelerate to standby timing, are accomplished by rewriting the appropriate data in the Beam Matrix.

The Master Pattern Generator is responsible for generating the proper sequence of beam codes in response to general strategies received from higher level computing nodes and from lower level data, indicating experiment and machine readiness. The MPG is also responsible for collating diagnostic requests for higher level programs with the sequence of beam codes it is generating and attaching appropriate command codes to the beam code. For example, a process might request a beam position monitor scan of the trajectory of a particular pulse down the machine; such a scan is synchronized by PDUs loaded in response to a command code.

There are four operational modes allowed for each PDU channel:

1) 360 Hz at a pre-set time with respect to the fiducial,

2) Preset time associated with a particular beam code,

3) Preset time at a base rate (10–180 Hz), and

4) Single pulse on a specific beam pulse.

The PDU output time can be adjusted in 8.4 ns steps and has an rms jitter of less than 1 ns. Further fine adjustment can be achieved with vernier delay units. Each PDU will be monitored with a companion diagnostic device which can measure time intervals between the fiducial and specific PDU output channels (or external inputs).

The timing system additionally provides synchronized pulse trains for use

in the Damping Rings. Further special Damping Ring applications include time and pulse height measurement and feedback for the kickers. Pulsed steering devices are also controlled through the timing system with pulsed digital-to-analog devices.

7.4 THE SOFTWARE SYSTEM

The software for the SLC control system has three major levels: System software, Facilities, and Applications. The System level includes not only language and network support but also the software that defines the underlying architecture. It includes standardized routines for terminal I/O, touch panel communication, knob handling, database access, message services, error reporting, and display generation. These routines are carefully layered to isolate the other software levels from the details of network protocols. They provide structured and disciplined access to system resources.

The SLC Facilities provide standard functions and displays for each of the major hardware systems, including Timing, Klystrons, Beam Position Monitors, Magnets, and Status. Each Facility has a dedicated job in the microclusters, a collection of control, display, and I/O routines in the Host, and a well defined set of functions and error codes for message communication. Systems and Facility code is designed, written, and maintained by the SLC software group. It encompasses a broad set of tools for use by the Applications programs.

Applications code provides the customization necessary for the individual machine groups while making extensive use of the Systems and Facilities software. The Applications level includes specific database entries, touch panel layouts, tailored displays, and functions not provided by the standard Facilities.

The basic architecture in the VMS Host machine is centered on the three shared data structures described below: the database, the configurations and the T-Matrix. This implies that the Host machine is necessarily a single memory system. A second Host machine with parallel data structures is used for system development. This machine has a full copy of the database and T-Matrix with identical values for all parametric data but no attempt is made to have the control and returned data reflect the current state of the production machine. Each machine runs its own copies of the control and support programs. Communication between the two machines is over a standard DECNET link.

The programming language used for the SLC control system is FORTRAN 77. The host software is written in VAX extended FORTRAN, with some system and utility routines in MACRO, the VAX assembly languages, or PL-M. The Micro-cluster software is written primarily in Intel FORTRAN 86, with some support routines PLM 86 or ASM86 assembler. All of the micro-cluster software is developed and compiled on the Host.

7.4.1 Data Structures

Data for the SLC controls system is stored in three interrelated data structures. The first, called the database, stores static and quasi-static information about the machine. This information describes all control connections, device characteristics (e.g. magnetization polynomial fits), and quasi-static machine characteristics (e.g. values of magnetic fields). The database is hierarchical, identifying devices by symbolic names, locations, and sequence numbers. Actual data is retrieved by reference to secondary symbolic device attributes. No attempt is made to store information in the database relevant to only one pulse of the machine.

Information organizing the quasi-static values of large sets of devices is stored as "configurations." A configuration is a formatted file identifying specific devices, secondary controllable attributes, and values for these attributes. The canonical example of a configuration is a set of explicitly identified magnets and their field values describing an operable lattice on the machine. Standardized facilities have been developed for the manipulation of configurations, e.g. saving or restoring configurations delineated by sector, region, or full machine.

The data structure used to configure the machine to a previously developed "Beam Definition" on a pulse basis is called the T-Matrix. It can handle data for all the timing elements of the machine (PDUs) for up to 256 separate beams.

The Database: is a structure designed explicitly for the distributed control architecture of the SLC control system. It consists of a master section in the Host machine that is divided into sections for each microcluster. These sections are

further divided into supertypes according to access requirements. The supertypes are:

1) Internal pointers (write accessible only by the database generation code),

2) Parametric data (write accessible only by the database generation code),

3) Control data (write accessible only by the Host),

4) Returned data (write accessible only by the microclusters), and

5) Local data (not accessible by the microclusters).

Supertype Sections 1 through 4 are maintained in each microcluster. Data updating of a non-local section is done over the network in response to specific update requests or "out of tolerance" conditions. Data transfers between the microcluster and the Host are managed by a DataBase EXecutive process (DBEX).

Proper access to the database is provided by a set of structured routines that include transparent updating of non-local sections and list facilities for multiple, rapid accesses. Database generation is an off-line activity, and has two major phases: definition of the schema, i.e. the definition of primary and secondary names and their attributes; and a second stage which consists of declarations of the existence of a specific device with values for its secondary characteristics. In this approach, the design of the first phase is part of the control system design, and is critical to basic operation of the control facilities. The second phase is an applications task, essentially ensuring that actual devices are properly described. Stand alone facilities to examine and edit database values exist.

The database on the Host is implemented using a memory segment of about 10 megabytes in size. Management of this block is done entirely by the VAX Virtual Memory System. The remote Multibus microclusters only support 1 megabyte of address space with the present configuration, and the local database size is of some concern.

Configurations: The database contains the (supposedly) accurate description of the present state of the machine. Configurations are used to store and

manage future and past states of the machine, in the sense of storing the output of TRANSPORT or other beam design software for future use, or for saving a state of the machine for possible future use. Configurations save only the directly controllable parameters of the machine, i.e. magnetic field values as opposed to magnet power supply connection data. In general, controllable parameters have a CONfiguration value coming from a stored configuration or possibly from an online calculation, a DESired value which starts from the CON value but which may be adjusted by operators or feedback control loops, and an ACTual value indicating the last reported measurement of the relevant sensor.

Structurally, a configuration is a VMS ASCII file. A hierarchy exists in the sense that a Sector configuration is a set of device identifiers and values (with suitable headers), a Region configuration is a list of Sector configurations, and a Machine configuration is a list of Region configurations. The configuration facilities maintain an index to the configurations and permit manipulation of the configuration components. The configurations are stored as ASCII files to permit easy examination and modification with a text editor. Saving a configuration is essentially copying ACTual or DESired values to a configuration file; specifically what is saved is determined by a configuration template file. Restoring a configuration is essentially copying values from the configuration files into database CONfiguration and DESired values.

The T-Matrix: In addition to the quasi-static description of the machine which is primarily magnetic field values and "nominal" values of the RF amplitudes and phases, the behavior of the machine on a given pulse is determined by the triggerable devices, e.g. thyratrons for klystrons, phase shifters for SLED control, or kickers for beam manipulations in the Damping Rings. As previously described, all timing is derived from the MPG by counting the fourth subharmonic of the RF following an AC line synchronized fiducial. A "Beam Definition" is a set of values for those counters. The control system can support up to 256 independently defined beams, whose sequence is arbitrary and determined by the

Master Pattern Generator. The data structure containing all of the timing information is stored in the Host machine as the T-Matrix. The appropriate subsets of the T-Matrix are transferred to the corresponding microclusters, to be stored in either local memory or in the PDUs (counters) themselves, depending on what generation PDU modules are in use. Timing facilities exist to manipulate elements of the T-Matrix and transparently communicate changes over SLCNET to the microclusters.

While elements of the T-Matrix are in units of 1/(119 MHz) or "ticks," the elements are more easily understood as relative times to two additive displacements. The first displacement is called TREF, and has a value in the database for each PDU. For a beam injected 1024 microseconds after the fiducial, as measured by an arbitrary but well defined procedure at the injector, TREF is the count required in the PDU for it to produce a pulse synchronized with the arrival of a beam derived pulse from the Beam Position Monitor module in the same CAMAC crate as the PDU. Defining times relative to TREF removes the beam and fiducial propagation times from the problem, thus leaving only delays associated with the controlled device. For example, in this way a distribution of thyratron trigger times is directly meaningful in terms of thyratron delay characteristics. The second displacement is called TNOM, for a nominal beam time relative to the reference beam (at 1024 microseconds after the fiducial). TNOMs are defined for each beam and each microcluster. An example of the use of TNOM is a value of 8 ticks (1/2 damping ring revolution) for the kicker to extract the second electron bunch. This use of TNOMs then permits one canonical device time to be kept in the database for each device function, and simple software routines can manipulate the data to define various beams.

The manipulation of timing elements has then had two stages, which are rather unrelated. The first is an offline exercise in designing beams, deciding what devices will be used on a particular beam code, and determining how this structure will interact with other activities in the machine. For example, different

beams might be used to store bunches in the Damping Ring, separately extract bunches, "stack" bunches in the damping ring, store e^- in PEP, store e^+ in PEP, etc. These exercises are performed using an interactive program called Beam Design Language.

The T-Matrix, like the database and configurations, is stable across Host crashes and normal system development. Additionally, the set of BDL commands that define the T-Matrix are normally saved as a file so it can be regenerated even when the physical components of the machine have changed. Finally, the sections of the T-Matrix can be saved and restored in a manner similar to configurations.

7.4.2 Communications Structures

7.4.2.1 High-Level Network Protocols: The SLCNET communication link between the Host computer and the microclusters is used to perform the following major logical functions:

- The initial loading of the remote microclusters, including the loading of their operating system. Only a minimal bootstrap program to operate the network is stored in PROM on the SBCs.
- Maintenance of the SLC database by passing messages between the database executive and the microclusters using "Database Services" high level protocol.
- Control of microcluster activity and relay of responses using the "Message Services" high level protocol described below.
- Implementation of the cross debugging facilities.
- Communication with the COWs, transmitting graphics for the displays and touch panel, and receiving touch panel and knob data.
- Driving remote line printers. A VMS spooler transmits printer queues over the network to dedicated line printer micro nodes.
- The protocols for these functions are described in detail in the SLCNET manual (Ref. 2).

7.4.2.2 Message Services: Communication among processes in the SLC system passes either through the shared data structures or through the SLC message service. Messages are used to convey commands to the microclusters and command completion responses back to the VAX. They are also used for error messages or for data from a single pulse such as beam position monitor readings. All SLC messages have a simple structure consisting of ten words of header information followed by up to 502 words of data. The header includes source and destination specifiers, a time stamp, a function code, and a data length word. The source and destination are 4 character ASCII names to identify either a

VAX process or a microcluster. VAX names are of the form V0nn where nn is the SLCNET interrupt used by the process; microcluster names are the standard database names. The function code has two bytes, a high byte to identify the Facility and a low byte to specify the explicit function to be executed. A standard set of interface routines are available to construct messages, to synchronize commands and responses from multiple microclusters, to implement single pulse commands through the MPG, and to signal error messages.

7.4.2.3 Error Reporting: The SLC control system uses a uniform protocol for error reporting which is based on the VMS Message Utility. The same protocol is used by stand-alone VMS programs, by components of the VMS SLC control system, and by the microclusters under iRMX. When an error condition is detected, it is reported using one of a set of predefined error messages. Each message is associated with a 32 bit word called the message code, a unique message symbol that is generated by the message compiler, and a message text and formatting directives for any parameters of the message text. The SLC error message scheme has two basic pieces; a message originator and a message receiver. The message originator sends the message code and any parameters to the message receiver using the SLC Message service. The message originator needs to "know" only the message code, defined symbolically in FORTRAN "Include" files, and the message text and formatting is handled entirely by VMS. The receiving routine takes the SLC Message buffer, acquires the message text using the VMS system services, formats the message using SLC format conventions, and outputs the formatted message. Error messages from microclusters or SCPs are sent first to PARANOIA (see section 7.4.3.2) which obtains and formats the message text and puts it in the error log. The message is then relayed by PARANOIA to the remote destination for display.

7.4.3 Host Software

7.4.3.1 Console Programs: Each user of a console (COW or CALF) has his own copy of the SLC Control Program (SCP). The SCP is the console interface

to the database, configurations, T-Matrix and the Message services. The SCP manages the console, translates user directives, and generates displays. The SCP handles only one user, and there is no requirement that all SCP's be identical. Because there is a separate copy of the SCP for each user, the SCP code is relatively easy to optimize and debug. The single user software is conceptually and actually much simpler than a multiuser version would be, and development is made possible by the coexistence of several versions of SCP. A natural consequence of the SCP design is that the SCP executes interactively on a terminal (as opposed to batch). This terminal is used to receive messages from the SCP and other processes, and to conduct dialogs that are unsuited for touch-panel communication.

The primary control interface for each console is a flexible touch-panel system. The touch-panel is a transparent screen capable of sensing the position of an operator's fingers, and it is backed up by a general-purpose monochrome CRT display. Each panel is generated interpretively from a fixed format text file. A logical name facility is used to provide communication between the application code and the panel description code. The logical name routines allow data to be moved from the panel, and allow the panel to manipulate displays and subroutines that have been identified to the logical name service. The structure is deliberately limited to ensure that the panels may be easily understood and debugged. System routines read and interpret the panel files and implement the buttons when pushed. Additional routines provide for output of character data to the panel from the user software.

The COW supports up to eight knobs for the input of quasi-continuous variables to the program. The actual hardware consists of 250-count shaft-encoders polled at 5 Hz by hardware. Also each knob has a software-writeable legend of 16 characters per knob. Four knobs are simulated by the CALF software. A standard set of knob access routines are available for use by the Facilities and Applications.

Essentially all Facilities and Applications code is structured into two classes of subroutines referred to as 'actions' and 'displays.' A 'display' is a subroutine which generates information to be conveyed to an operator by a COW. Usually these routines generate graphics displays using the UNIFIED GRAPHICS package; they may also generate certain line printer and terminal displays. 'Displays' are always called by the Display EXecutive subroutine DEXEC. They are made known to the SCP system by a call to a Logical Name routine. An 'action' is a routine which may exercise an actual control function or gather and process data either for a display or the database. A suitable collection of actions constitutes a GROUP. One member of the GROUP is usually a driver for the other actions, and is identified to the SCP system by a call to a Logical name routine. The distinguishing feature of a GROUP is that it may be scheduled for execution in various periodic modes. After any GROUP is executed the SCP will call DEXEC to generate any requested displays. The GROUP structure allows various functions to be executed periodically, ie the BPMO display may be regenerated regularly by scheduling the GROUP which acquires data from the SLC. Then DEXEC can call the actual BPMO display, and the system will translate the graphics buffers and transmit them to the COW.

The Host software for each Facility is pre-linked into a module (a VMS shareable image) which may then be linked with other such modules into a version of the SCP. Each Facility module contains an initialization routine, a GROUP driver if appropriate, and all 'display' and 'action' routines for that Facility. These modules are then declared to the VMS operating system by means of the VMS Install utility, so that the code and fixed data sections may be shared by all active consoles. The sharing of code significantly reduces the load on the Host machine when multiple consoles are active. The pre-linking of each Facility into a module makes minor revisions transparent to the user and major revisions uniform across the system.

7.4.3.2 PARANOIA: is a Host process with two major responsibilities, error handling and machine monitoring. All errors detected by the SCPs or other Host programs are sent to a dedicated mailbox for Paranoia; those detected in the microclusters are sent to a dedicated SLCNET interrupt owned by Paranoia. Paranoia receives the messages, logs them, formats them, and broadcasts them to the appropriate control consoles. Messages from a SCP or detected in a microcluster while executing a command from a SCP are broadcast only to the originating SCP. Messages generated by the monitoring activities of either Paranoia or the microclusters themselves are broadcast to all active consoles.

Paranoia's monitoring activities are an evolving collection of diagnostic functions. It requests periodic checks of machine parameters such as magnet settings, klystron phases, and temperatures from the individual microclusters. Error conditions reported are metered and broadcast to the consoles. Paranoia also checks the microclusters, consoles, and network and performs various maintenance and cleanup tasks. As the system develops and recurrent problems are recognized, additional monitoring functions will be added to PARANOIA. Future improvements will include global error-analysis algorithms and more sophisticated diagnostics.

7.4.3.3 Other Host Programs: In addition to PARANOIA and the individual SCP programs running each COW or CALF console, several other programs are included in the Host software. The DataBase EXecutive process, DBEX, handles all network transfers of database information between the VAX and the microclusters. When a VAX program changes control data in the database, the database access routines send a message to DBEX requesting that the appropriate information be updated in the microclusters. When database information is returned by a microcluster, it is sent to DBEX which then writes the new values to the VAX database.

Other programs provide network monitoring and diagnostics, error log formatting and filtering, time logging of data, and CAMAC or database checking.

7.4.4 Microcluster Software

The microcluster software was designed to take advantage of the multi-tasking capabilities of the iRMX operating system. Each microcluster runs 10 to 15 jobs which timeshare according to their assigned priorities. The jobs are organized by function, with a separate job for each of the Facilities, e.g. Magnets or Klystrons, plus a number of additional server jobs. Each Facility job is responsible for performing all of the monitoring and local control algorithms for its class of devices. These jobs execute commands received through the message service and use a shared common database. Network input in the form of database updates or messages is handled by two separate network server jobs. At initialization, each job creates its own mailbox to receive communications from other jobs or from the VAX via the message server job. All messages are in a standard message service format. Each job performs its own network output to the Host, including database updates, response messages and error reporting. These jobs carry out the following services:

- The Main Job is responsible for creating all of the other individual jobs when the micro is booted. It always creates the Database, Message, and CAMAC server jobs plus a list of additional jobs which are specified dynamically when the microjob is linked. The jobs for the various facilities are not created until a full copy of the local database has been received to guarantee that valid database information is available for initialization.

- The Database Job receives all database updates from the VAX including the full copy of the local database which is downloaded when the micro is booted. As each block of database information is received, it is stored directly in the microcluster's local copy of the database.

- The Message Job is the network server for all messages from the VAX to the microcluster. As each message is received, the high order byte of the function code is used to determine the facility to be exercised, and the message is sent to the mailbox of the appropriate job.

- The Virtual CAMAC Job performs CAMAC operations requested directly

by the VAX. It does not process CAMAC operations for the other jobs in the microcluster which have their own direct access. It may be used to bypass the normal software algorithms for diagnostic purposes or to execute CAMAC operations not provided by any of the existing facilities.

- The Timing Job is responsible for the synchronization of devices on a pulse to pulse basis. It maintains the local copy of the Beam Matrix, initializes and programs pulsed devices, and performs all operations necessary to configure the machine for the next beam as each beam code interrupt is received.

- The Klystron Job performs control and monitoring functions for the klystrons and subboosters. It downloads the Parallel Input Output Processors, transmits to them database values and function requests, and executes the closed loop phase setting algorithm.

- The Magnet Job is responsible for all closed loop analog control and monitoring. In addition to magnets, this includes stepping motors, attenuators and other miscellaneous devices with DAC control and ADC readback. Locally implemented algorithms include closed-loop setting, device calibration, and magnet standardization.

- The Beam Position Monitor Job reads the stripline position monitors and SLC toroid charge monitors. The BPM's are gated and processed in response to a command broadcast by the MPG. The BPM job reduces the data to transverse positions in millimeters and asynchronously transmits the data to the VAX using the Message services.

- The Status Job is responsible for monitoring of analog signals such as temperatures and vacuum gauges, and for monitoring and control of a wide variety of digital input and output devices.

- The Crate Job monitors the CAMAC crates attached to each microcluster and reports whenever a crate is taken offline. When a crate is turned on, it

detects the change of state, initializes CAMAC modules as needed, sends messages to other jobs to perform additional initialization, and reports the new status of the crate. When requested by the VAX, it can also exercise the crate verifier and report any problems detected.

7.4.4.1 Software Development: All microcluster software is generated on the Host machine using modern cross compilers and linkers. Additionally, cross debuggers are used to debug a microcluster program interactively. (A cross debugger is one which executes on the Host, uses symbol tables resident on the Host, and targets the micro cluster over the network through the micro's operating system). In this architecture, compilers, linkers, editors and other language support of the micro operating system are irrelevant and have not been implemented; neither has the micro's disk or other virtual memory management facilities been used. Instead a rather minimal real-time support nucleus has been generated with enhancements to support the cross debugger.

7.4.5 Specialized Equipment Programs

7.4.5.1 Magnet control: The Magnet Control facility consists of general-purpose command and display routines in the Host and setting and monitoring routines in the microcluster. All parametric information including magnetization polynomials, power supply transfer functions, channel assignments, tolerances, and set points are stored in the database. The microcluster has a repertoire of five commands:

1) CHECK sets status lists indicating whether set points and actual values are within Check tolerances;

2) TRIM sets actual values to within Trim tolerances, iterating if necessary;

3) CALIBRATE determines the power supply transfer function and checks whether it is within tolerance of the database nominal value;

4) STANDARDIZE cycles a magnet so that it is at a known point on its hysteresis curve; and

5) PERTURB sets a magnet current by extrapolation from its current value without using the readback system (Perturb is used for making changes small compared to setting tolerances for some feedback applications and for hand knobbing of magnets).

Magnets fall into two general classes, loosely defined as small and large, and more accurately defined as those controlled by channels of a standard DAC and SAM, and those controlled by a Power Supply Controller (PSC). The PSC controls one power supply, provides on-off and reversing control and status returns. In general, the "small" supplies are considered to be safe and do not require detailed interlocking, while the "large" supplies are considered hazardous. The control system supports several well defined combinations of supplies and magnets:

- A small supply is controlled by a DAC, the current is read by a SAM, and the power supply drives one magnet. The power supply may be one channel of a current controller fed by a bulk supply.
- A large supply is controlled by a PSC, its shunt voltage is monitored by the PSC, and it drives one magnet.
- A PSC controls a large power supply powering a series string of magnets, each of which has a controllable shunt. These shunts are controlled by DAC and SAM channels.

In addition, either a small or a large supply may be used to provide a single set of controls for several magnets connected in a series string.

7.4.5.2 Klystron Control: The software for RF control is divided into three functional levels which correspond to three processors involved. At the lowest level, in the PIOP, the software takes the form of firmware resident in ROMs and of a compiled PL/M program which gets downloaded into the 64k byte RAM. The firmware contains the bootstrap program and the self-test routines while the compiled program consists primarily of the routines which operate the PAD in

one of four modes:

- In the tracking mode, the phase of the reference signal is kept locked to that of the klystron by means of the control voltage on the PAD phase shifter whenever the klystron phase drifts away.
- In the jitter mode, the PAD phase shifter is kept fixed and the program computes phase variations from pulse to pulse.
- In the hybrid mode, a combination of the previous two modes, the phase adjustment is activated only if the klystron phase has drifted by a relatively large amount.
- In the fast-time-plot mode, the program successively delays the measurement trigger by a fixed amount (normally 67 nsec) and performs 64 phase or amplitude measurements to span over the envelope of the klystron pulse. The data is stored in the fast time plot block where it is made available for reading by the micro and VAX computers.

The PIOP also performs the data reductions, averaging computations and hardware checks.

At the middle level, the software resident in the microcluster memory contains the routines which control the position of the phase-shifter and the level of the RF drive to the klystron.

At the highest level, in the VAX, applications programs support the control and monitoring of the klystron station by means of touch-panels, knobs and displays, to allow the selection of any linac sector and perform the following functions:

- Read the phase and amplitude values of all the klystrons in the sector.
- Display detailed information on the phase and amplitude detector of each klystron.
- Change the input phase value for each klystron by means of a knob.

- Trim the phase of each klystron to the desired reference value.
- Saturate each klystron by modulating the drive and reading the detected output amplitude value.

Also scheduled for later implementation are the following functions:

- Monitoring of klystron beam parameters and power levels.
- Operation of the klystron station in open or closed phase-lock loop.
- Triggering of the modulator pulse according to a beam pattern.
- Control of the SLED cavities tuners.

7.4.5.3 Beam Position Monitor Control The BPM facility is used to gather and display BPM and toroid data on a pulse-to-pulse basis. The data obtained depends not only on the set of BPMs or toroids being used, but on several other parameters selected by the operator. Since different operators may be requesting data with different parameter settings at roughly the same time, the data gathered does not characterize the hardware at that time and is not kept in the database.

BPM software is divided between the host and the microcluster. Routines in the microcluster issue necessary CAMAC commands (or in some cases prepare to issue them) and reduce the raw data read from the BPM or toroid modules to the form expected by the Host before sending it back to the Host via the Message Service. BPM software in the Host may be used to request calibration or measurement of BPMs or toroids in a specified range of microclusters under certain conditions. The conditions to be selected include: beam, time slot, bunch, and attenuation setting as well as the range of microclusters. Typically, the operator will define one or more such sets of parameters (each set is known as a "measurement definition") and do a calibration for each. He may then take data for any of the calibrated measurement definitions. Returned BPM calibration data is both displayed and written to a disk file (toroids are calibrated off-line). Measurement data may be displayed or returned to higher-level histogramming

or Modemling software for further analysis.

The database contains parameters for each BPM electronics module, each stripline monitor, and each toroid. This data is rarely changed unless a module has been added or replaced.

Procedures used to calibrate BPMs or to take measurements of BPMs or toroids all have roughly the same form. Initially, the Host requests all microclusters in the active range to prepare for the operation to follow. Preparation includes setting up (but not executing) two CAMAC packages: the first will program the timing device (PDU or PSU) used to gate the BPMs; the second will read the BPMs. When the microcluster has completed preparation, it sends a response back to the Host, indicating the status of the operation.

Each time data is to be read, the Host sends a request to the MPG for two special codes to be broadcast. When the first code is broadcast, the previously-prepared microclusters will execute the first CAMAC package. The BPMs will receive the necessary gate, and when the beam passes, will digitize and hold the data from the striplines. On the second broadcast, the BPMs are read. Finally, the microclusters convert the data to its final form and send it back to the Host.

Figure 7.5.1

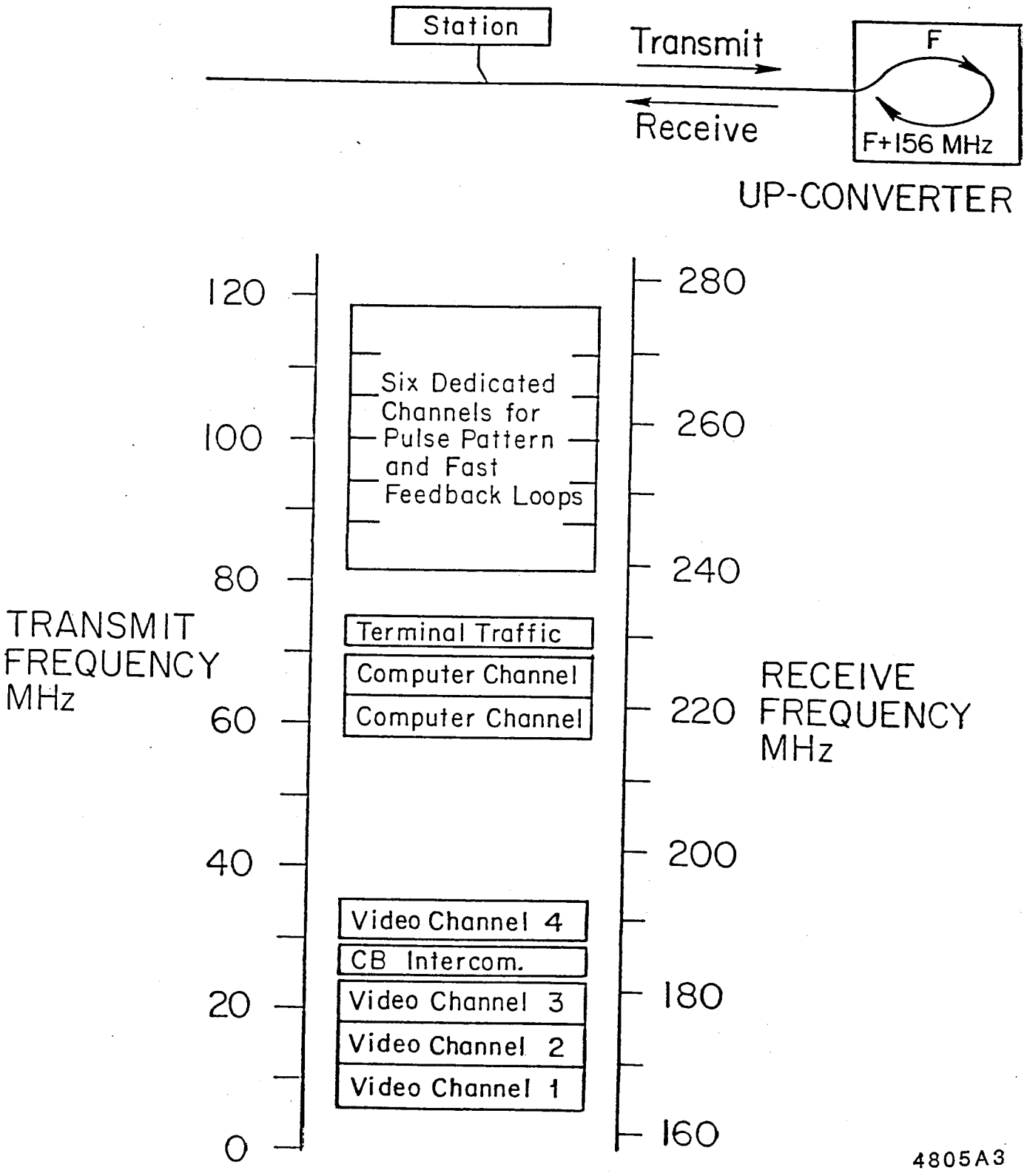
Station
Transmit
Receive
F
F+156 MHz
UP-CONVERTER
120
100
80
60
40
20
0
TRANSMIT FREQUENCY MHz
Six Dedicated Channels for Pulse Pattern and Fast Feedback Loops
Terminal Traffic
Computer Channel
Computer Channel
Video Channel 4
CB Intercom.
Video Channel 3
Video Channel 2
Video Channel 1
280
260
240
220
200
180
160
RECEIVE FREQUENCY MHz
4805A3

7.5 COMMUNICATIONS NETWORK

7.5.1 Broadband Cable

Almost all SLC Communications are based on the use of a midsplit broadband 3/4 inch coaxial cable system. The midsplit configuration was chosen because it provides a low band spectrum of 5 to 120 MHz and a high band spectrum of 160 to 300 MHz. Nearly all signals are transmitted on the low band toward the injector end of the SLC. Three frequency bands are then up-converted and sent back down the coaxial cable. Since nearly all signals are up-converted in this manner, any signal can originate from any point on the cable and be received at any point on the cable. This mode requires twice the cable bandwidth but results in the maximum flexibility for the users.

As can be seen from Figure 7.5.1, the cable carries four 6 MHz video channels with frequency agile modulators, 40 channels of voice, using citizens band transceivers, two 2 Mbaud SLCNET data channels (see Section 7.2.3), five 2 Mbaud point-to-point data channels, one 2 Mbaud broadcast data channel as well as three "one-way" dedicated video channels. The cable also has several 300 kHz channels for terminal-to-VAX communications using the Sytek Localnet 20 system. A combination of Frequency Division Multiplexing (FDM) and Time Division Multiplexing (TDM) is used. The video, voice and point-to-point data channels use FDM, whereas the two 2 Mbaud data channels, and the terminal-to-VAX data channels use TDM. Special modems have been developed for the cable system. The 2 MBaud TDM modems are frequency agile and Multibus compatible. The Video Modems are frequency agile and have eight multiplexed video inputs. All modem parameters are controlled by the network software.

The coaxial cable is installed in all equipment areas, control rooms and laboratory development areas. Connection to the cable is achieved by a special RG59/u double shielded "drop" cable connected to the nearest cable tap (directional coupler). Approximately 5 miles of cable are now installed but eventually over 7 miles will be in place. A pilot carrier, which is up-converted at the injec-

tor, is also provided. Cable levels are read at all cable amplifiers and levels are transmitted back to the central computers on a separate cable, thus providing cable diagnostics.

The cable passes through areas of high electrical noise and a high level of isolation must be maintained otherwise the system performance is degraded. The noise isolation of a properly installed wide-band cable system can be 80 to 100 dB.

The cable system trunk amplifiers are powered from three points on the site. Amplifier power is also carried on the 3/4 inch cable. In-house installation and maintenance is done on this cable system, since, in case of failure, a rapid response to repair is needed, since the accelerator cannot operate without a working cable system.

7.5.2 Tunnel Radio Communications (SLC Tunnel Antenna)

An active bidirectional distributed antenna system will be installed in the BSY and SLC Arcs. This system will be an enhancement and extension of a tunnel antenna system previously installed in the PEP tunnels. The purpose of the system is to permit radio communications between handheld radios in the tunnels, between these radios and the control room radios and to provide radio paging signals in the tunnels. It also provides communications for the Palo Alto Fire dispatch center while firemen are in the tunnels. Earlier tests in the PEP tunnels proved that passive antennas (antenna above-ground coupled to an antenna in the tunnel) were ineffective. The passive antenna approach worked reasonably well in BSY but is not effective in a smaller tunnel due to the smaller diameter and the "RF lossy" concrete walls.

The SLC tunnel radio system will be extended to operate from 150 MHz to 420 MHz. (The PEP system is frequency limited to 150 to 170 MHz). "In-going" signals will be collected by an above-ground antenna and carried throughout the tunnels with a "distributed twin-lead" antenna and periodic amplifiers to provide unity gain throughout the system. The "out-going" signals are collected

by a second "distributed twin lead" antenna and periodically amplified by similar amplifiers. These signals are received and detected by FM receivers which apply the audio to the base band wire line control and monitoring site radio system for distribution to control rooms, gate guards and other users. Above ground, site radio signals are collected and sent into the tunnels, as previously described, to provide half duplex communications. The expanded tunnel radio system will be an integral part of the SLC UHF radio system.

7.5.3 UHF Radio System

A new UHF radio system is being installed for SLC. The system will permit handheld radios to communicate above ground, underground (in the SLC Arcs), and from above ground to/from the Arcs. The system has two full-duplex repeater stations. One repeater will facilitate the communication within the Arcs, and between the Arcs and the ground alcove. A second repeater will permit a handheld portable radio to connect to the SLAC phone system to place calls and to accept calls either above ground or in the Arcs.

The handheld radios will have six channels, i.e., two dual-frequency channels for repeater operation as well as four simplex channels. Eight new UHF frequencies have been assigned to SLAC for this service. The repeaters, their duplexers and antennas will be installed at Pump Station 1 (adjacent to Sector 30). The repeaters will receive signals from their antennas (above ground signals) as well as from the tunnel antenna system. UHF repeater signals will be carried into the Arcs by the "In-going" tunnel antenna system.

7.6 PROTECTION SYSTEMS

7.6.1 The Personnel Protection System (PPS)

The Personnel Protection System for the SLC will be consistent with the PPS philosophy and design incorporated in the linac. It will have "access modules" at the CID injector, north and south damping rings, positron source, north and southwest adits of the arcs, and IR hall. The "access module" consists of a door and inner gate with emergency exit, keybank, access sign, intercom and TV camera.

The collider arcs will be divided into two PPS zones with a third for the final focus. Emergency shutoff buttons will be located on the walls of the IR hall and the aisle side of the arcs. Beam shutoff ion chambers (BSOIC) will be located in occupied areas outside of the shielding block of the IR hall.

The system will be monitored and controlled through the computer control system, but a hardwire "enable" signal from MCC to each zone will provide protection of control functions from other computer terminals.

The PPS will also control the tunnel lighting and paging system during the two-minute tape warning that occurs prior to beam operation.

7.6.2 Machine Protection & Beam Containment

Accelerator components are protected by the PLIC system, the Tone Interrupt system, and the "50 microsecond" permissive system, which stop the production and injection of electron beams into the accelerator, as described in the SLAC Blue Book. To provide additional protection against any accident in which the electron beam might burn its way through its shielded enclosure and threaten people, a "Beam Containment System" is provided, which, in addition to operating the Tone and Permissive Systems, also stops the production of energetic electron or positron beams by shifting the timing of klystrons so that no more than one sectors worth (1 or 2 GeV) of energy can be acquired by any beam originating from field emission or other accidental cause.

Sensors of various kinds operate the Beam Containment System. Some, such as ion chambers, detect radiation outside the normal beam path. Others consist of pairs of current-monitor toriods equipped with circuits that detect a loss of beam current between an upstream device and its downstream partner. It is planned to install five such pairs of toroid charge monitors and comparators, and to adjust the circuits to shut off any beam that has suffered charge loss which represents enough power loss to cause damage to components in an arc.

REFERENCES

1. SLC Hardware Manual, Edited by W.S. Friar. To be published.
2. SLCNET Reference Manual, SLCNET Development Group. To be published.
3. SLC Control System, Basic Users Guide, Joanne Bogart, et al. To be published.
4. Stanford 2-Mile Accelerator, R.B. Neal, editor, SLAC, 1968.

Preliminary copies of 1–3 can be obtained from the I & C Software Group.

CHAPTER 8.

SLC ALIGNMENT HANDBOOK

8.5.2 Step 2 = Prealigning the Pedestals

8.5.3 Step 3 = Smoothing the Magnets

8.6. CALIBRATION

8. ALIGNMENT DESIGN

8.1. PROBLEM AND DEMANDS

8.1.1 General

An ideal linear collider would consist of two linear accelerators pointed at each other. As SLAC has only one linear accelerator, the idea of the SLC project is to make one LINAC do the job of two. This will be done by accelerating both a positron bunch and an electron bunch, separating these two bunches at the end of the LINAC, turning them around and colliding them. To bring the two bunches to the collision point is the job of two beamlines, the arcs. These two collider arcs consist of a string of about 1000 bending magnets which will be set up in an underground tunnel.

The purpose of the alignment is to translate theoretical magnet position data into the real world.

8.1.2 Design Coordinate System

8.1.2.1 Coordinate System of TRANSPORT The three-dimensional position of the bending magnets is given by the data of the program TRANSPORT. In this program the following coordinate system is used (Fig. 8.1.1):

- the Z-axis of the right hand coordinate system lies in the vertical plane of the LINAC and points perpendicular to the vertical (direction of gravity) at the origin of the coordinates,
- the X-axis points perpendicular to the Z-axis and to the vertical,
- the Y-axis is defined by the vertical at the origin of the coordinates
- the origin of the coordinates is defined by LINAC station 100+00 ($Z = 0.0, X = 0.0, Y = 77.6425$m).

Figure 8.1.1 Coordinate System Used in TRANSPORT.

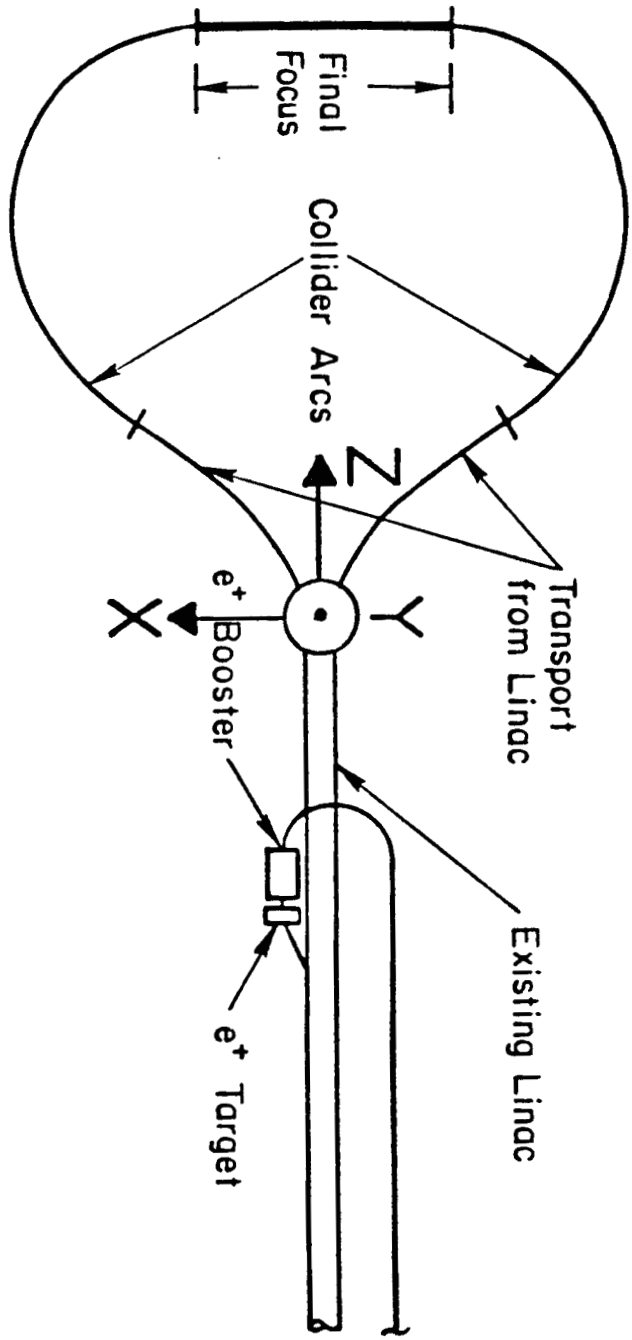

Figure 8.1.2 3 Translations: from Z_0, X_0, Y_0 to $\bar{z}_i$, $\bar{x}_i$, $\bar{y}_i$.

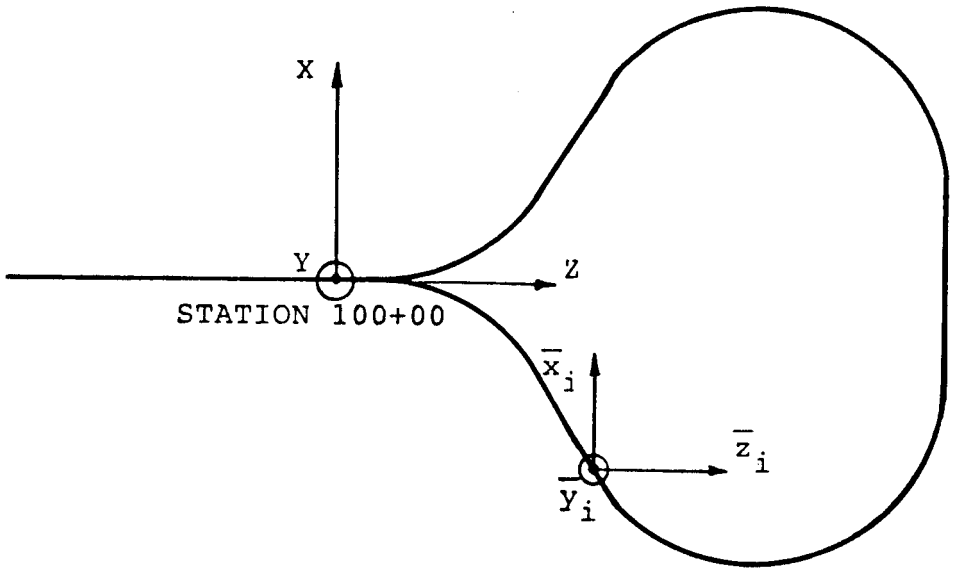

Figure 8.1.3 The $\bar{z}'_i$, $\bar{x}'_i$, $\bar{y}'_i$ coordinate system.

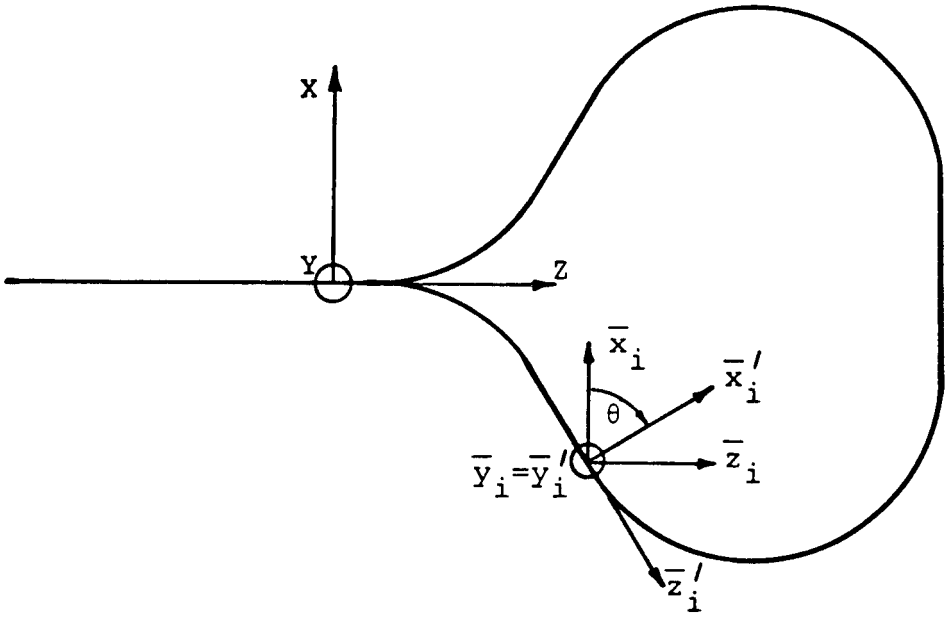

These three coordinates describe the three translations of the six degrees of freedom of a beam following coordinate system. The remaining three rotations of the six degrees of freedom are defined by the angles:

$$\theta = \text{"yaw"}$$

$$\phi = \text{"pitch"}$$

$$\psi = \text{"roll"}.$$

Figure 8.1.4 The $\bar{z}_i''$, $\bar{x}_i''$, $\bar{y}_i''$ coordinate system.

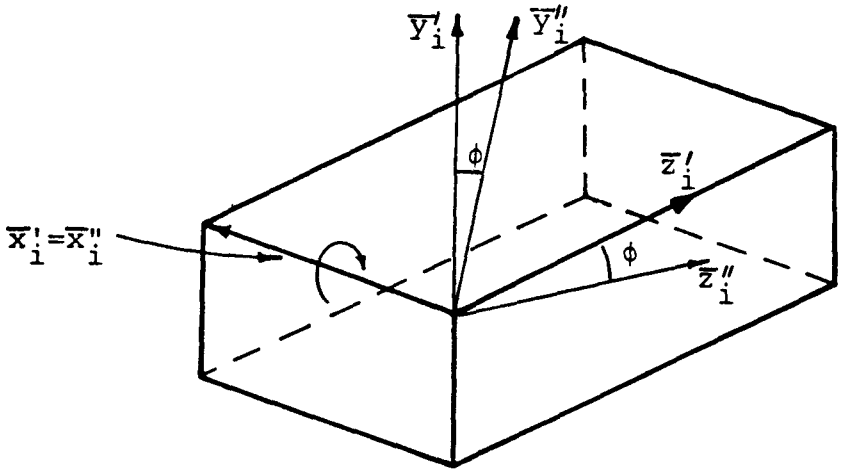

The whole transformation can be divided into the following steps:

1.–3. Three translations from Z_0, X_0, Y_0 with $Z_i - Z_0$, $X_i - X_0$, $Y_i - Y_0$ to a coordinate system $\bar{z}_i$, $\bar{x}_i$, $\bar{y}_i$, whose planes are still parallel to the origin system (Fig. 8.1.2).

4. Then the $\bar{z}_i$ and $\bar{x}_i$ axes are rotated by an angle θ (yaw) around the $\bar{y}_i$ axis to obtain a $\bar{z}_i'$, $\bar{x}_i'$, $\bar{y}_i$ ($\bar{y}_i = \bar{y}_i'$) coordinate system (Fig. 8.1.3).

5. The once rotated $\bar{z}_i'$, $\bar{x}_i'$, $\bar{y}_i'$ system is then rotated by an angle ϕ (pitch) around the $\bar{x}_i'$ axis. This results in the twice rotated system $\bar{z}_i''$, $\bar{x}_i''$, $\bar{y}_i''$ ($\bar{x}_i' = \bar{x}_i''$) (Fig. 8.1.4).

Figure 8.1.5 The $\bar{z}_i'''$, $\bar{x}_i'''$, $\bar{y}_i'''$ coordinate system.

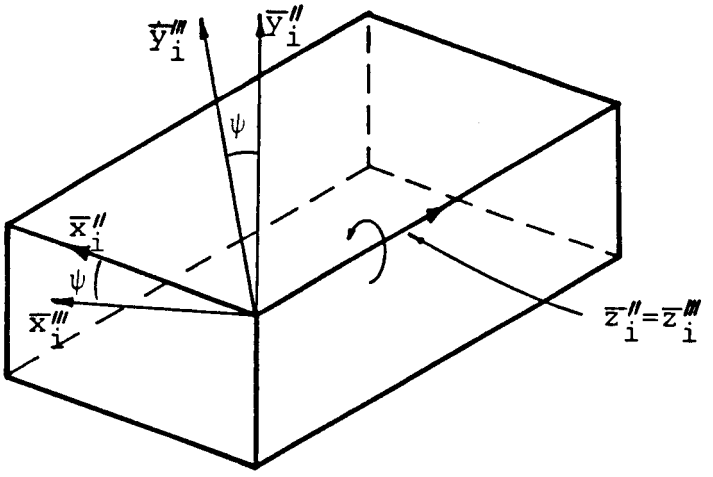

6. Finally the $\bar{z}_i''$, $\bar{x}_i''$, $\bar{y}_i''$ system is rotated by an angle ψ (roll) around the $\bar{z}_i''$ axis to obtain the desired $\bar{z}_i'''$, $\bar{x}_i'''$, $\bar{y}_i'''$ ($\bar{z}_i'' = \bar{z}_i'''$) beam-following coordinate system. For convenience, let $\bar{z}_i'''$, $\bar{x}_i'''$, $\bar{y}_i'''$ equal z_i, x_i, y_i (Fig. 8.1.5).

The signs of all rotation angles used in the alignment procedures are determined using the right-hand rule. However, this is not the case in TRANSPORT so a sign conversion between TRANSPORT angles and surveying angles must be made. The following chart explains the sign changes:

TRANSPORT	Alignment
θ rotation is positive when the z-axis turns towards the x-axis	θ rotation is positive when the z-axis turns towards the x-axis. This is the **same** as TRANSPORT.
ϕ rotation is positive when the z-axis turns towards the y-axis	ϕ rotation is positive when the y-axis turns towards the z-axis. This is the **opposite** from TRANSPORT.
ψ rotation is positive when the x-axis turns towards the y-axis	ψ rotation is positive when the x-axis turns towards the y-axis. This is the **same** as TRANSPORT.

The complete rotation matrix corresponding to the above rotations is formed

from three single rotation matrices:

$$R = R_{(\psi)} R_{(\phi)} R_{(\theta)}$$

with

$$R_{(\psi)} = \begin{pmatrix} 1 & 0 & 0 \\ 0 & \cos\psi & \sin\psi \\ 0 & -\sin\psi & \cos\psi \end{pmatrix}$$

$$R_{(\phi)} = \begin{pmatrix} \cos\phi & 0 & -\sin\phi \\ 0 & 1 & 0 \\ \sin\phi & 0 & \cos\phi \end{pmatrix}$$

$$R_{(\theta)} = \begin{pmatrix} \cos\theta & \sin\theta & 0 \\ -\sin\theta & \cos\theta & 0 \\ 0 & 0 & 1 \end{pmatrix}.$$

The product matrix is

$$R = \begin{bmatrix} \cos\phi\cos\theta & \cos\phi\sin\theta & -\sin\phi \\ \sin\psi\sin\phi\cos\theta - \cos\psi\sin\theta & \sin\psi\sin\phi\sin\theta + \cos\psi\cos\theta & \sin\psi\cos\phi \\ \cos\psi\sin\phi\cos\theta + \sin\psi\sin\theta & \cos\psi\sin\phi\sin\theta - \sin\psi\cos\theta & \cos\psi\cos\phi \end{bmatrix}.$$

The total transformation equation is as follows:

$$\begin{bmatrix} z \\ x \\ y \end{bmatrix} = [R] \begin{bmatrix} Z \\ X \\ Y \end{bmatrix}_i + \begin{bmatrix} Z_i - Z_0 \\ X_i - X_0 \\ Y_i - Y_0 \end{bmatrix}$$

$$= \underline{R}\underline{X}_i + \underline{k}_i.$$

Since R is orthogonal, i.e. $R^t = R^{-1}$, the inverse transformation can be written as follows:

$$\underline{X}_i = \underline{R}^t[\underline{x}_i - \underline{k}_i].$$

8.1.2.2 Coordinate System of an Achromat Although each magnet of all 46 achromats (see Fig. 8.1.6) has a different roll-value defined in the z_i, x_i, y_i coordinate system, in fact all magnets of an achromat are lying in a sloped plane.

Figure 8.1.6 Layout of achromats on the arcs.

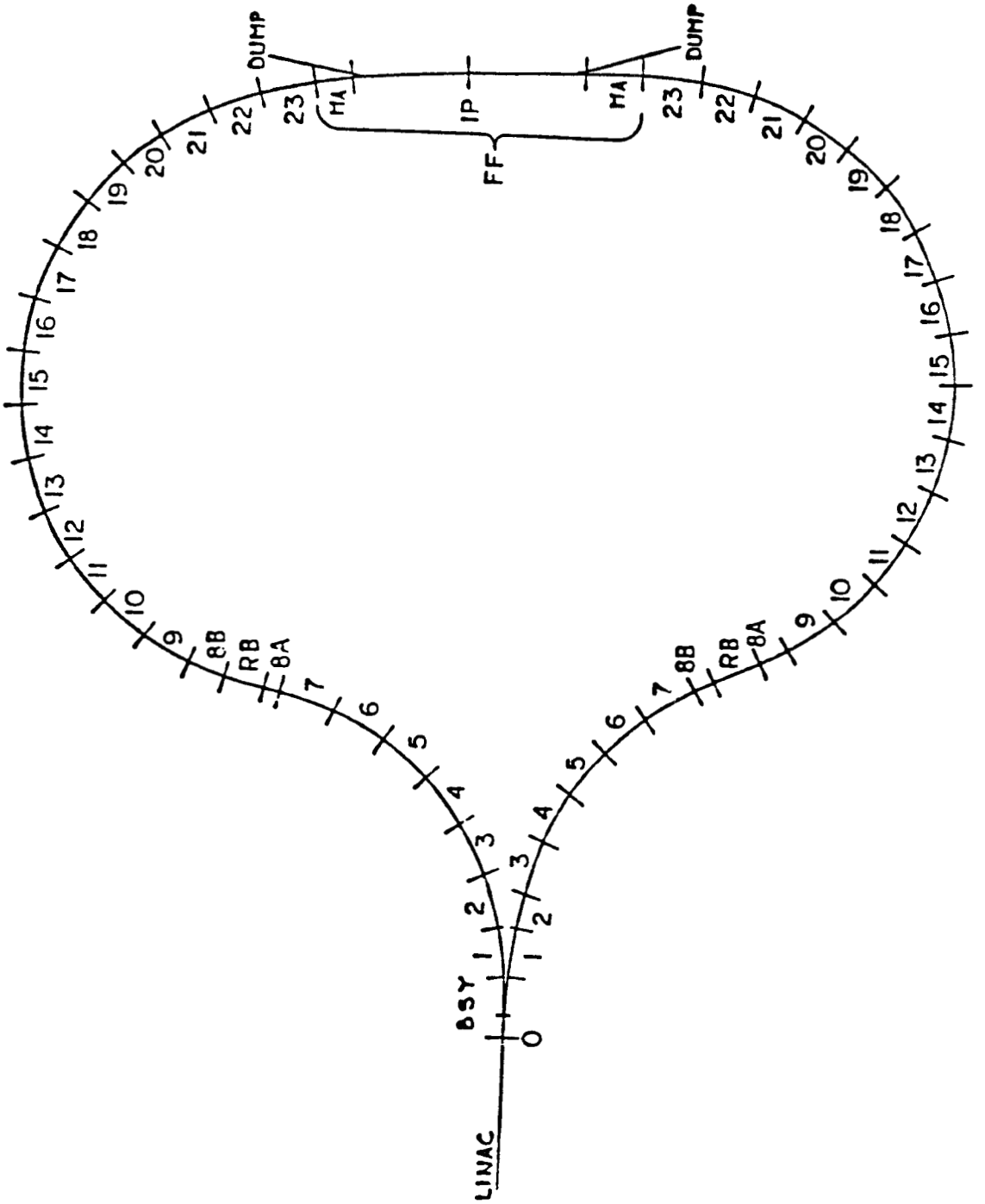

As we have to perform magnet adjustments in this sloped plane, it will be useful to define an additional coordinate system which is adapted to the geometry of an achromat. We will adopt the beam following coordinate system whose origin is the first vertex point of an achromat. The geometry and mathematics associated with this system have been explained in the previous section.

8.1.2.3 Information Taken from TRANSPORT Output Fig. 8.1.7 shows an example page of output from TRANSPORT. The first labeled columns contain coordinates in the TRANSPORT coordinate system (i.e. Z, X, Y system) of points along the beamline. The next three columns contain the values of the sequential rotation angles described above. These angles relate only to the sequentially rotated coordinate systems; i.e. the roll angle is not the roll to be measured with respect to gravity.

For the alignment, Z, X, Y coordinates of magnets and vertex points as well as the values of the sequential rotations are required to transform $(Z,\ X,\ Y)_i$ coordinates to $(z,\ x,\ y)_i$ coordinates. A seventh piece of information not found on the TRANSPORT output is a roll angle (call this Ψ') which is measured with respect to gravity. Refer to section 8.2.2.2.

Figure 8.1.7 An Example of TRANSPORT output.

X_i Y_i Z_i θ_{yaw} ϕ_{pitch} ψ_{roll}

```
*DRIFT*        3.    "DR  "    0.15289 FT
  215.958 FT                  -2.4341    253.9465   165.8262 FT       -2.007    -0.271     9.990 DEG
*BETA*        16.    "SEXD"    1.   -0.22697D-08
*BEND*         4.    "DFOC"    4.10597 FT          5.96976 KG    32824.69183    (  916.595 FT  ,   0.257 DEG )
  220.064 FT                  -2.5869    253.9255   169.9293 FT       -2.260    -0.316     9.989 DEG
*BEND*         4.    "DFOC"    4.10597 FT          5.96976 KG    32824.69183    (  916.595 FT  ,   0.257 DEG )
  224.170 FT                  -2.7579    253.9013   174.0316 FT       -2.513    -0.360     9.988 DEG
*DRIFT*        3.    "DR  "    0.15289 FT
  224.323 FT                  -2.7646    253.9003   174.1844 FT       -2.513    -0.360     9.988 DEG
*DRIFT*        3.    "DR  "    0.15289 FT
  224.475 FT                  -2.7713    253.8993   174.3371 FT       -2.513    -0.360     9.988 DEG
*BETA*        16.    "SEXF"    1.    0.13580D-08
*BEND*         4.    "FFOC"    4.10597 FT          5.96976 KG   -32823.69183    (  916.595 FT  ,   0.257 DEG )
  228.581 FT                  -2.9604    253.8719   178.4386 FT       -2.766    -0.405     9.986 DEG
*BEND*         4.    "FFOC"    4.10597 FT          5.96976 KG   -32823.69183    (  916.595 FT  ,   0.257 DEG )
  232.687 FT                  -3.1676    253.8413   182.5393 FT       -3.019    -0.449     9.984 DEG
*DRIFT*        3.    "DR  "    0.15289 FT
  232.840 FT                  -3.1756    253.8401   182.6919 FT       -3.019    -0.449     9.984 DEG
*DRIFT*        3.    "**A "    0.0     FT
  232.840 FT                  -3.1756    253.8401   182.6919 FT       -3.019    -0.449     9.984 DEG
*DRIFT*        3.    "DR  "    0.15289 FT
  232.993 FT                  -3.1837    253.8389   182.8446 FT       -3.019    -0.449     9.984 DEG
*BETA*        16.    "SEXD"    1.   -0.22697D-08
*BEND*         4.    "DFOC"    4.10597 FT          5.96976 KG    32824.69183    (  916.595 FT  ,   0.257 DEG )
  237.099 FT                  -3.4089    253.8051   186.9442 FT       -3.271    -0.494     9.982 DEG
*BEND*         4.    "DFOC"    4.10597 FT          5.96976 KG    32824.69183    (  916.595 FT  ,   0.257 DEG )
  241.205 FT                  -3.6523    253.7681   191.0428 FT       -3.524    -0.538     9.980 DEG
*DRIFT*        3.    "DR  "    0.15289 FT
  241.358 FT                  -3.6617    253.7667   191.1954 FT       -3.524    -0.538     9.980 DEG
*DRIFT*        3.    "DR  "    0.15289 FT
  241.511 FT                  -3.6710    253.7652   191.3480 FT       -3.524    -0.538     9.980 DEG
*BETA*        16.    "SEXF"    1.    0.13580D-08
*BEND*         4.    "FFOC"    4.10597 FT          5.96976 KG   -32823.69183    (  916.595 FT  ,   0.257 DEG )
  245.617 FT                  -3.9325    253.7250   195.4455 FT       -3.777    -0.583     9.977 DEG
*BEND*         4.    "FFOC"    4.10597 FT          5.96976 KG   -32823.69183    (  916.595 FT  ,   0.257 DEG )
  249.723 FT                  -4.2120    253.6817   199.5417 FT       -4.030    -0.627     9.975 DEG
*DRIFT*        3.    "DR  "    0.15289 FT
  249.876 FT                  -4.2227    253.6800   199.6942 FT       -4.030    -0.627     9.975 DEG
*DRIFT*        3.    "**A "    0.0     FT
  249.876 FT                  -4.2227    253.6800   199.6942 FT       -4.030    -0.627     9.975 DEG
*DRIFT*        3.    "DR  "    0.15289 FT
  250.029 FT                  -4.2334    253.6783   199.8467 FT       -4.030    -0.627     9.975 DEG
*BETA*        16.    "SEXD"    1.   -0.22697D-08
*BEND*         4.    "DFOC"    4.10597 FT          5.96976 KG    32824.69183    (  916.595 FT  ,   0.257 DEG )
  254.135 FT                  -4.5310    253.6318   203.9416 FT       -4.282    -0.672     9.972 DEG
*BEND*         4.    "DFOC"    4.10597 FT          5.96976 KG    32824.69183    (  916.595 FT  ,   0.257 DEG )
  258.240 FT                  -4.8466    253.5820   208.0351 FT       -4.535    -0.716     9.969 DEG
*DRIFT*        3.    "DR  "    0.15289 FT
  258.393 FT                  -4.8587    253.5801   208.1875 FT       -4.535    -0.716     9.969 DEG
```

8.1.3 Required Alignment Accuracy

8.1.3.1 Alignment Tolerances Within the Arcs The magnets' theoretical positions are calculated by the TRANSPORT program. Tentative placement accuracies are as follows:

1. The length of both arcs must be equal to their theoretical length with an accuracy of:

$$\sigma_{arc.l.} = 15mm.$$

2. The absolute accuracy of one magnet position with respect to the theoretical position in the ZX- and ZY-plane is:

$$\sigma_{theo.p.} = 5mm.$$

3. The two arcs must each point to the beamline position of the final focus in the zx- and zy-plane with an offset accuracy of:

$$\sigma_{arc.o.} = 0.2mm.$$

Figure 8.1.8 Offset of the two arcs—$\sigma_{arc.o.}$

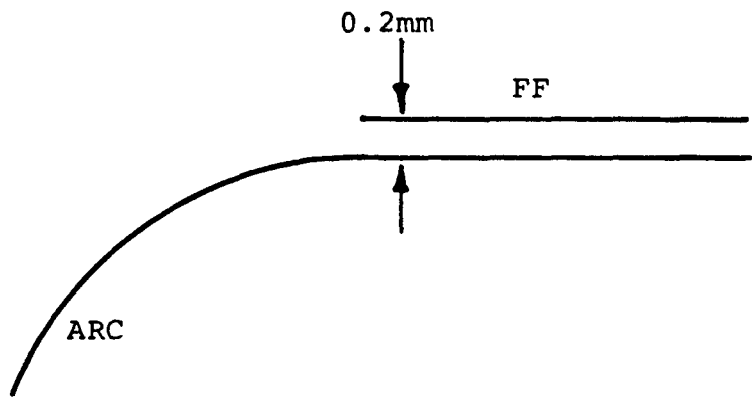

4. The direction of the last achromat of each arc must be connected to the direction of the final focus beamline in the zx- and zy-plane with an angular accuracy of:

$$\sigma_{arc.a.} = 0.05mrad.$$

Figure 8.1.9 $\sigma_{arc.a.}$

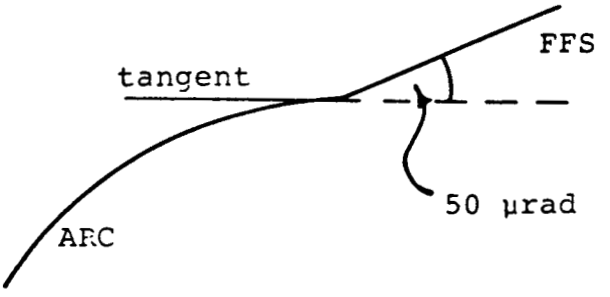

5. The distance in z-direction between the last achromat of each arc and the first of the final focus magnets must be measured with an accuracy of:

$$\sigma_{arc.ff.} = 0.5mm.$$

Figure 8.1.10 $\sigma_{arc.ff.}$

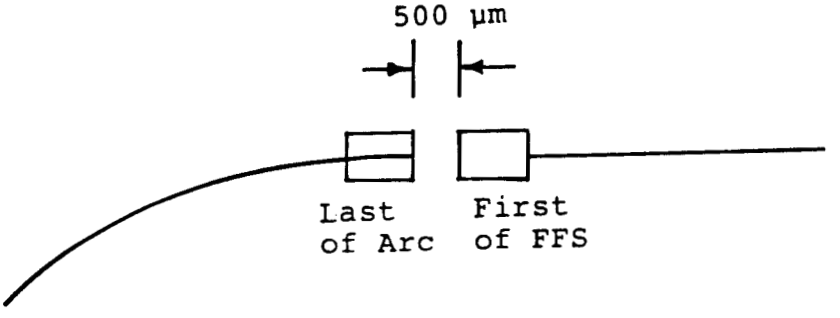

6. Two achromats must be connected to each other in the zx- and zy-plane with an angular accuracy of:

$$\sigma_{achr.a} = 0.04mrad.$$

Figure 8.1.11 $\sigma_{achr.a}$.

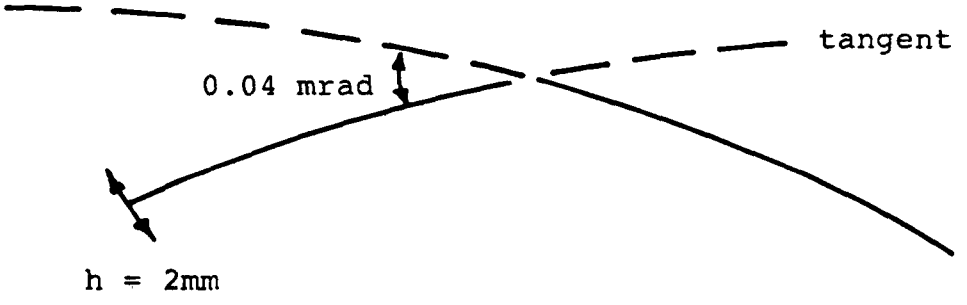

7. Two achromats must point toward each other in the zx- and zy-plane with an offset accuracy of:

$$\sigma_{achr.o.} = 0.4mm.$$

Figure 8.1.12 $\sigma_{achr.o.}$

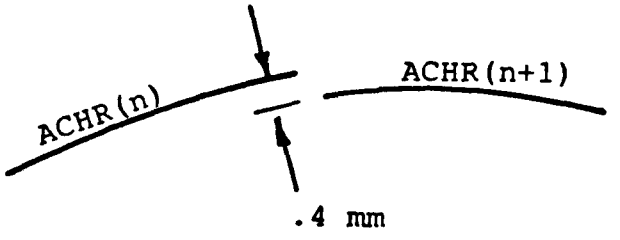

8. The distance in z-direction between the last and the first magnet of neighbouring achromats must be aligned with an accuracy of:

$$\sigma_{achr.d.} = 0.5mm.$$

Figure 8.1.13 $\sigma_{achr.d.}$

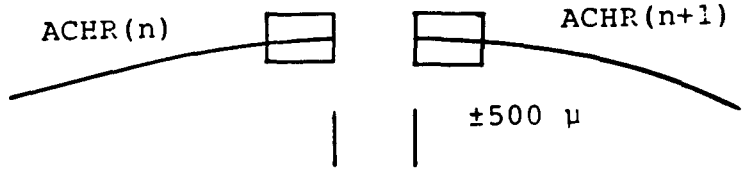

9. Within an achromat two magnets must be connected to each other in the $\overline{zx}$- and $\overline{zy}$-plane[1] with an angular accuracy of

$$\sigma_{mag.a.} = 0.04mrad.$$

Figure 8.1.14 $\sigma_{mag.a.}$

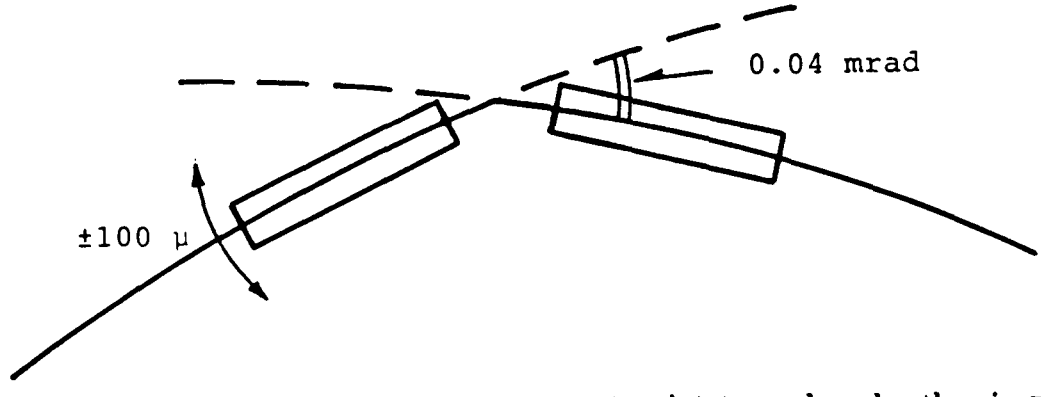

10. Within an achromat two magnets must point toward each other in $\overline{zx}$- and $\overline{zy}$-plane with an offset accuracy of

$$\sigma_{mag.o.} = 0.1mm.$$

---

[1] The $\overline{z}, \overline{x}, \overline{y}$ is a coordinate system which is defined with respect to the plane of an achromat. It is explained in section 8.1.2.2.

Figure 8.1.15 $\sigma_{mag.o.}$

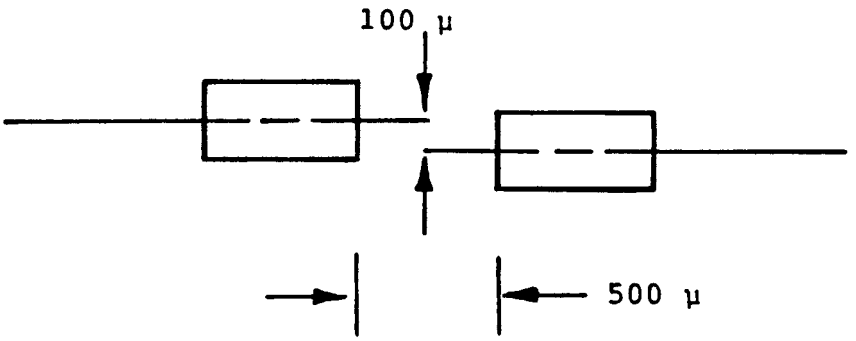

11. The distance in z-direction between two magnets within an achromat must be adjusted with an accuracy of

$$\sigma_{mag.d.} = 0.5mm.$$

12. 'Roll' must be adjusted with an accuracy of

$$\sigma_{roll} = 2.0mrad.$$

Figure 8.1.16 Accuracy of 'Roll' Adjustment

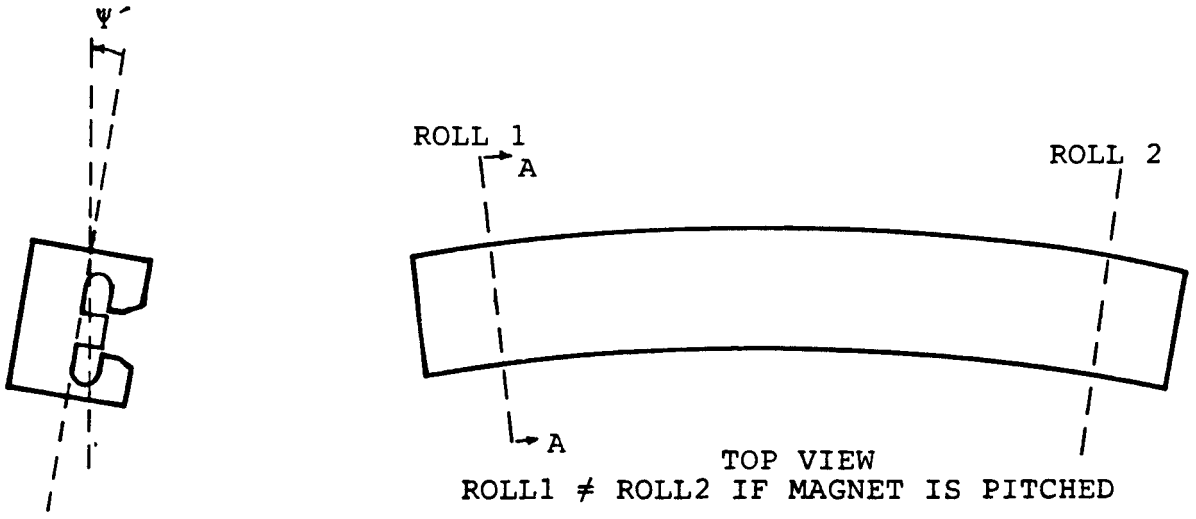

8.1.3.2 Alignment Accuracy for the Final Focus

Simulations are in progress.

8.2. GEODETIC COORDINATE SYSTEMS

All our measurements on the surface are done with respect to gravity at the location of the control points. Only in very small systems could we neglect the variation of gravity due to the curvature of the earth. Therefore we have to look for a reference system which closely describes the real world, and which can be used to transfer the measured data into the coordinate system of TRANSPORT and vice versa.

Figure 8.2.1 Gravity field of the Earth.

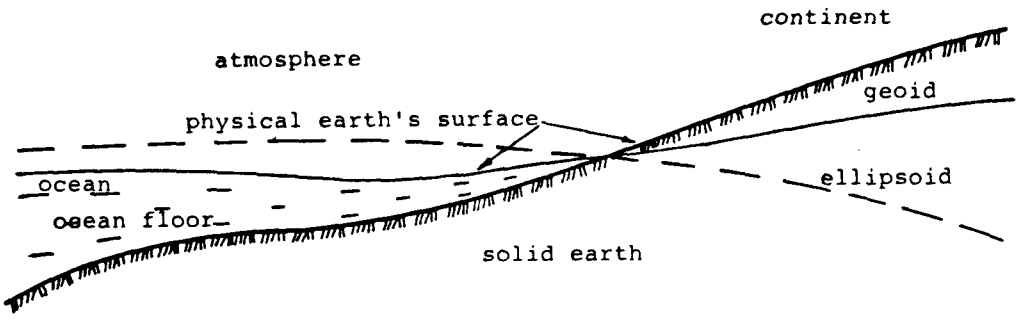

The majority of the observed parameters used in geodesy refer to the earth's gravity field. This gravity field may be described by equipotential level surfaces (Fig. 8.2.1). For computations in global geodesy, geodetic surveying reference systems with a defined metric and curvature are required. Because of its simple equation, a rotational ellipsoid flattened at the poles is well suited as a geodetic reference surface (Fig. 8.2.2).

Often the ellipsoidal normal and local gravity vectors differ. For most calculations of two-dimensional position coordinates these differences can be neglected, but for applications involving calculation of height coordinates they may become

Figure 8.2.2 The geoid compared with geodetic reference ellipsoid.

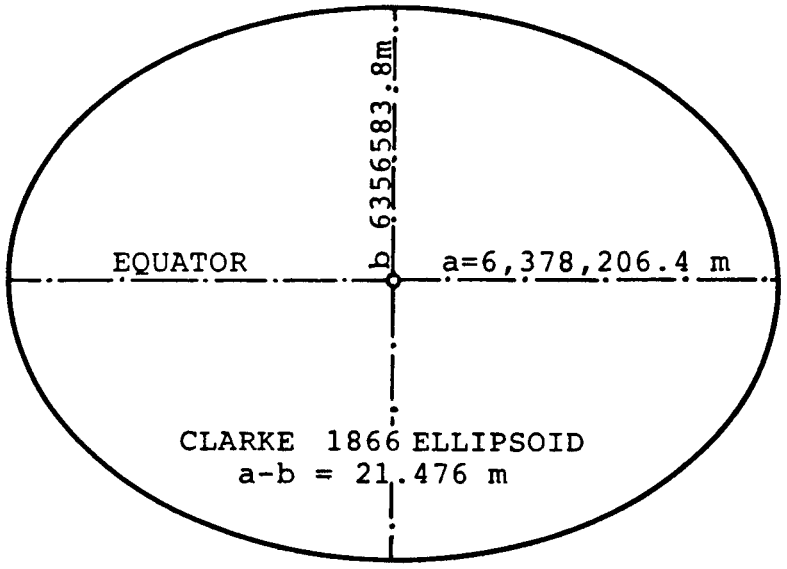

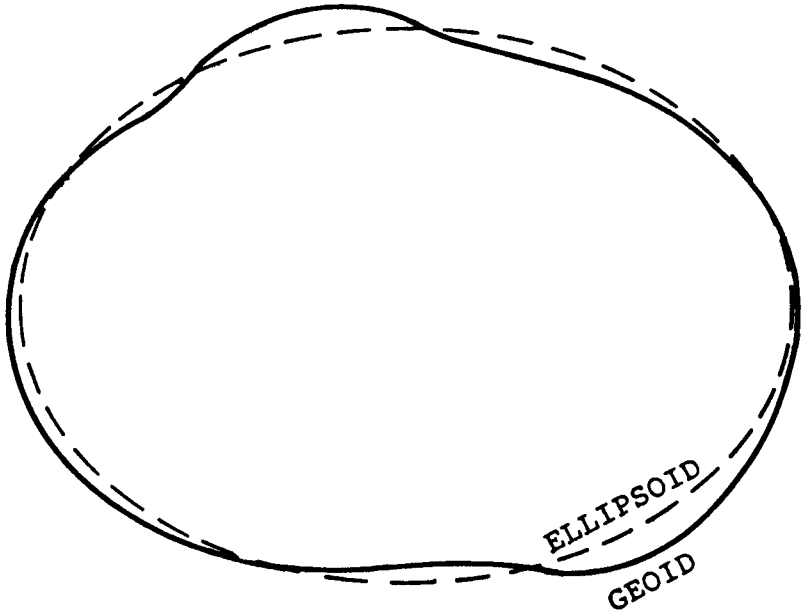

significant. Therefore, a reference surface that is determined by gravity is needed when height coordinates are to be used. This reference surface, which is determined by the uneven distribution of the earth's masses is termed the geoid. It can be described as follows:

Let us consider the water of the ocean as freely moving homogeneous matter, which is subject only to the force of the earth's gravity. Upon attaining a state of equilibrium, the surface of such an idealized ocean assumes a level surface of the gravity field; we may regard it as being extended under the continents.

Due to the earth's uneven distribution of masses we often find deviations between the physical plumb, to which the measurement refers, and the ellipsoidal normal. This means that the curvature of the geoid has discontinuities at abrupt density variations of the earth's masses. Consequently, the geoid is not a good reference system for position determinations. However, it is well suited as a reference surface for height differences which are supplied by spirit leveling in combination with gravity measurements.

8.2.1 Geodetic Height Coordinate System

8.2.1.1 Theoretical Background of Height Determination In plane surveying the height of a point with respect to the geoid is often defined as the linear distance reckoned along the curved plumb line from the geoid to the surface point. However, the direction of the gravity vector along the plumb line is changing because of an uneven distribution of masses (i.e. the equipotential level surfaces are not parallel). Therefore, the actual values of gravity are required between the geoid and the earth's surface to compute the length of the plumb line. Direct measurements of gravity values along the plumb line inside the earth are not possible, so a hypothesis regarding the mass distribution must be formed to compute a mean gravity along the plumb line from a measured value of gravity on the surface.

Figure 8.2.3 Determining differences in height.

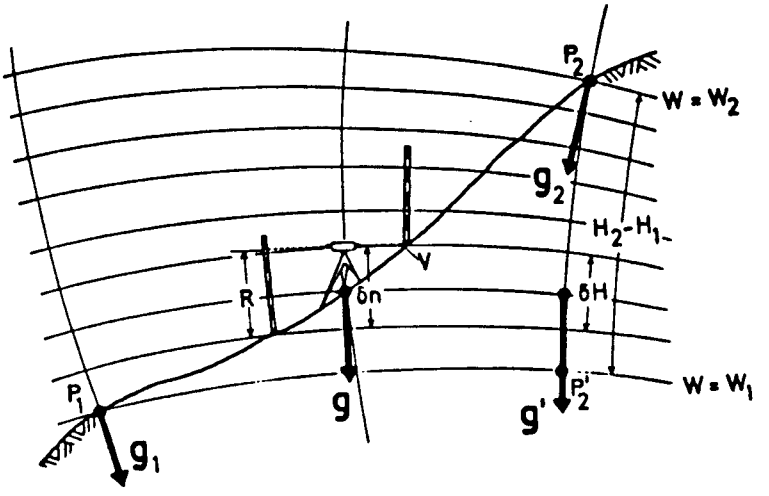

In geometric leveling on the surface of the earth, the differences in height are determined using horizontal lines of sight between points in close proximity to each other (Fig. 8.2.3). The leveled height differences, δn, between the rod stations is given by the difference between the backsight R and the foresight V readings. Because of the quasi-differential distance between the rod stations, the convergence of the equipotential surfaces may be neglected, as well as the change in curvature of the equipotential surfaces that pass through the telescope. Then, δn corresponds to the separation of the equipotential surfaces that pass through the rod stations. The leveled height difference between points P_1 and P_2 is yielded by summing the observed δn's:

$$\Delta n_{1,2} = \sum_{1}^{2} \delta n.$$

The difference in theoretical heights is calculated as the length difference of the plumb lines between the geoid and the earth's surface at the control points P_1 and P_2. Since the equipotential surfaces are not parallel, Δn depends on the path taken and the result of leveling does not correspond to a difference in theoretical

heights. This means that a definite determination of height is possible only by considering gravity.

The non-parallelism of equipotential surfaces can be seen by leveling a closed circuit. The sum of the leveled height differences, in addition to the measuring errors, consists of the path dependent orthometric excess ϵ:

$$\oint \delta n = \epsilon.$$

The orthometric excess ϵ would vanish if the geopotential numbers, c, could be calculated.

$$c = g\,\delta n.$$

In order to do this, gravity observations along the leveling lines must be made.

Gravity measurements at SLAC during LINAC construction revealed no significant gravity anomalies. Due to this fact and the small size of the SLC site, errors due to orthometric excess become negligible.

8.2.2 Geodetic Elevation Coordinate System

In geometric leveling we determine height differences with respect to local gravity, whereas TRANSPORT (see section 8.1.2.1) defines the elevation of each point with respect to the direction of gravity at the origin of the TRANSPORT coordinate system. This means that TRANSPORT defines elevations relative to a plane, while geodetic leveling defines elevation with respect to a curved surface. To convert from one system to the other, a mathematical model must be determined for each system.

Assuming a homogeneous distribution of masses in the earth, it is possible to approximate the geoid by a reference system with a defined metric and curvature, normally an ellipsoid. In our case, the geoid can be locally approximated by the Gaussian sphere, which has the same tangent plane as the ellipsoid at the origin

of the TRANSPORT coordinate system. Its radius is defined by $r = \sqrt{MN}$, with M being the meridian radius curvature and N the radius of curvature in the prime vertical. For more details see section 8.2.3.1.

To get an estimate of the elevation difference between the Gaussian sphere (often referred to as the best osculating sphere) and the ellipsoid at the latitude of the SLC (37.5 deg), the following calculations, based on Clark's ellipsoid, are made. Assuming that the arc length from point Z (Fig. 8.2.4), where ellipsoid and sphere have the same tangent plane, to an arbitrary point P are nearly the same on ellipsoid and sphere, the elevation difference d between the two reference systems can be approximately calculated by:

$$d \approx \frac{1}{2}(K_1 - K_2)l^2$$

d =difference between the reference systems

l =arc length from Z to P

K =curvature of the arcs.

Figure 8.2.4 Divergence of Gaussian sphere and ellipsoid.

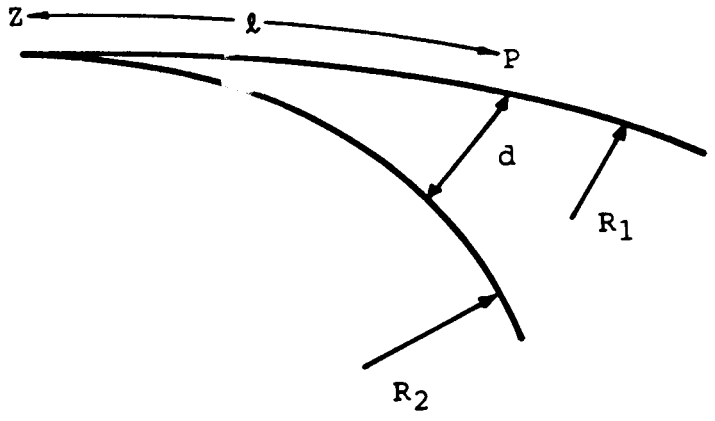

With $K_1 = \frac{1}{\sqrt{MN}}$ and $K_2 = \frac{\cos^2 A}{M} + \frac{\sin^2 A}{N}$ the following table results.

Figure 8.2.5 Gaussian Sphere vs. Ellipsoid.

A(deg)	l(m)	d(mm)
0	500	−0.04
45	500	0
90	500	+0.04
0	1000	−0.2
45	1000	0
90	1000	+0.2

As can be seen, the differences between the two reference systems are negligible.

8.2.2.1 Transformation between geodetic and TRANSPORT elevations

As seen from figure 8.2.6 the gravity vector varies depending on the central angle γ. Taking this into account, the following reduction formula to transform measured elevations above the sphere to those above the plane defined by TRANSPORT are valid.

$$
\begin{aligned}
(r + h_s)^2 + s^2 &= (r + h_n)^2 \\
(r + h_s) &= \pm\sqrt{(r + h_n)^2 - s^2} \\
h_s &= \pm\sqrt{(r + h_n)^2 - s^2} - r \\
\Delta e &= h_n - h_s
\end{aligned}
$$

with $r = \sqrt{MN}$ for the osculating sphere, or for computations on the ellipsoid

$$\frac{1}{r} = \frac{\cos^2 A}{M} + \frac{\sin^2 A}{N}.$$

Assuming $s = 1$ km and $h_n = 100$ m, then $h_s = 99.921$ m. Due to this fact we obtain an elevation difference Δe between plane and sphere of 0.079 m, which must be taken into account.

8.2.2.2 Corrections of Measured Tilts As explained in section 8.1.2.3, the tilt angle 'roll' must be set with respect to gravity at the origin of the coordinate

Figure 8.2.6 The curvature correction.

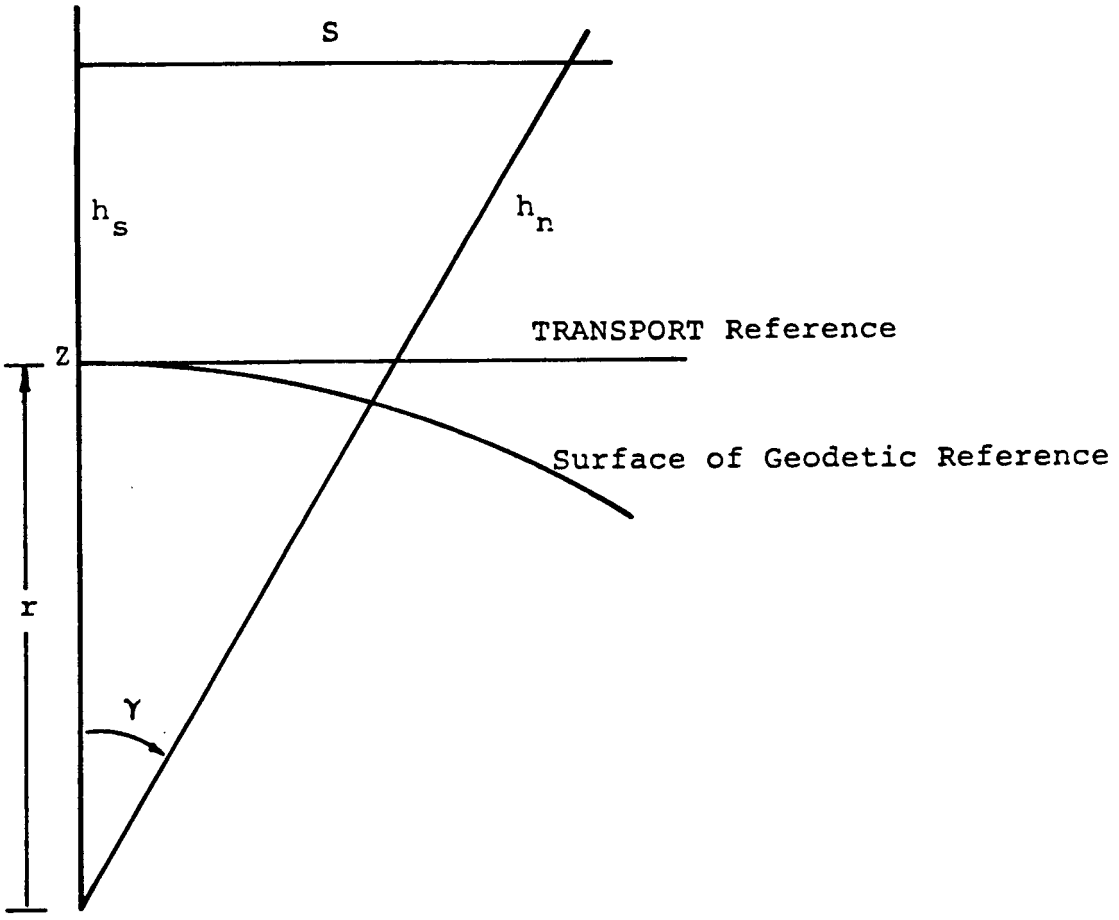

system. Since the inclinometer measures with respect to local gravity, we must examine whether the differences in the direction of gravity due to the curvature of the ellipsoid are significant or not.

With an approximation of the geoid as a sphere, the following formula to correct 'roll' measurements can be found:

$$\varphi = \frac{s}{r} \cdot \cos\alpha.$$

The mathematical context is shown in Figs. 8.2.7, 8.2.8, 8.2.9. In the worst case the following correction values are obtained (Fig. 8.2.10):

Figure 8.2.7 Correcting for 'Roll'—Top view.

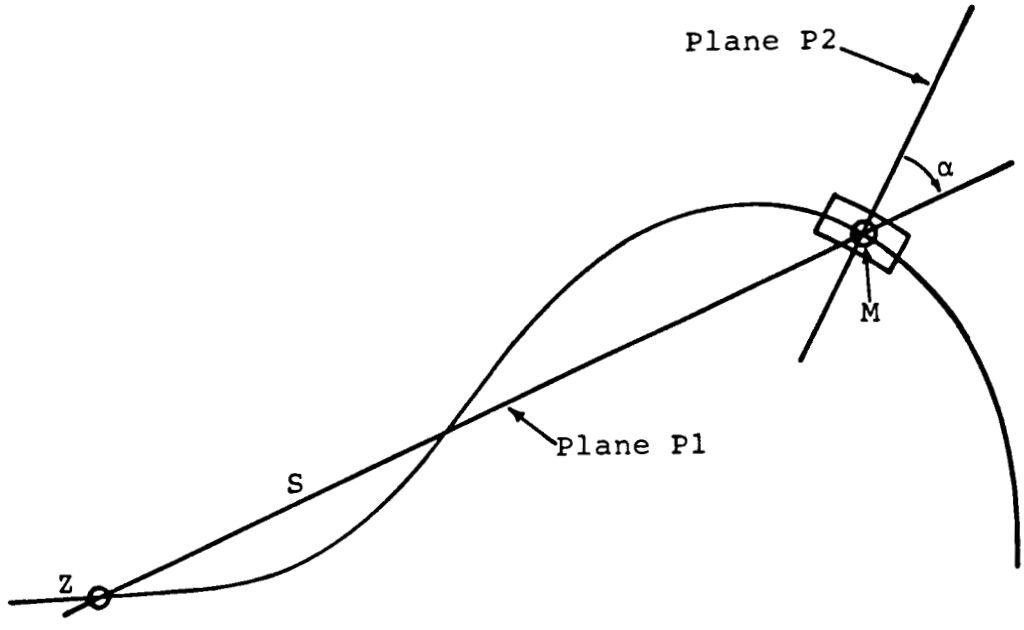

with:

Z =origin of TRANSPORT coordinate system

S =distance $\overline{ZM}$

$P1$ =vertical plane through Z and M

$P2$ =vertical plane through M in which roll is measured

Figure 8.2.8 Correcting for 'Roll'—Side view.

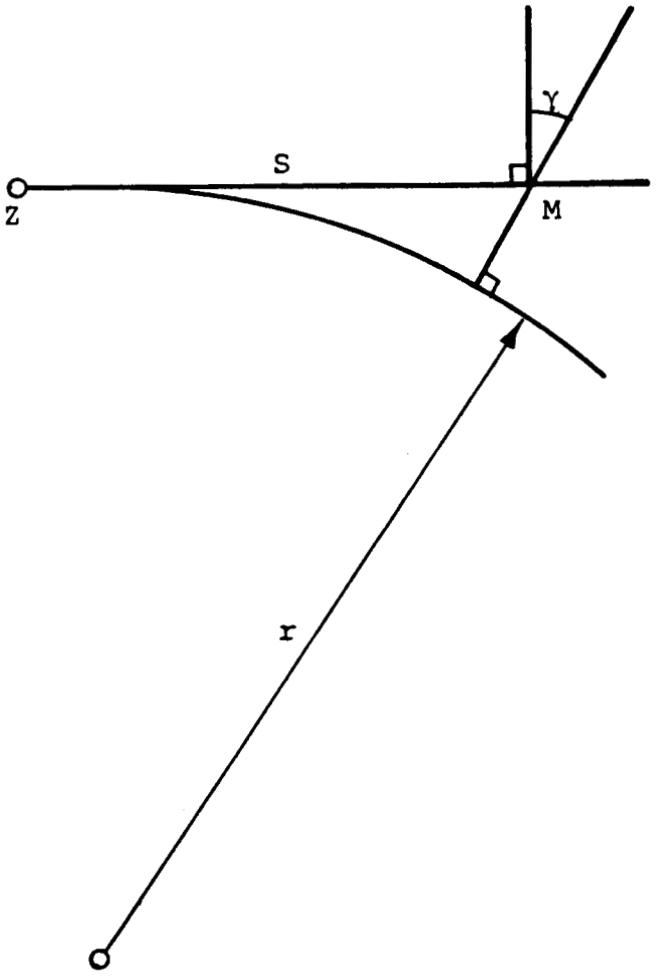

$$\sin\gamma = \frac{s}{r}$$

with:

r =radius of the best osculating sphere.

Computed and described in section 2.2.1

As γ is a small angle,

we can write:

$$\gamma = \frac{s}{r}$$

Figure 8.2.9 Correcting for 'Roll'—Deviation from Gravity.

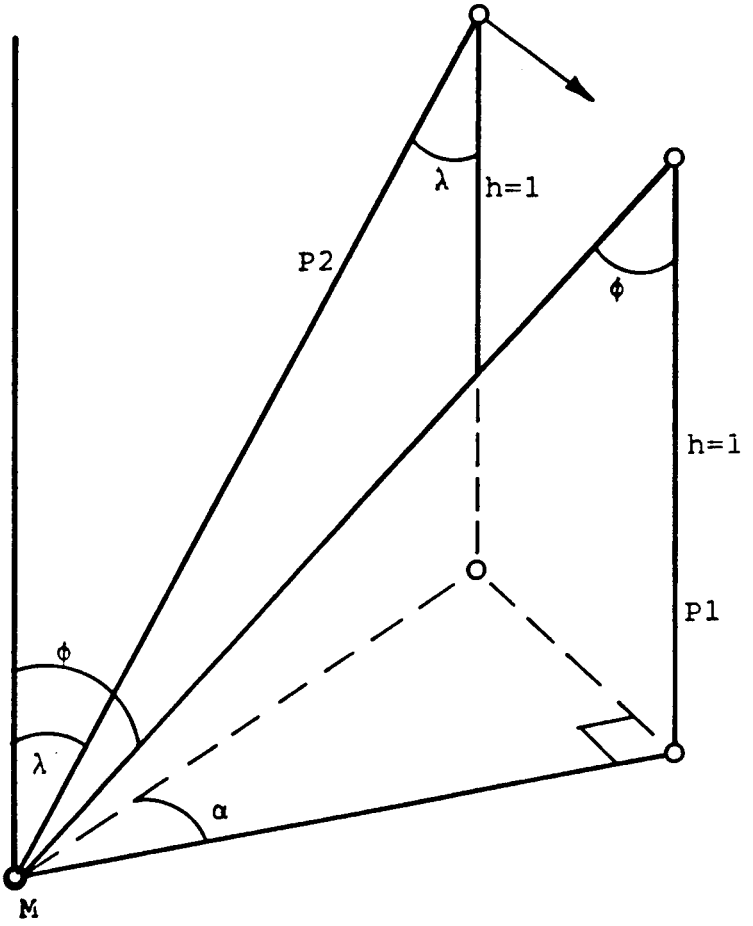

The projection of the deviation of gravity in plane $P1$ into plane $P2$

$$\tan \phi = \tan \gamma \cdot \cos \alpha$$

As ϕ and γ are very small angles we can also write

$$\phi = \gamma \cdot \cos \alpha$$

Evaluating γ we obtain

$$\phi = \frac{s}{r} \cdot \cos \alpha$$

Figure 8.2.10 Correction Values

s [m]	α [degree]	$\Delta\psi$ [mrad]
0.0	0	0
500.0	0	0.08
500.0	90	0
1000.0	0	0.16
1000.0	90	0

In comparison with the required accuracy, one sees that the value of this correction is not significant with respect to the accuracy of 'roll.' A similar correction would be applied to the 'pitch,' but since this tilt will be set by leveling techniques no correction is necessary.

8.2.2.3 Summary: Height Coordinate System

- We assume that gravity anomalies are insignificant.
- The height reference system in which the adjustment is performed is the Gaussian sphere.
- To translate these heights into the TRANSPORT height coordinate system and vice versa we have to compute correction values Δe_i.
- Correction values for 'roll' are not significant and are consequently neglected.

8.2.3 Position Coordinate System

8.2.3.1 Theoretical Background As described above, the geoid is not a mathematical reference system with defined metric and curvature. However, the earth's surface may be closely approximated by a rotational ellipsoid with flattened poles.

The rotational ellipsoid is created by rotating the meridian ellipse about its minor axis. The shape of the ellipse is thereby described by two geometric parameters: the semimajor axis a and the semiminor axis b (Fig. 8.2.11).

Figure 8.2.11 The rotational ellipsoid.

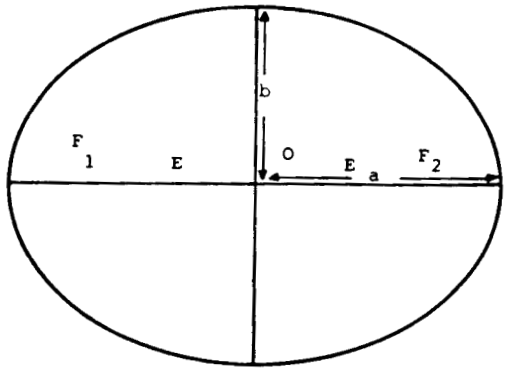

Figure 8.2.12 A spatial Cartesian coordinate system.

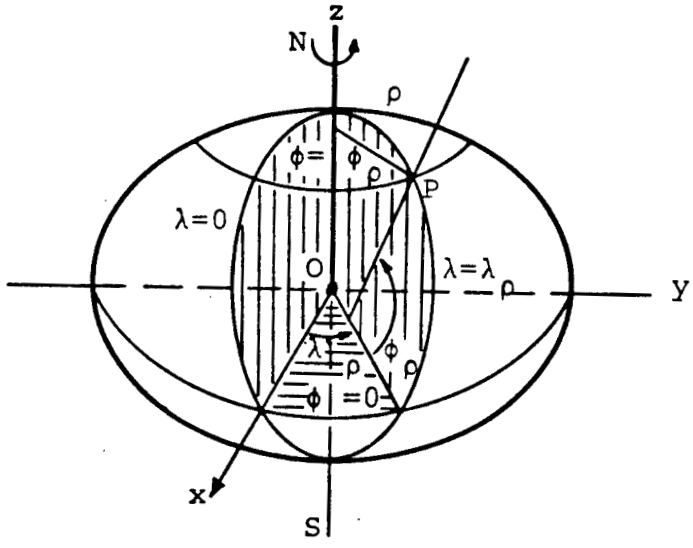

Often a system of spatial X, Y, Z Cartesian coordinates is used (Fig. 8.2.12). The origin of the system is situated at the center O of the figure, the Z-axis coinciding with the minor axis of the ellipsoid. The equation of the surface of the ellipsoid is then given by

$$\frac{X^2+Y^2}{a^2}+\frac{Z^2}{b^2}=1.$$

The system of ellipsoidal geographic coordinates is defined by the geographic latitude φ and the geographic longitude λ. φ is the angle measured in the

meridian plane between the equatorial plane of the ellipsoid and the surface normal at P. λ is the angle measured in the equatorial plane between the zero meridian and the meridian of P (Fig. 8.2.12).

Figure 8.2.13 The principal radii of curvature.

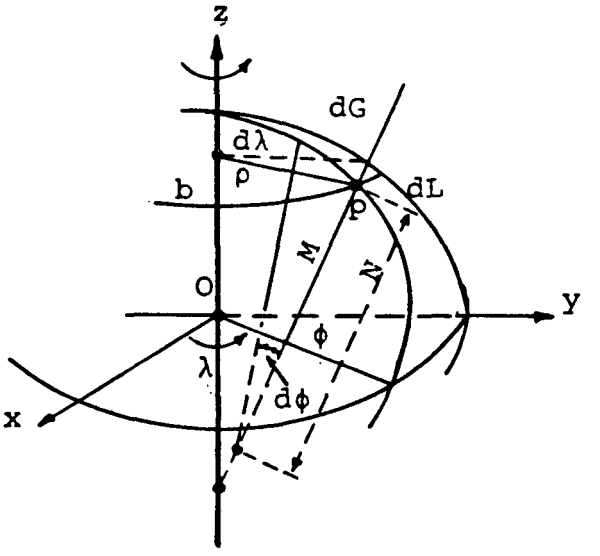

The meridians and parallels are the lines of curvature of the rotational ellipsoid. The principal radii of curvature are therefore in the plane of the meridian (meridian radius curvature M) and in the plane of the prime vertical, perpendicular to the meridian plane (radius of curvature in the prime vertical N), see Fig. 8.2.13.[3] The following formulas show the relationship between the ellipsoid parameters a and b and the radii of curvature M and N.

$$M = \frac{C}{V^3}$$

$$N = \frac{C}{V}$$

$$V = \sqrt{1 + e'^2 \cos^2 \varphi_0}, \qquad \varphi_0 = \text{latitude of origin of coordinates}$$

$$C = a\sqrt{1 + e'^2}$$

$$e'^2 = \frac{a^2 - b^2}{b^2}$$

[3] Wolfgang Torge, GEODESY, New York, 1980, S.145

The curvature of an arbitrary normal section at an azimuth A is computed according to Euler's formula by

$$\frac{1}{r} = \frac{\cos^2 A}{M} + \frac{\sin^2 A}{N}.$$

Here, r is the radius of curvature of the normal section. The geodetic azimuth A is defined as the angle measured in the horizontal plane between the ellipsoidal meridian plane of P_0 and the vertical plane determined by the normal to P_0 and by the point P_i; A is reckoned from the north in the clockwise direction. For our purposes we can neglect differences in the direction of north (between 'geographic north' and 'grid north'='convergence of meridians') and we will compute A by use of our coordinates:

$$A = \tan^{-1}\left(\frac{Y_i - Y_0}{X_i - X_0}\right).$$

For our purpose the CLARK's ellipsoid of 1866 is used to obtain the best osculating sphere at the origin of TRANSPORT. Clark's ellipsoid is defined by the following parameters:

$$a\,(\text{semimajor axis}) = 6,378,206.4m$$
$$b\,(\text{semiminor axis}) = 6,356,583.8m.$$

For the latitude of 37.5° the following is valid:

$$e'^2 = 0.006815$$
$$C = 6,399,902.552$$
$$V = 1.002147$$
$$N = 6,386,190.603$$
$$M = 6,358,854.777.$$

The radius of the best osculating sphere is

$$R = 6,372,508.033.$$

8.2.3.2 Adjustment Reference Shapes Generally the adjustment of a position net would be done on an ellipsoid or best osculating sphere depending on the size of the net. Therefore it is necessary to reduce the terrestrial measurements, distances, and directions to this reference shape. After adjustment, coordinates can be easily transformed to a plane, such as that defined by TRANSPORT. All further computations, e.g. deformation analysis, can be done in the plane, where the mathematical relationships are much easier. In our case, in addition to the terrestrial measurements, space system data from the global positioning system (GPS) is available. GPS derived coordinates are three-dimensional coordinates related to a specific point in our net.

In a three-dimensional adjustment, space system data and terrestrial data can be adjusted in one step, without reducing the original measurements to the reference surface. In this case the distance measurements must only be corrected for meteorological and calibration conditions.

8.2.3.3 Reduction of Distances

8.2.3.3.1 Meteorological Corrections. Every distance measured with an EDM can be expressed as:

$$D = K_0 + U\overline{D}$$

D =corrected distance

$\overline{D}$ =measured distance

K_0 =offset correction

U =scale factor

Ideally K_0 should be zero and U be one, but due to the actual atmospheric conditions and the actual modulation frequency, these values are slightly changed. Therefore the measured distance must be corrected. The meteorologically corrected distance is:

$$D_1 = \overline{D} + (N_0 - N) \times 10^{-6}\overline{D}$$

N =actual refractive index of air

N_0 =internal refractive number of the instrument depending on the actual modulation frequency

8.2.3.3.2 Calibration Correction. Every EDM in connection with a reflector has an offset and a cyclic error. The distance D_1 has to be corrected for these systematic errors.

$$D_2 = D_1 + A + Z$$

A =offset error dependent on the distance

Z =cyclic error dependent on the distance

8.2.3.3.3 Geometric Corrections. Having done the previous corrections, the distance must be reduced to compensate for:

1. The bending of the beam from the instrument to the target due to temperature gradients.
2. The tilt and elevation above the reference surface.
3. The curvature of the earth, in this case approximated by the Gaussian sphere.

Figure 8.2.14 Reduction of distances

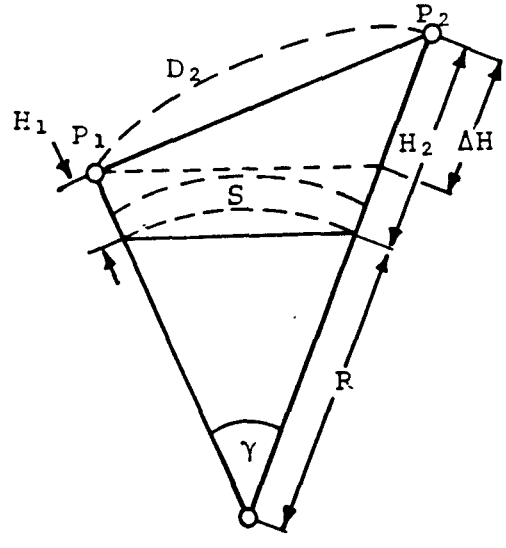

Referring to the above statements, the distance reduced to the reference surface is:

$$S = D_2 + K_1 + K_2 + K_3$$

with:

$$K_1 = (1-K)^2 \cdot \frac{D_2^3}{24R^2}$$

R =radius of the Gaussian sphere

K =coefficient of refraction

$$K_2 + K_3 = D_2 \left(\sqrt{\frac{1 - \left(\frac{\Delta H}{D_2}\right)^2}{\left(1 + \frac{H_1}{R}\right)\left(1 + \frac{H_2}{R}\right)}} \right)$$

K_1 must be taken into account only if there are distances greater than 10 km. Otherwise it is negligible.

8.2.3.4 Reduction of Angles The theodolite angles are measured around the vertical. At every station the theodolite is leveled with respect to the gravity vector, which is different in direction from station to station. Since we will make the adjustment in the plane of the ZX coordinates, we have to reduce the angles with respect to the direction of gravity at the origin of the coordinate system. The treatment, therefore, is the same as for the effect of dislevelment of the theodolite. The formula is given by

$$\Delta\alpha = \Delta g \tan\beta \sin\Delta A$$

with

Δg = variation in the direction of gravity

β = vertical angle

A = azimuth of variation of gravity

An estimation shows that for our purpose $\Delta\alpha$ can reach about 20". Therefore in our calculations it must be taken into consideration.

8.2.3.5 Summary: Position Coordinate System

- position coordinate system is the ZX-plane of TRANSPORT
- reference shape for the measurements is the CLARK ellipsoid 1866
- the measured distances must be reduced by several corrections to be transferred into the plane coordinate system
- the measured angles must also be reduced.

8.3. DATA HANDLING

The huge amount of data which must be collected to obtain the high accuracy for the beam line necessitates the use of an "electronic field book." Once the data is entered, it can be used by other computers and programs to calculate results quickly. The electronic fieldbook also allows field checks for error detection. If a check fails, the specific observation may be repeated.

For our project the Epson HX, a small hand-held computer, will be the electronic fieldbook. Field data will be passed to an IBM PC for correction and storage. Finally, adjustment will be performed on a mainframe with the capacity to handle the many unknowns.

Figures 8.3.1 and 8.3.2, at the end of this section, show the entire procedure—from collecting the data to the final storage—for both the elevation net and position net.

8.3.1 Error Calculations

8.3.1.1 Error Propagation Before observation begins, it is important to estimate the errors at specific points. The size of these errors is highly dependent on the net configuration, which itself is dependent on the topography, the number and kind of measurements, and the accuracy of the instruments used. To obtain estimates of these errors, special error propagation programs are used. The accuracy of the instruments is limited and the net configuration is fixed, so that only the number and kind of measurements (often referred to as the observation plan) can be varied to obtain smaller error ellipses.

HOEHE 2 is the program for error propagation in a free elevation net. A free elevation net contains no benchmarks at a specific elevation.

NETZ 22A is the program for error propagation in a free position net. A free position net constrains no points to fixed coordinate values. It processes distances, directions, gyro and offset measurements and calculates:

- expected free position errors
- confidence interval for the reference variance and 95% confidence level factor
- expected absolute and relative error ellipses
- expected *a posteriori* distance, direction, gyro and offset errors
- output file for program NETZ 24 containing the variance-covariance matrix for the tunnel connection points.

NETZ 24 is used for error propagation in a connected subnet. It processes the same measurements as NETZ 22A and needs the output file of NETZ 22A to calculate:

- confidence interval for the reference variance and 95% confidence level factor
- expected absolute and relative error ellipses
- expected distance, direction, gyro and offset errors for a subnet position.

8.3.1.2 Adjustment of the Elevation Net Systematic, random, and gross errors exist in every measurement procedure. The concept of adjustment is based on the assumption that the observational errors are random only. Therefore, systematic and gross errors must be removed before adjustment to avoid biased estimates. Gross errors are eliminated by employing proper instrument techniques and data checks. Systematic effects, such as thermal expansion of graduated metal scales, must be computed and corrections applied. The systematic errors affecting all leveling observations are listed in section 8.4.3.2.1.

HOEHE 11 the level net adjustment program, allows constrained and unconstrained adjustment. In an unconstrained adjustment, only one elevation point is fixed, while in the other case two or more points are fixed. It also reduces elevations to the height coordinate system described in section 8.2.2.1. Two output files are created, one for later use with a data management program, the other for deformation analysis with HOEHE 3.

8.3.1.3 Adjustment of the Position Net For the reasons described in section 8.2.3.3 and 8.2.3.4 the original observations must be corrected for systematic and gross errors. To test the observations for gross errors, program CHECK is used. Different units such as feet or meters can be accommodated by CHECK. An output is created for later use in NETZ 11, the position net adjustment program. Constrained and unconstrained adjustment is possible. Constrained means two or more points of the network are fixed, while unconstrained means one point and one direction are fixed. With these constraints the orientation and scale of the net will be fixed, otherwise a free net as described in NETZ 22A would exist.

NETZ 11 processes distances, directions, gyro and offset measurements. It creates output files for later use in a data management program and NETZ 3, a program for deformation analysis. To use NETZ 3 for a deformation analysis between two position nets, the two nets must consist of identical points, although the observation programs need not be the same. The other output contains information about the adjusted coordinates and observations, the associated r.m.s. errors and the parameters for the error ellipses of each point of the net.

The output file created by CHECK can also be used by program NETZ 44, which calculates an adjustment of a free position net using the actual observations. It calculates the adjusted "free" coordinates and their error ellipses. Another program, NETZ 55, is a special version of NETZ 44. It uses only 1/6 as much core memory as NETZ 44, but requires more computation time.

8.3.2 Adjustment of a Three-Dimensional Net

To adjust terrestrial measurements and the space systems data we get from GPS, it is necessary to use new methods and programs. As can be seen from the previous sections, the elevation and position nets are strictly separate. Historically, these nets have always been separate, even in the adjustment phase. Today, in many cases, the measuring procedures are still separate, but the adjustment can be done in one step. To do this, program CHECK 3 is used first and then NETZ 13. CHECK 3 tests the observations for gross errors and creates an output file used in NETZ 13, a program which performs the three-dimensional adjustment of a constrained net. This program processes horizontal and vertical data and computes three-dimensional coordinates with corresponding error ellipsoids.

Using GPS it is now possible to make all observations for a three-dimensional net in one step. With this system it is possible to get three-dimensional coordinates of every point on any selected reference ellipsoid. Each position is determined independently, so that there is no error accumulation from point to point as in a traverse.

Figure 8.3.3 is a schedule of the adjustment procedure, showing each program and its special purpose.

Figure 8.3.1 Schedule 1.

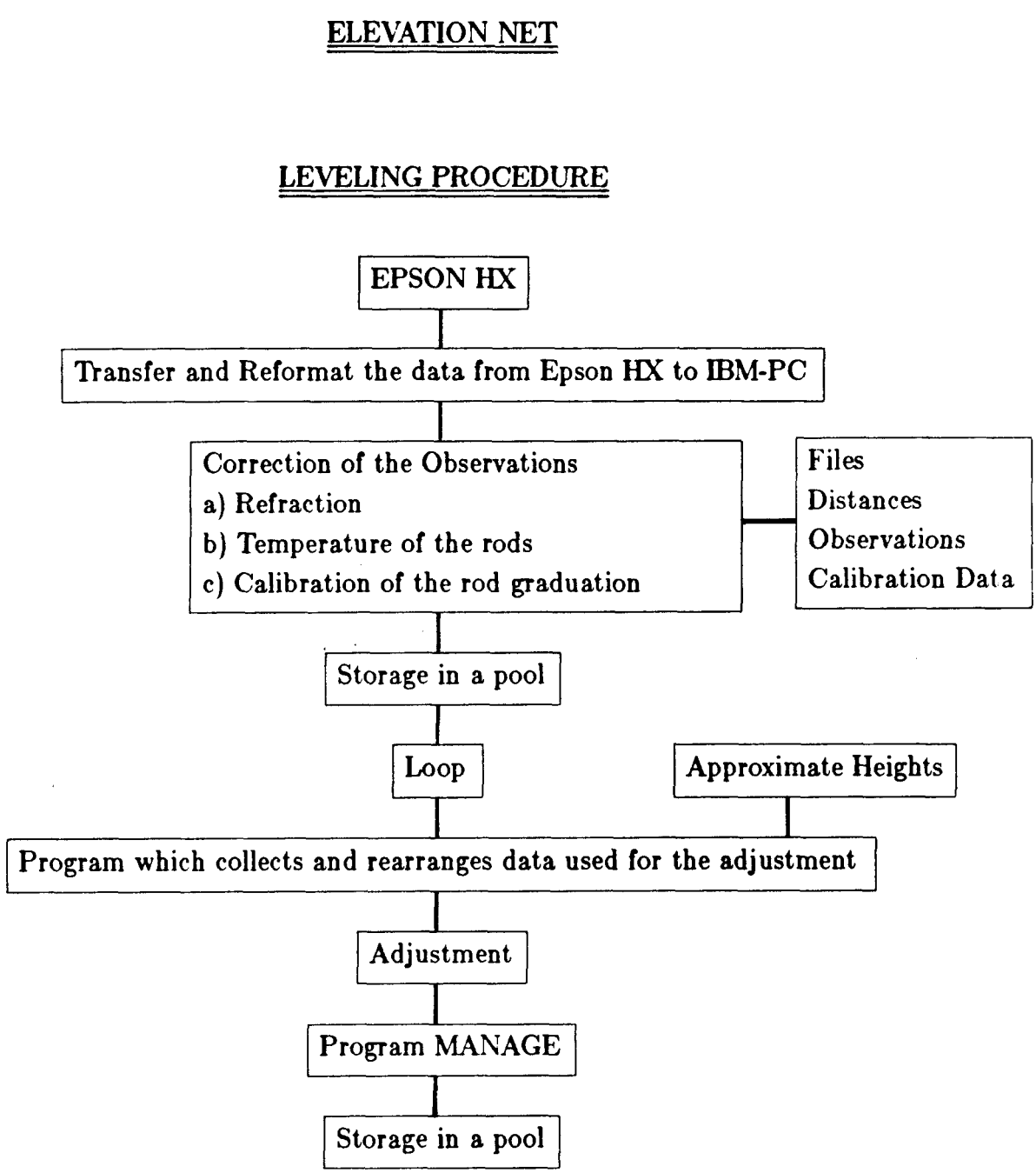

Figure 8.3.2 Schedule 2.

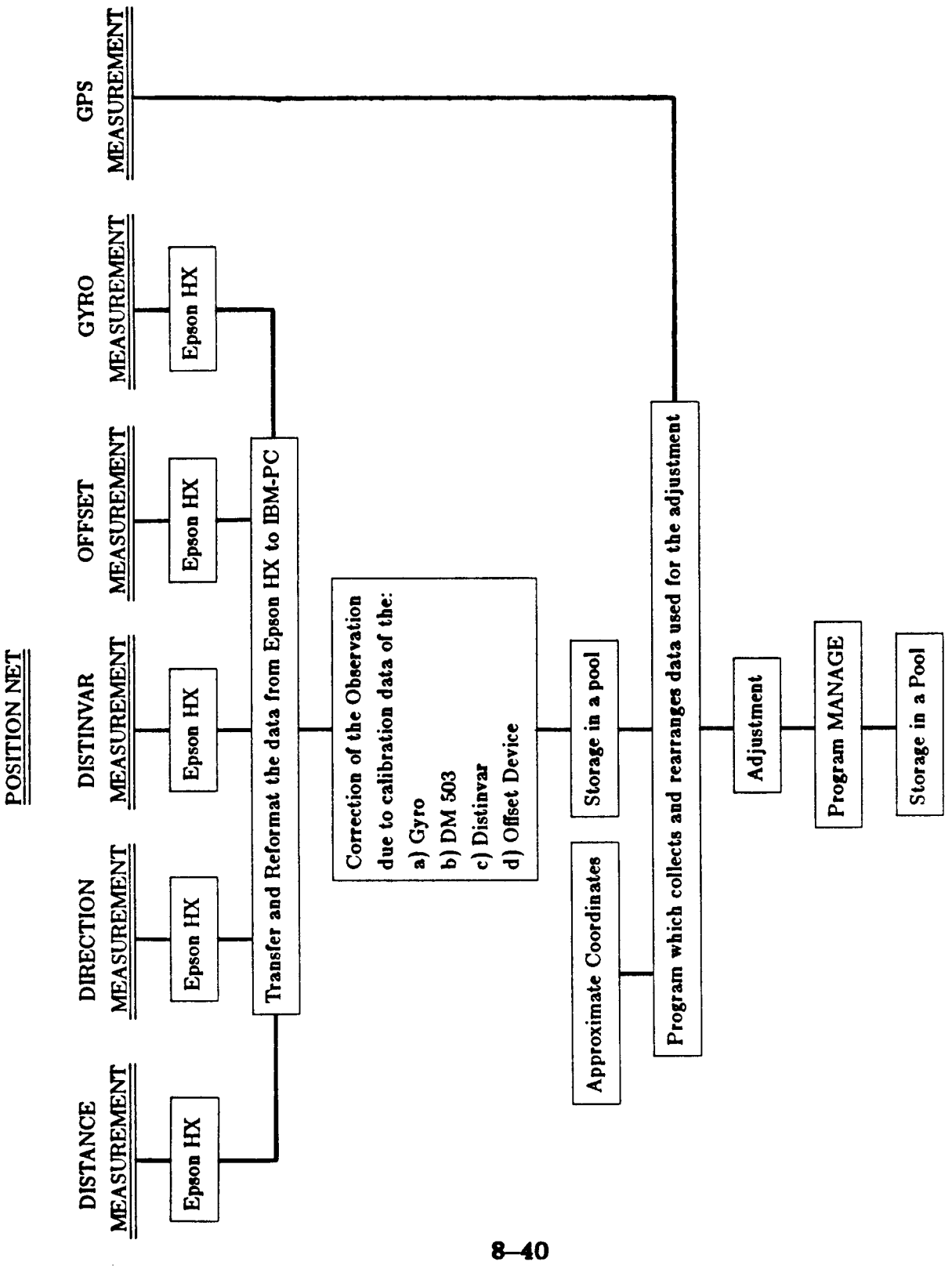

Figure 8.3.3 Schedule 3.

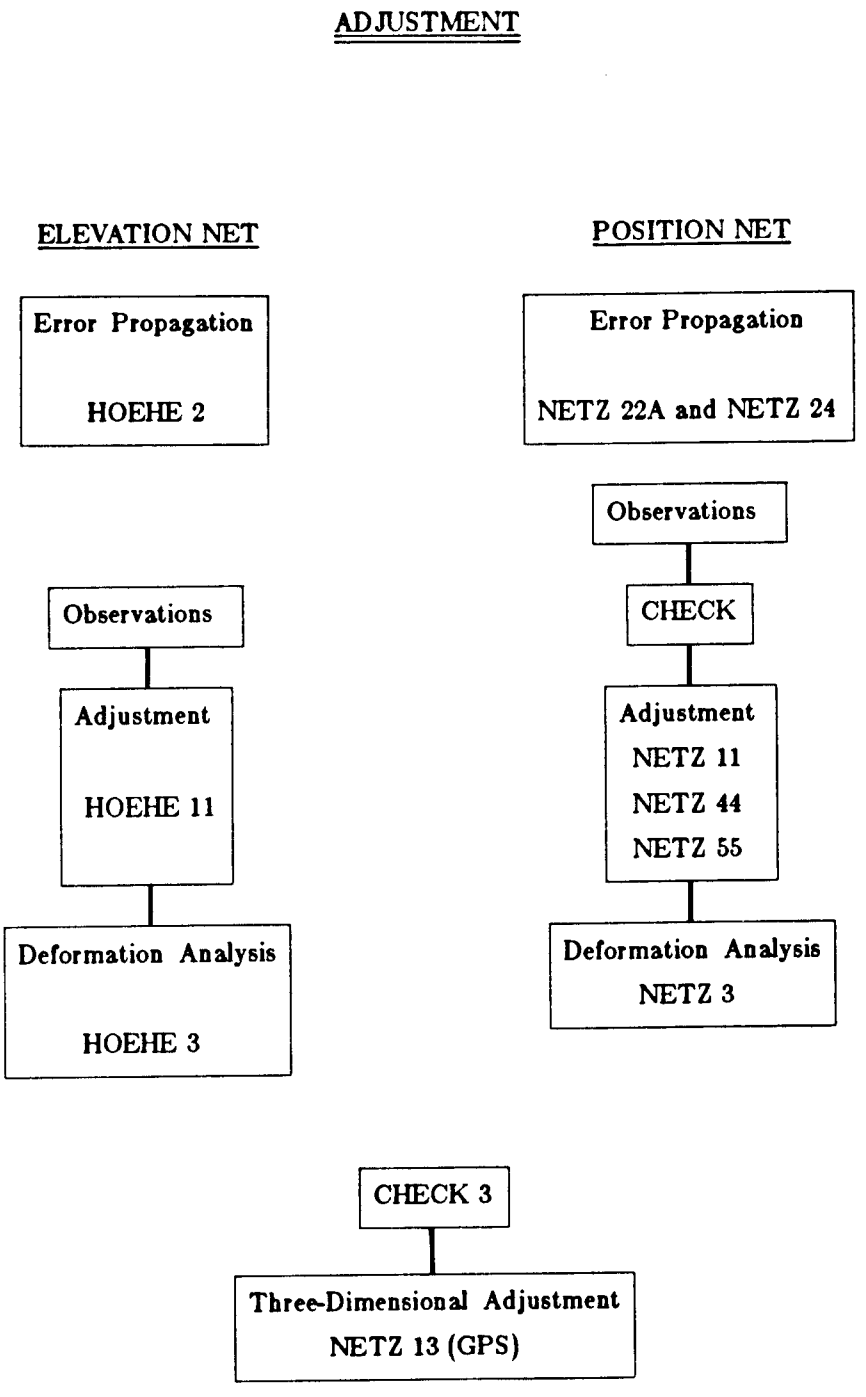

8.4. ALIGNMENT DESIGN

8.4.1 Procedural Considerations

8.4.1.1 Horizontal Positioning In each arc tunnel 500 magnets have to be placed to their three-dimensional coordinates. To place the magnets we need reference coordinates. Such a reference for the horizontal positioning could be a traverse, measured in each arc beginning from the beam switchyard and ending at the interaction point. To determine the bending points of the traverse we have to measure directions and distances. From experience it is known that directions can be measured with an accuracy of ± 0.5 mgon and distances to ± 0.05 mm.

Figure 8.4.1 Traverse error.

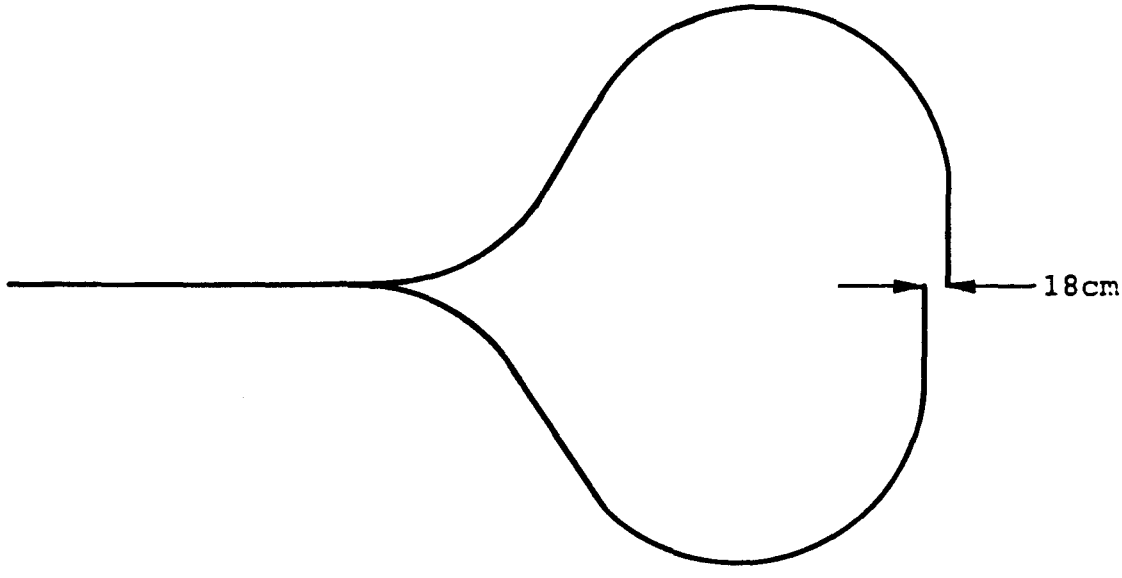

An error propagation of these measurements shows that the last point of each arc traverse would have a transverse error of ± 9 cm with respect to the first point because of the accumulation of measurement errors in a traverse. So

in the worst case we would have an offset at the interaction point of about 18 cm instead of a closure (Fig. 8.4.1).

To avoid this large offset the traverses must be stabilized by other measurements. For this purpose, two alternatives are available :

- gyrotheodolite measurements
- surface control net with transfer penetrations

8.4.1.1.1 Gyrotheodolite Measurements. With a gyrotheodolite (gyro) geographic north can be determined directly. If a gyro is used for measuring a traverse, there is no accumulation of direction errors. This is because the azimuth of each line is not a function of previously measured directions, but is an absolute measured value. Since the absolute accuracy of the gyro is less than the directions measured with a theodolite, both methods are usually combined. Whenever the accumulation of the direction measurement errors equals the accuracy of the gyro, a support measurement with the gyro is made (Fig. 8.4.2).

Available on the market are gyros with an accuracy of 20" to 30". Custom made high accuracy gyros are both designed by CERN and designed and built by the Berggewerkschaftskasse Bochum West Germany. The German gyro has an accuracy of ± 1", but a delivery time of at least one year and a price of about $80,000.

8.4.1.1.2 Surface Net with Penetrations. The second way for supporting the traverse is to determine control points on the surface and transfer the points down into the tunnel through penetrations.

According to the required accuracies, one point of the beam has to be positioned with respect to its theoretical position within ± 10 mm. An estimate shows that a 350 m long traverse, supported at its beginning and end, and assuming that these support points have a position error of about ± 5 mm, has in its middle

Figure 8.4.2 Gyrotheodolite measurements.

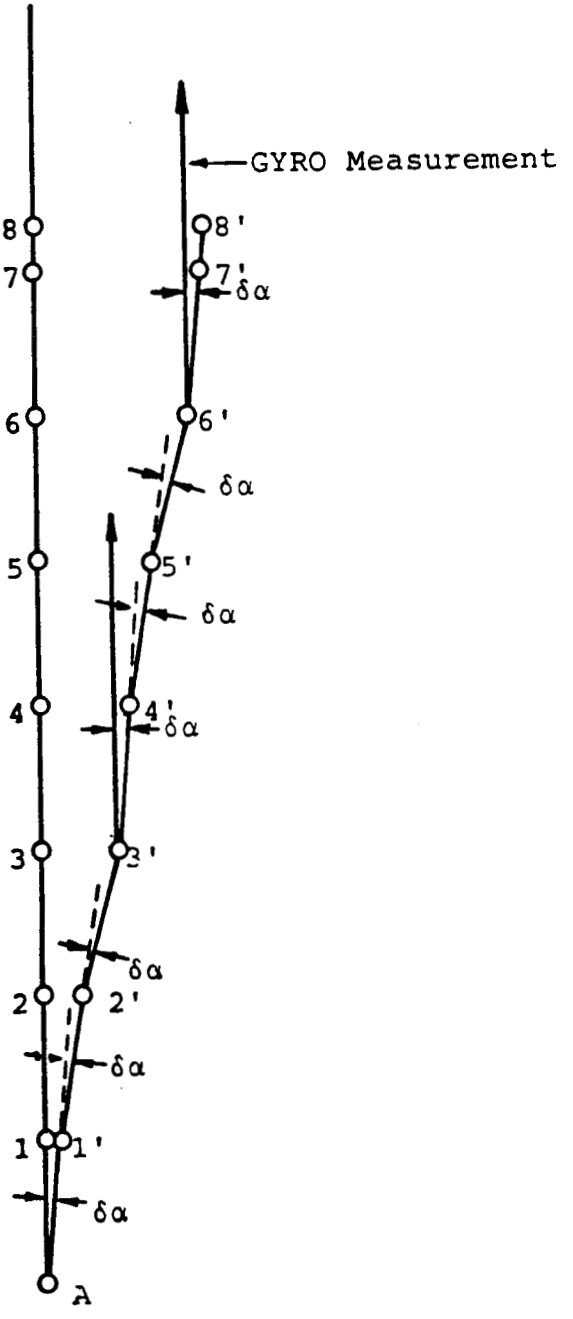

Figure 8.4.3 Maximum traverse error.

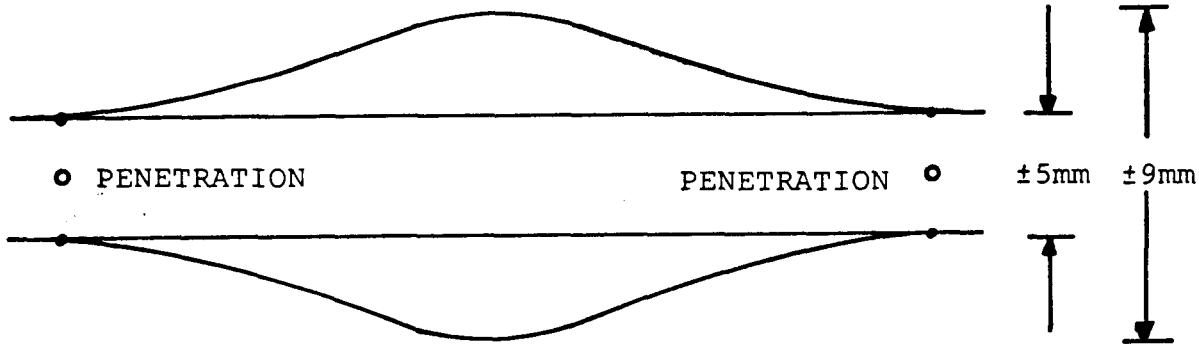

a maximum transverse error of about ±9 mm (Fig. 8.4.3). So a support point is required every 350 -400 m. A support point is a surface determined control point, whose coordinates are plumbed down through a penetration. Figure 8.4.4 shows the distribution of the penetrations for both arcs.

8.4.1.2 Vertical Positioning Taking into account random errors only, the vertical coordinate usually can be determined as precisely as required. But experience from DESY show that one has to reckon with systematic errors of unknown value. Often, these systematic errors are many orders of magnitude bigger than the random errors. Since there is no way to eliminate these systematic errors by a special measuring procedure, the only way to provide a control is by also having support points for the vertical position.

These support points could be established by using the penetrations to transfer elevation measurements made on the surface into the tunnel.

8.4.1.3 Summary As a high precision gyrotheodolite is not available on the market, and it is also necessary to support elevation points by using penetrations, in principle gyro measurements will not be used.

Figure 8.4.4 Distribution of penetrations.

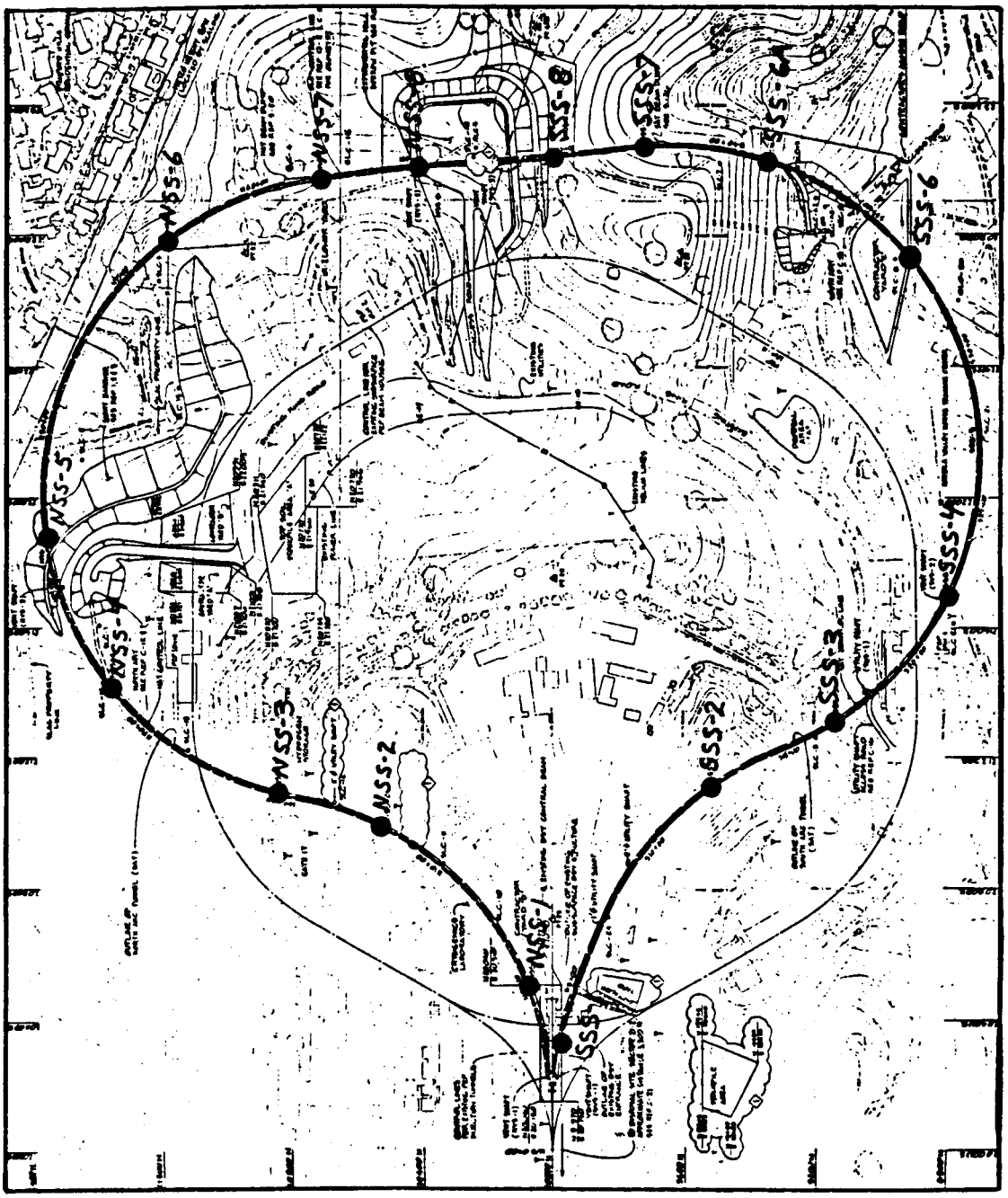

8.4.2 Connection of Geodetic- to TRANSPORT Coordinate System

As stated in section 8.1, the SLC will use the existing LINAC as its positron and electron source. This means that the new SLC components must be located and oriented very precisely with respect to the existing LINAC-BSY beamline. To ensure this, a strong, direct tie must be made between the LINAC-BSY beamline and the new SLC control network. This tie ensures that the same coordinate system will be used in all parts of the SLC project.

8.4.2.1 Tie to the Origin The origin of the TRANSPORT system is station 100+00 of the LINAC and its primary reference axis is in the direction of the LINAC beamline (see section 8.1.2.1). A three-dimensional survey must be made to bring the position of station 100+00 and the direction of the LINAC into the new net.

8.4.2.1.1 Translation. The XZ-position of the origin will be picked up by two traverses and a small net in the BSY area. This net will include two penetration points, the positions of which will be transferred to the surface with an optical plummet.

The Y-position of the beam will be brought to the surface with the same leveling techniques employed on the surface (see section 8.4.3.2). A level line beginning at station 100+00 will be observed through the southwest adit of SLC to a surface mark in the new net.

8.4.2.1.2 Orientation. Two methods are available for orienting the SLC net to the direction of the LINAC. The first involves conventional surveys in and over the BSY. This survey would "pick up" three points near the existing beamline and under the penetrations in the BSY. The points along the beamline would provide a reference direction for the surface net. This alternative has the following constraints:

- Strength of Connection

  The three points which would be used to define the direction of the LINAC

are only 120 m apart. This provides a weak connection. Unavoidable transfer errors will be multiplied by a factor of eight due to the short baseline.

- Time

  A BSY survey would take at least two weeks of tunnel surveying and two weeks of surface surveying.

- Equipment

  All the necessary equipment to conduct the survey will be prepared by the end of 1984.

The second alternative is to use the new Macrometer satellite technology now available on the market. Here the NAVSTAR Global Positioning System and the principles of V.L.B.I. are utilized. This alternative has the following characteristics:

- Strength of Connection

  Since intervisibility of net points is not necessary for the Macrometer, a number of points along the LINAC can be connected to the SLC surface net. An accuracy of 2 p.p.m. is guaranteed, thus providing a stronger connection to the LINAC than a conventional survey. Figure 8.4.5 shows the points along the LINAC and in the SLC surface net which would provide a strong solution to the problem.

- Time

  The actual Macrometer data gathering procedure can be completed in a week's time. Necessary offset measurements in the LINAC can be finished within two days.

- Measurement of the Positron Return Line Length

  The Macrometer will also provide a precise distance from the beginning of Sector 0 to Sector 20. With conventional surveying techniques, this would be more expensive and less precise.

Of the two alternatives the second is the best. The strength of the Macrometer connection is far superior to that obtained by a BSY survey. Also, the timing of the satellite survey is more flexible.

Figure 8.4.5 Net for Macrometer satellite survey.

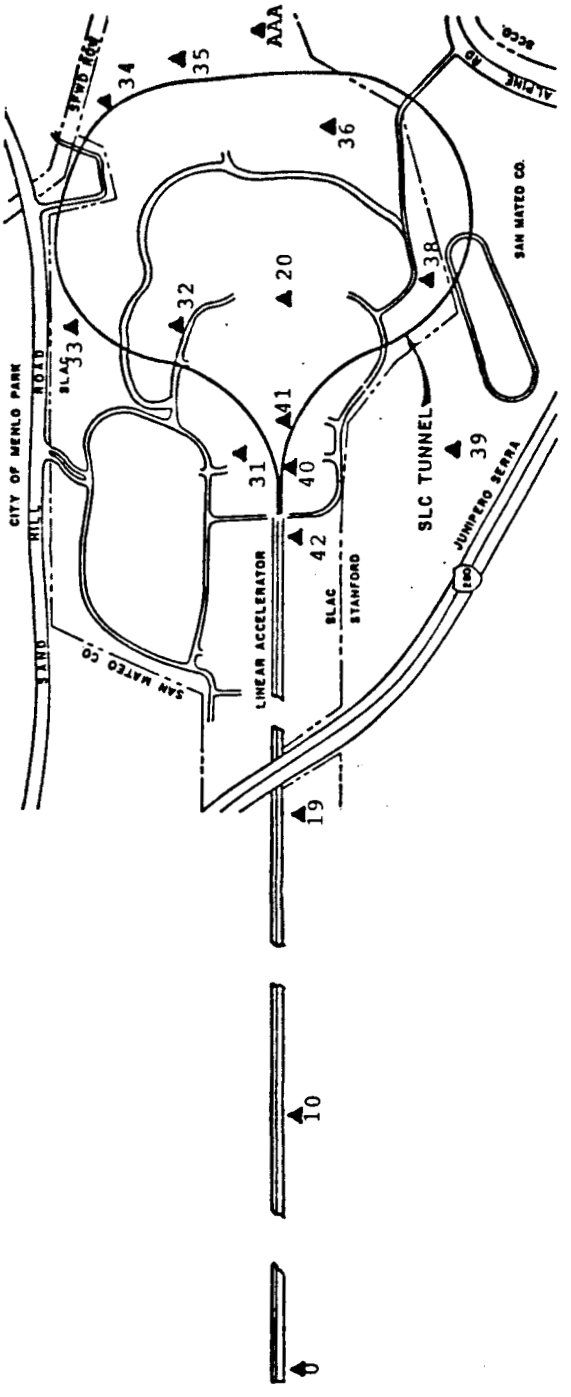

Figure 8.4.6 Proposed geodetic net.

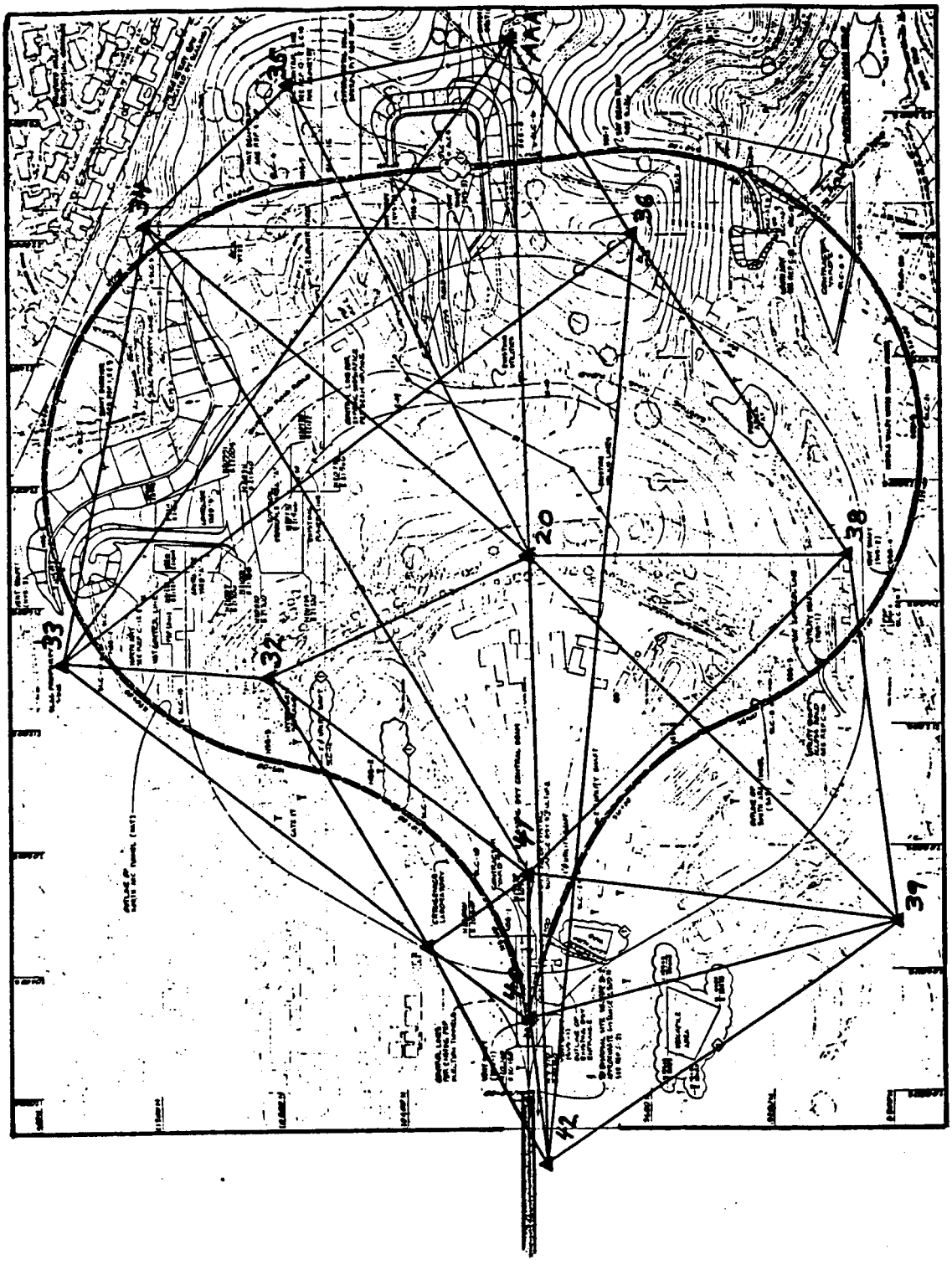

8.4.3 Surface Surveying

8.4.3.1 Horizontal Coordinates To compute the coordinates of the penetration points, those points must be joined together by a geodetic net. Because of problems with the topography and stability, the penetration points are not suitable as control points. Therefore we have to locate points in the SLC area which have view-connections to each other and to the neighbouring penetrations. Together, these will form a strong enough geometric figure that the control points are determined within the necessary accuracy. Fig. 8.4.6 shows the position net design.

8.4.3.1.1 Measurement Procedure. For the determination of geodetic positions, distance and direction measurements are used. These measurements affect the accuracy of a net point in different ways. Direction measurements determine a point in its transverse direction, while distance measurements determine the longitudinal component. Because of disadvantageous error accumulation in direction measurements for longer lines of sight, it is often attempted to replace direction measurements with distance measurements. The error accumulation of direction and distance measurements with respect to different distances is shown in Fig. 8.4.7:

Figure 8.4.7

distance [m]	S [mm] Theod. E2	S [mm] DISTINVAR	S [mm] DM 503
10	0.08	0.05	–
50	0.39	0.05	2.0
100	0.78	–	2.0
500	3.89	–	2.5
1000	7.78	–	3.0

A best observation scheme for the control and penetration points can only be found by an error propagation of a so called free net. A software package based on the recently developed theory of free nets has been acquired and used

for simulation (see section 8.3). Fig. 8.4.8 shows the error ellipses of the control points and of the penetration points determined by the proposed measurement procedure in the optimized net.

8.4.3.1.2 Design of the Forced Centering System. To determine the coordinates of the penetration points and to transfer these coordinates through the penetrations into the tunnel we have to use a theodolite, a rangefinder and a plummet. Furthermore, for measurements in the tunnel we will use a subtense bar, an offset device and a mechanical distance measuring device. All these instruments must fit into the same forced centering system. The problem is that we have to use equipment of different manufacturers with different forced centering systems.

The following requirements must be met by the required SLC forced centering system:

- adaptability of CERN, Kern, Wild and SLAC made instruments,
- repeatability of centering within 1/100 mm,
- centering pin must be a tube to provide possibility of plumbing down,
- possibility of integrating a cross-slide,
- insensitivity to tension applied by the Distinvar,
- simple handling,
- insensitive to canting,
- insensitive to dust.

Figs. 8.4.9, 8.4.10, and 8.4.11 show three different designs which vary according to which of the above arguments was given the most importance.

The design of Fig. 8.4.11 was chosen because of:

- most homogeneous solution,
- adapter consists in all possibilities only of one part,
- most insensitive to tension,
- cheaper than design of Fig. 8.4.10.

8.4.3.1.3 Physical Design of the Control Points. The control points must be marked in such a way that it is possible to center and fixture the measurement

Figure 8.4.8 Error ellipses of the free net control points.

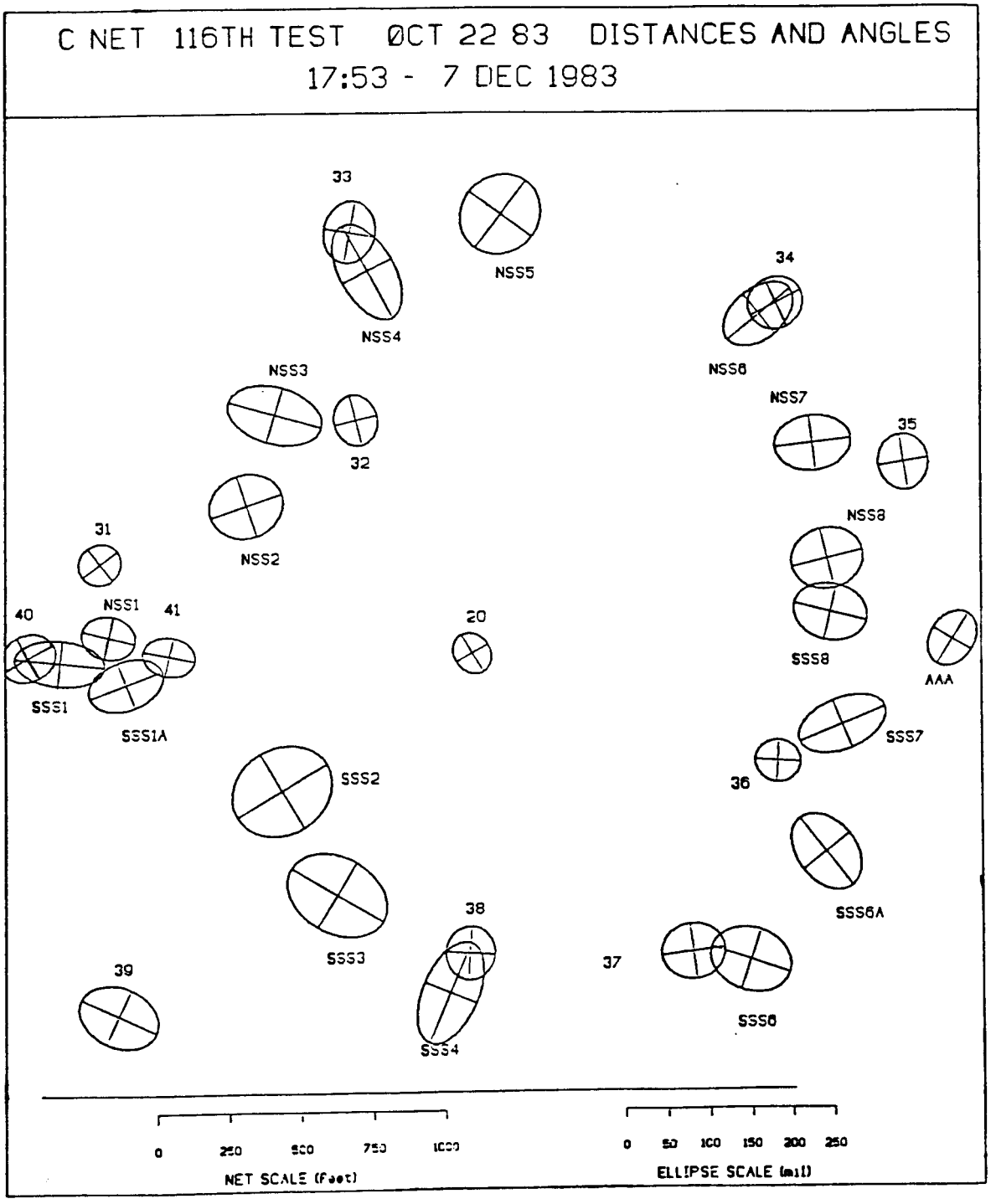

Figure 8.4.9 A design for the forced centering system. (I)

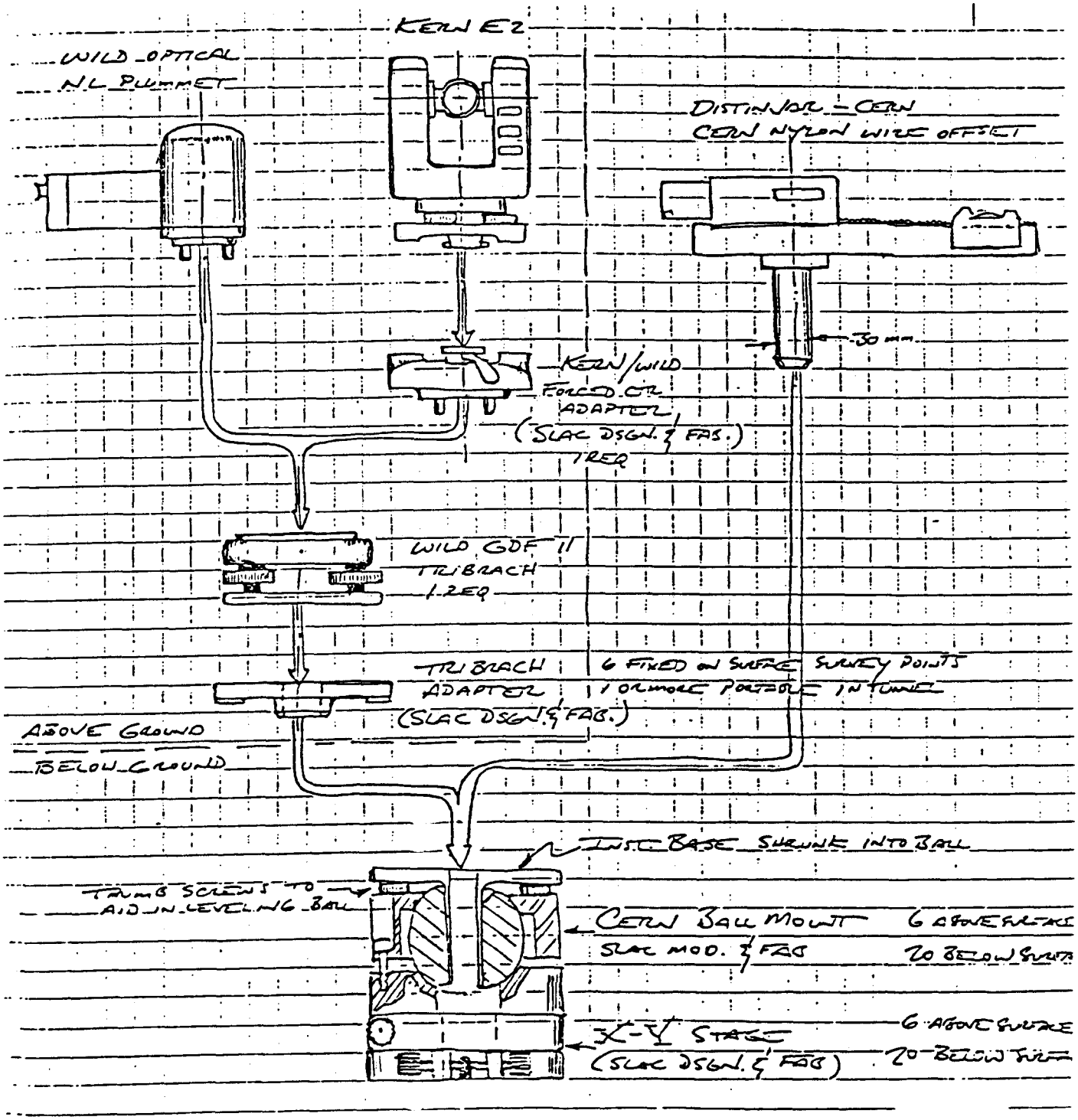

Figure 8.4.10 A design for the forced centering system. (II)

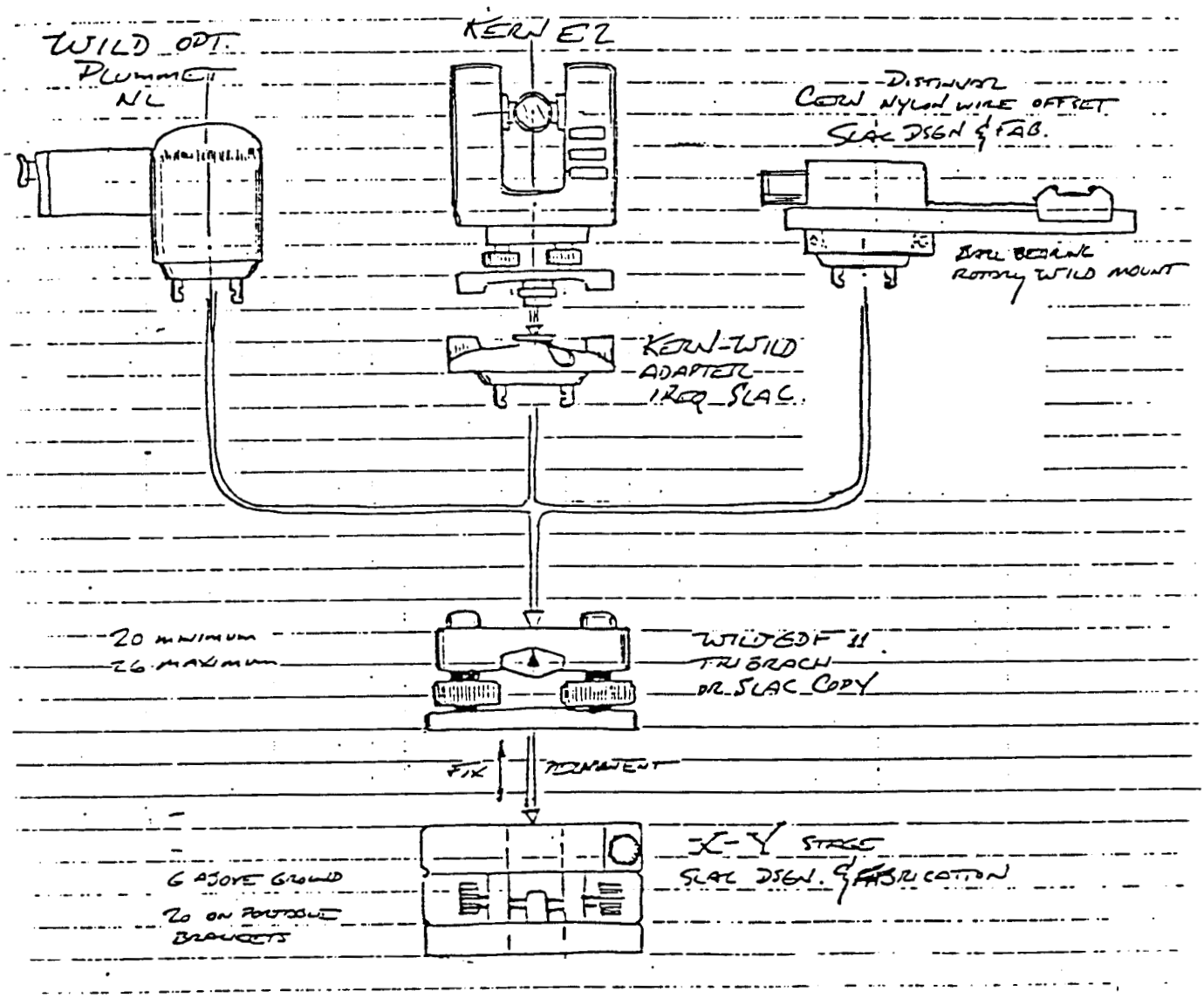

Figure 8.4.11 A design for the forced centering system. (III)

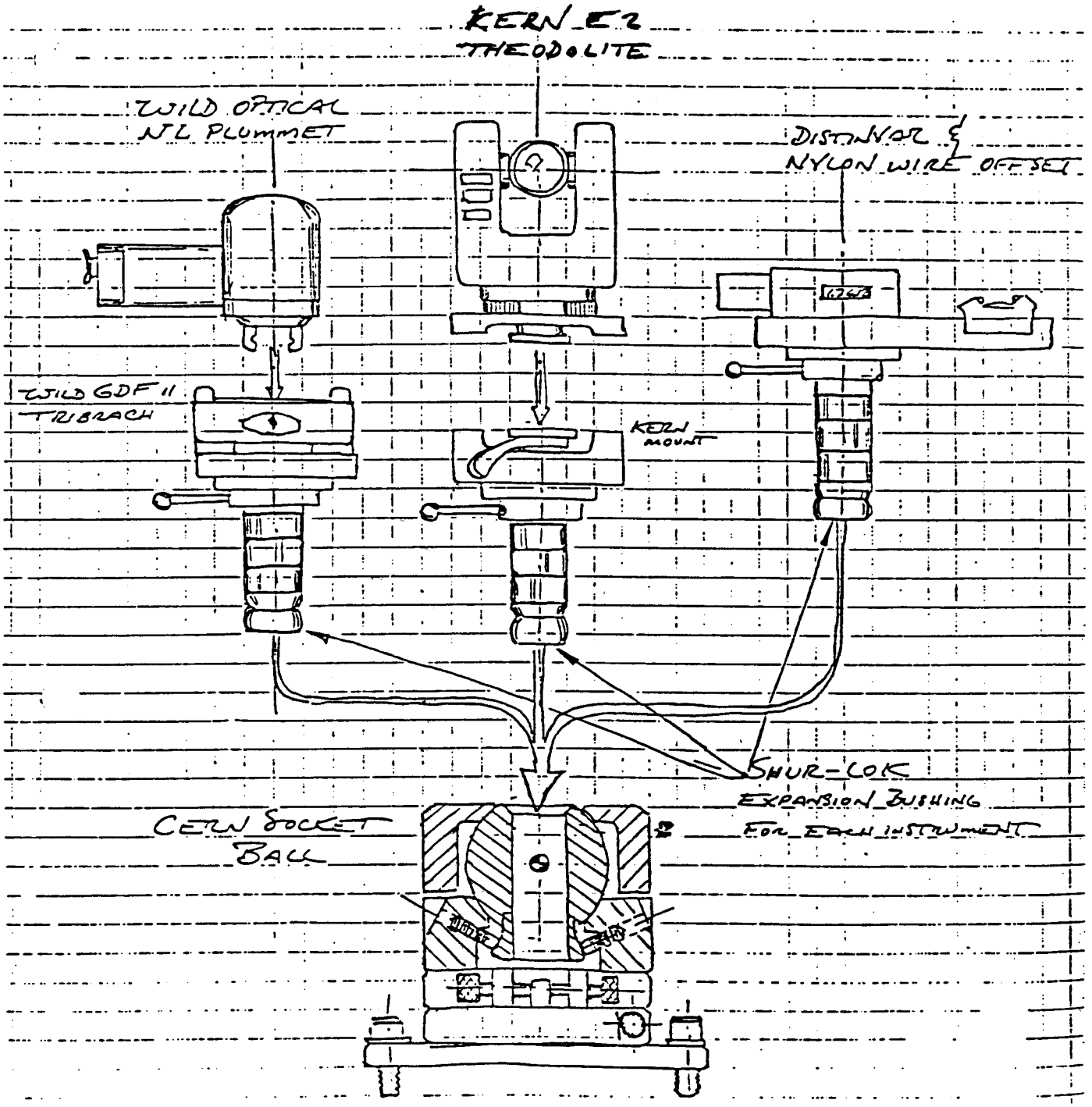

instruments over the points with an accuracy three times better than the accuracy of the net itself. It should also be possible to do the fixturing and the centering very quickly and simply.

These requirements do not allow the use of tripods to center and fixture the measurement equipment. Therefore, following the CERN, DESY, and Fermilab examples, concrete monuments were built (Fig. 8.4.12). Where that was not possible, steel frame towers (Fig. 8.4.13), with forced centering plates on their tops were constructed. The monuments should be stable enough so that no changes in their positions occur during the measurement period. Since it does not seem possible to build the monuments and steel frames so rigid that over one and a half years no changes occur, we have to repeat the net measurement in shorter time periods. To get an idea of the stability of the control points the first repetition should be made six months after the first. With that knowledge it can then be decided how often the measurement must be repeated.

8.4.3.1.4 Physical Design of the Penetration Points. Above the opening of the penetrations we must provide a fixturing for the measuring equipment. The fixturing design should have a modular structure and should also be interchangeable, because the height over the penetrations, at which the measuring equipment must be fixtured, is different at each point depending on the topography. Furthermore, we don't need fixturings for all penetrations, because the SLC schedule doesn't allow us to wait until the whole tunnel is ready and then to determine all penetration points together. Rather, we have to determine the penetration points according to the tunnel progress step by step. It seems to be enough to provide fixturings for six penetrations.

8.4.3.1.5 Instruments Needed. To measure distances and directions, a DM 503 EDM attached to a Kern E2 theodolite will be used. In addition to this, a

Figure 8.4.12 Concrete monuments.

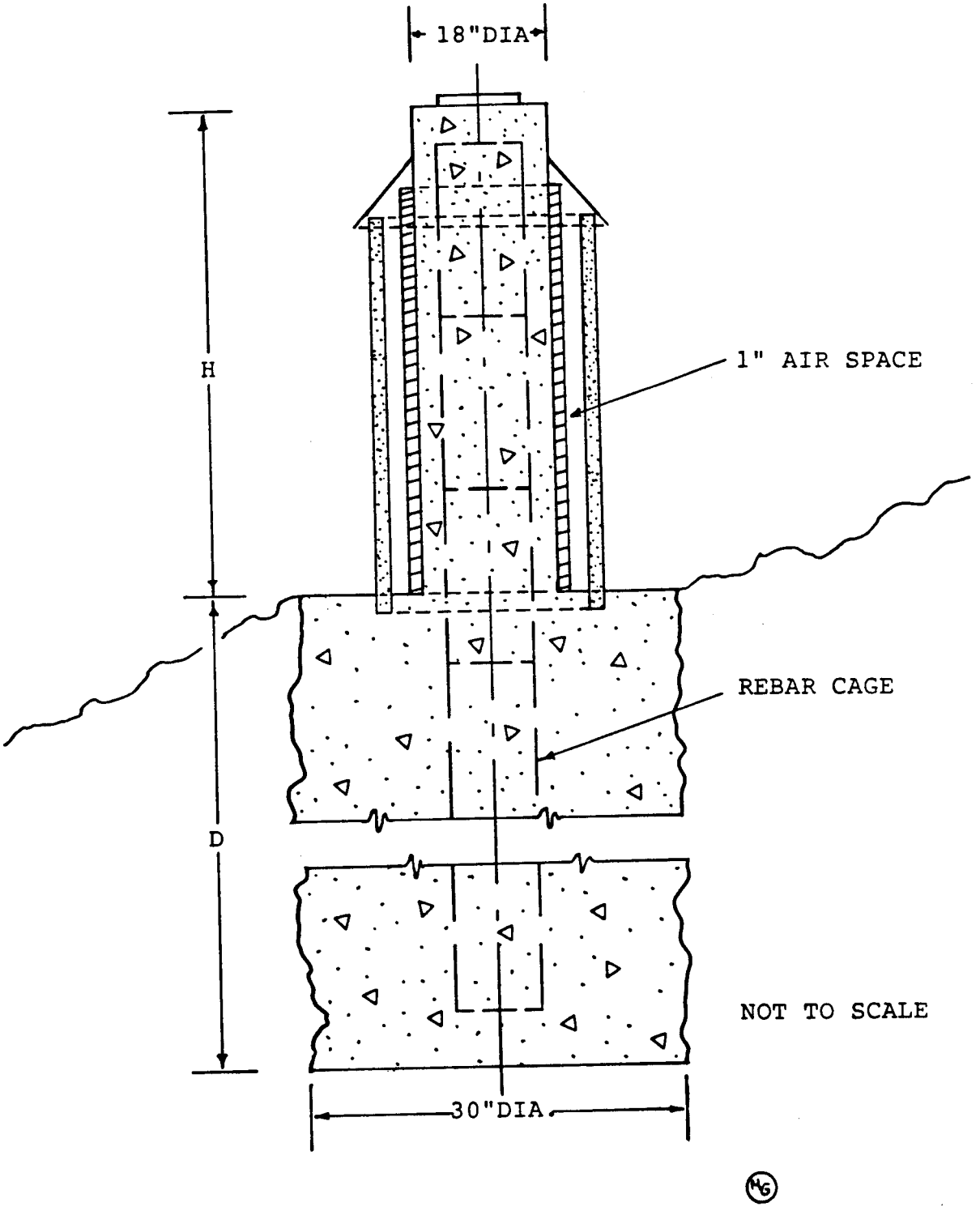

Figure 8.4.13 Steel frame monuments.

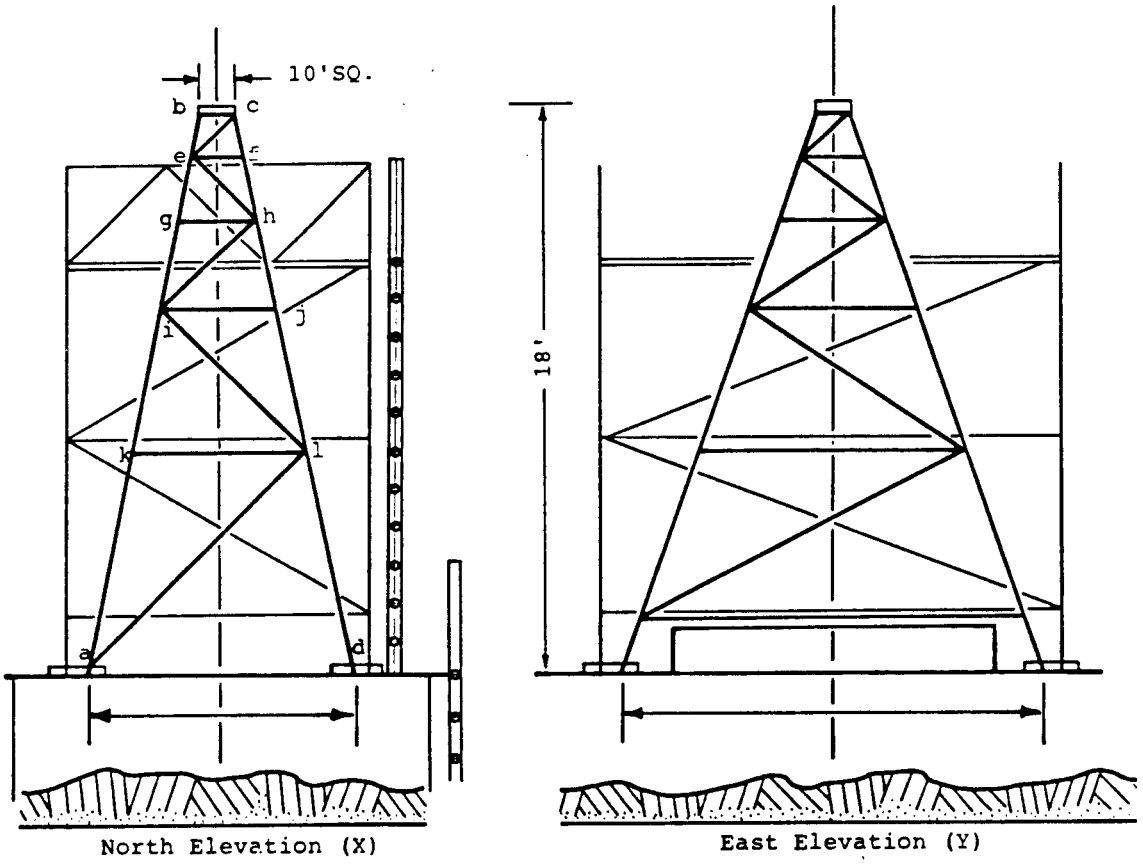

plummet, a subtense bar, and special devices to obtain information about the atmospheric conditions are available. Calibration facilities are needed to calibrate the rangefinder and the subtense bar (see section 8.6).

8.4.3.2 Vertical Coordinates To connect elevation measurements in the tunnel to those on the surface, elevations from the surface net will be transferred through the penetrations. Therefore we need bench marks near each penetration. The accuracy of these points should be comparable to the horizontal accuracy, ±2 mm.

As shown above, we also have to determine the height of the control points and the penetrations with an accuracy of ±(3–5) mm (refer to section 8.2.2.3), to reduce sloped distance measurements.

Consequently, we must establish an elevation net with bench marks near the penetrations and the position control points, with an accuracy of ±2 mm.

Figure 8.4.14 Difference in height between bench marks.

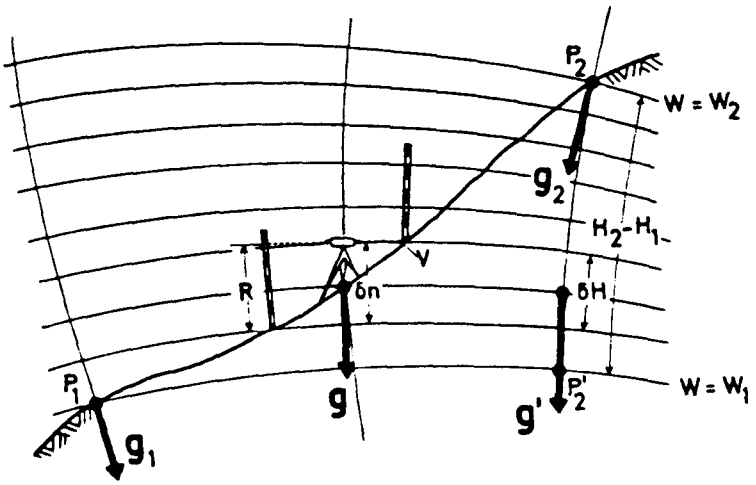

8.4.3.2.1 Measurement Procedure. The accuracy of precise leveling depends on personal, instrumental, topographical, and atmospheric influences. Since the difference in height, Δn, between two bench marks is composed of numerous

Figure 8.4.15 Bench mark design.

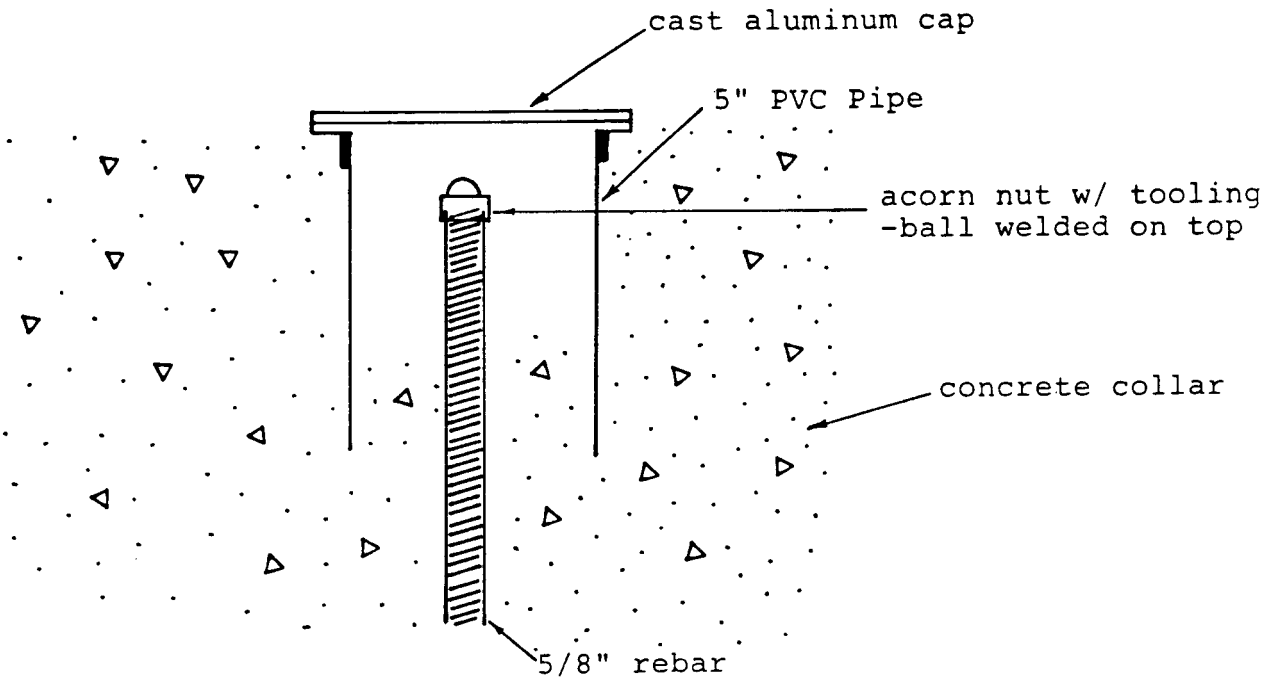

- it has a shortest focusing length of only 0.5 m,
- it is comfortable to handle,
- it is very sturdy,
- calibration can be done at SLAC,
- it is in the lower price range of its order,
- it has a short time of delivery.

For the leveling procedure a pair of rods for each instrument is needed. The rods must be made of invar, and double-scaled with 5 mm graduations. For use on the surface they should be 3 m long with brace poles. The best rods which are available on the market with a short time of delivery are offered by Kern and Wild. We chose the rods from Kern, because Wild protects the rods with a transparent varnish coat which causes difficulties for rod calibration with an automatic microscope.

8.4.3.2.4 Transfer of Heights. As indicated above, for supporting the elevations

measured in the tunnel, we have to transfer heights measured on the surface through the penetrations into the tunnel.

For this purpose we will use invar tapes, cut and calibrated to the special height difference of each penetration. We will use invar tapes instead of invar wires because invar tapes are much more stable than the wires. For each special transfer length we will cut the tape, and fix at the two ends small scales like the graduated scales of the level rods. The exact length between the two scales will be calibrated on the interferometer bench. Since in most cases the transfer length is longer than the range of the calibration bench, we have to do the calibration in two steps.

To do the transfer measurement the calibrated tape will be fixed at a tripod over the opening of the penetration on the surface and suspended down to the tunnel floor. There it will be connected to a spring scale and forced to the calibration tension. Then with two levels the height of the two scales are simultaneously read and transferred to the bench marks (Fig. 8.4.16).

8.4.4 Tunnel Surveying

8.4.4.1 Horizontal Coordinates To bring the 500 magnets of each arc to their correct positions we must have a reference. This reference can be obtained by measuring a traverse from the beginning to the end of each arc. It will be supported by surface coordinates plumbed down through the penetrations.

There are two alternatives to physically establish such a traverse. First, the pedestals themselves could be used as traverse points, or second, we could use separate monuments. The first alternative has the advantage that it produces a smooth beamline at minimal cost, since there would be no transfer errors from a separate monument network to the magnets. Such a system would be our choice for a machine on a level or sloped plane with magnets 20 to 50 m apart. However, for the SLC, with many arc magnets close together and frequently changing achromat planes, this turned out to be impractical. This alternative

Figure 8.4.16 Transfer of height measurements.

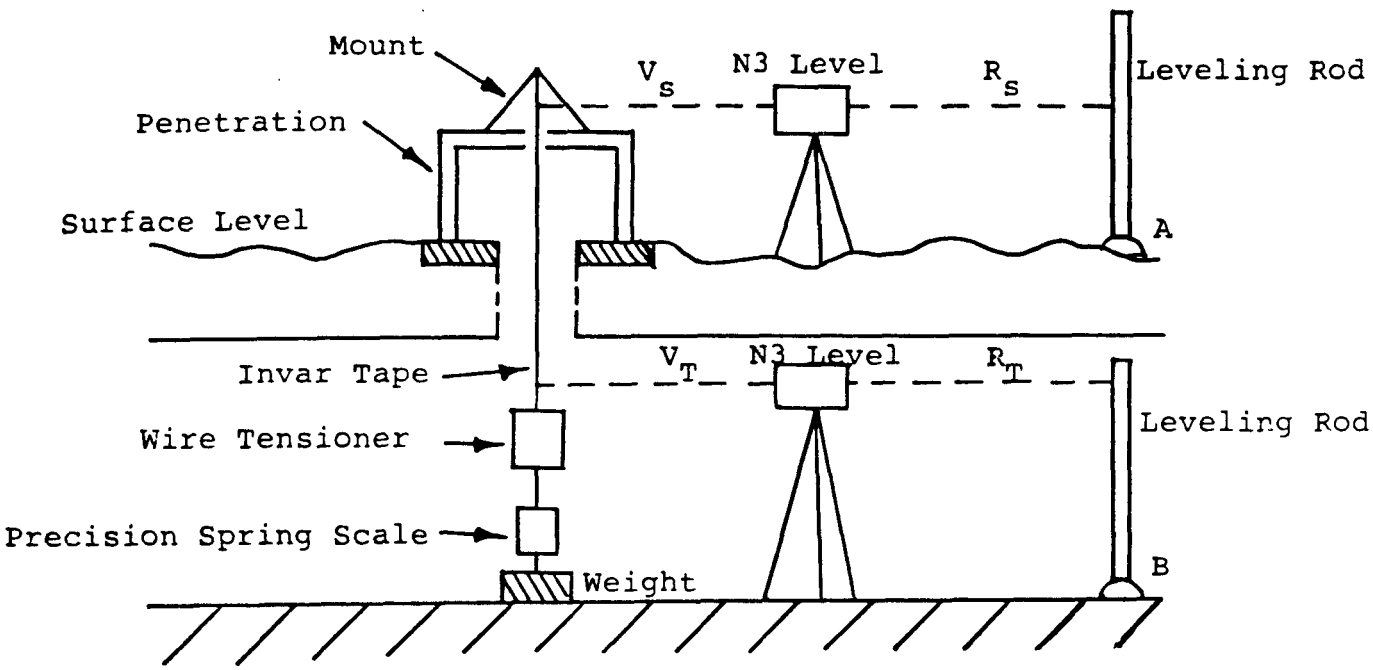

$$H_B = H_A + R_T - V_T - R_S + V_S$$

where:

H_A =Known height of point A

H_B =Height of point B, to be determined

R_T =Backsight in tunnel to leveling rod

V_T =Foresight in tunnel tape

R_S =Backsight on surface to leveling rod

V_S =Foresight in surface to tape

did not offer an obvious method to go from one achromat to the next. Moreover, it has the disadvantage that in moving the pedestals step by step to bring them to the correct position, our reference system would be lost every time. In order to reestablish our system, the traverse between at least two penetrations must be measured again. Also, it is possible that adjustments will have to be made at operating temperatures. Here scintillation due to the heated magnets prohibits the use of lines of sight over the magnets. Therefore, we have chosen the second alternative and will use monuments.

In section 8.5 it is shown that these monuments will not only be used for the traverse, but also for control of the construction survey and installation of the pedestals.

8.4.4.1.1 Measurement Procedure. The support points, which are plumbed down through the penetrations, provide starting and ending points for traverses in the arc. This makes it possible to run sections of the arc traverse without measuring the whole arc. Consequently, the arcs can be aligned section by section.

Figure 8.4.17 Traverse design.

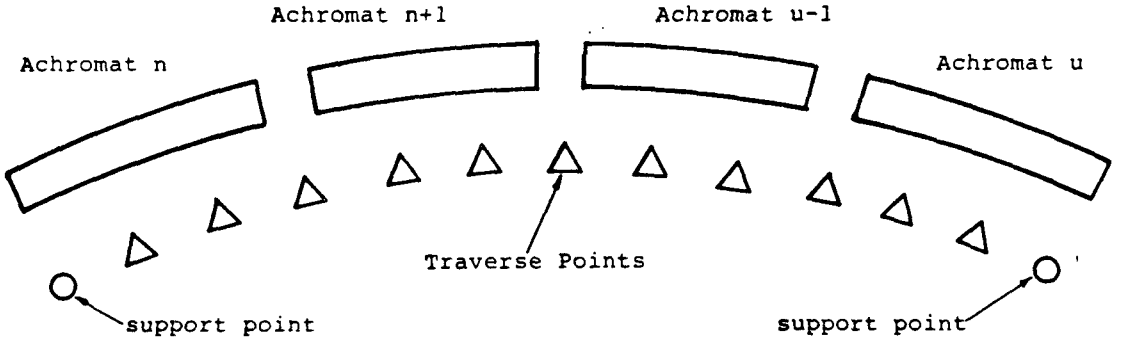

The arrangement of the traverse points takes into consideration that an achromat is the subsection in which the highest relative accuracy is required. This has guided us to the traverse design of Fig. 8.4.17.

A simulation of the adjustment has shown that three traverse points per achromat do not give the required accuracy. Therefore, the design of the traverse requires four points. The penetration points are seen as additional traverse points which are included in the measurement.[1]

The parameters of the traverse are distances and directions. These parameters are measured with a theodolite, a Distinvar, or a one meter subtense bar. To minimize the number of the required invar wires for the Distinvar, only two different distances are used.

The accuracy of the traverse points relative to the neighbouring points should be ± 0.2 mm according to the demanded accuracies (section 8.1.3.1). To attain this accuracy we have to measure the directions with an accuracy of ± 0.3 mgon and the distances with an accuracy of ± 0.2 mm per 100 m.

With a suitable measurement procedure the direction measurement can be done with this accuracy. Horizontal distances could easily be measured to twice the above accuracy with the Distinvar. For measuring the sloped distances a suitable reduction formula has to be found. The CERN reduction formula is assumed to work for slopes up to 5%, but has not yet been verified experimentally at SLAC.

The Distinvar must be calibrated for both horizontal and sloped distances. For more details refer to section 8.6.

8.4.4.1.2 Design of Tunnel Monuments. Since the tunnel is narrow we do not have the space for permanent monuments. Therefore we have to design a tripod which can be reinstalled with ease and great precision. The following requirements must be met by the design:

---

[1] Previously it was stated that the surface coordinates would be transferred down into the tunnel. But in reality we will go the opposite direction. For technical reasons, it is easier to bring the cross-hairs of a cross slide mounted plummet in alignment with the ground marks than to move the ground mark to coincide with the fixed plummet.

- stability better than the demanded accuracy (± 0.02 mm),
- stable against tension of the Distinvar (32 pounds),
- repeatability of position and height,
- easy handling.

A sketch of a design which would meet the requirements is shown in Fig. 8.4.18.

To reestablish the tripod ground marks are used. A possible design of those ground marks is shown in Fig. 8.4.19.

8.4.4.1.3 Instruments needed. The parameters of the traverse to be measured are directions and distances. For measuring the directions, the Kern E2 electronic theodolite, will be used. Suitable targets for short distances are not available on the market. Nonreflecting cones will be used for this purpose.

The Distinvar will be used to measure both horizontal and sloped distances. Slopes of 10% will be encountered. However, these slopes have never been measured to the required accuracies with the Distinvar. Although an attempt will be made to make the Distinvar usable for measuring the sloped distances, an alternative should be provided. A interferometer together with a feedback controlled reflector designed at CERN will be used to measure the most difficult distances. Fig. 8.4.20 shows a sketch of the CERN design.

In addition to these techniques a one meter subtense bar will be used to measure distances between points which cannot resist the Distinvar tension.

8.4.4.2 Vertical Coordinate A reference for the vertical position is needed similar to that for the horizontal position.

8.4.4.2.1 Measurement Procedure. The measurement procedure used for the determination of the bench marks in the tunnel is the same as used on the surface.

The vertical net is to be established with bench marks in the floor every 20 m. The traverse points can not be used as bench marks because the tripods are not permanently fixed. With the bench marks in the floor the heights of the

Figure 8.4.18 Sketch for a tripod design.

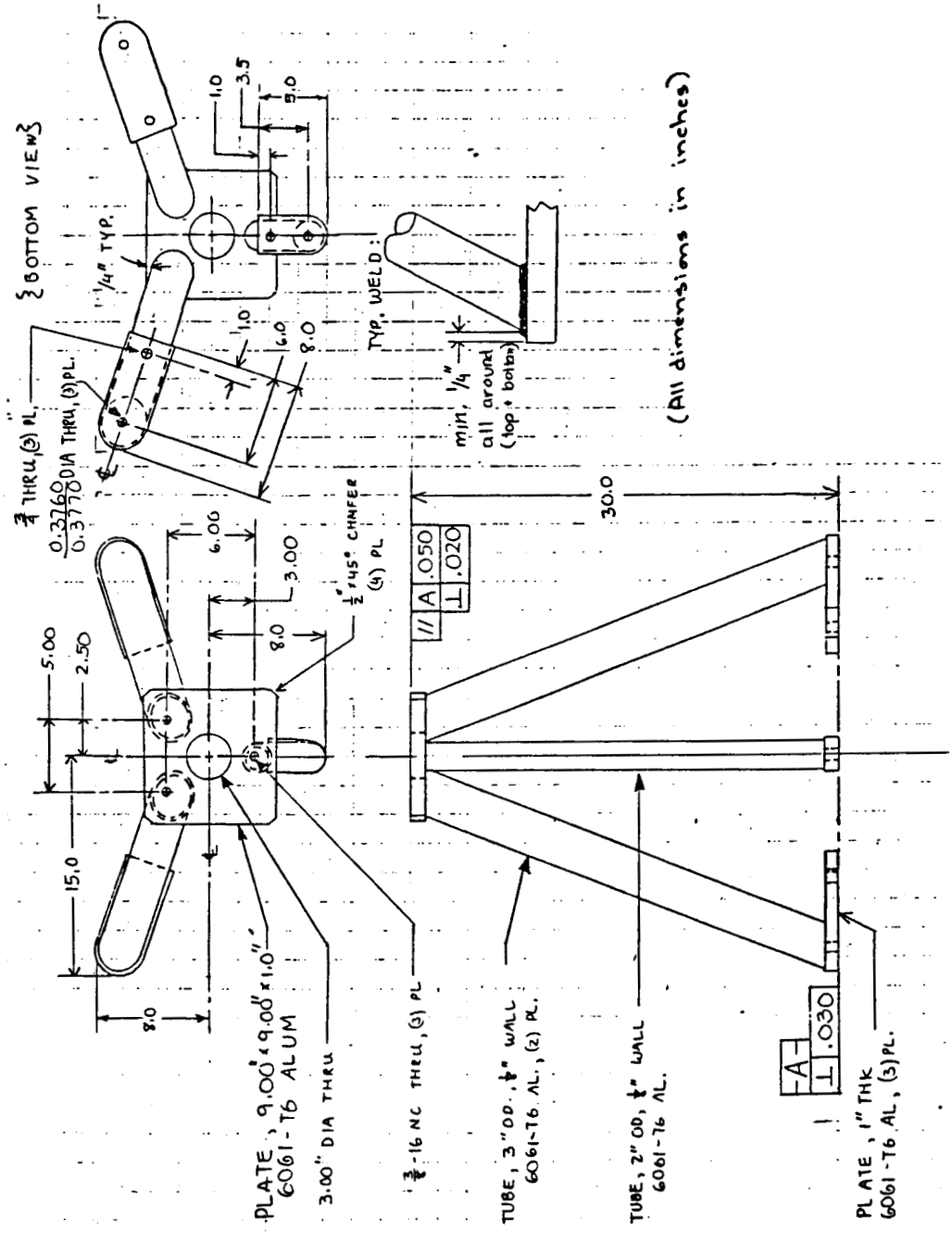

Figure 8.4.19 Sketch of a ground mark.

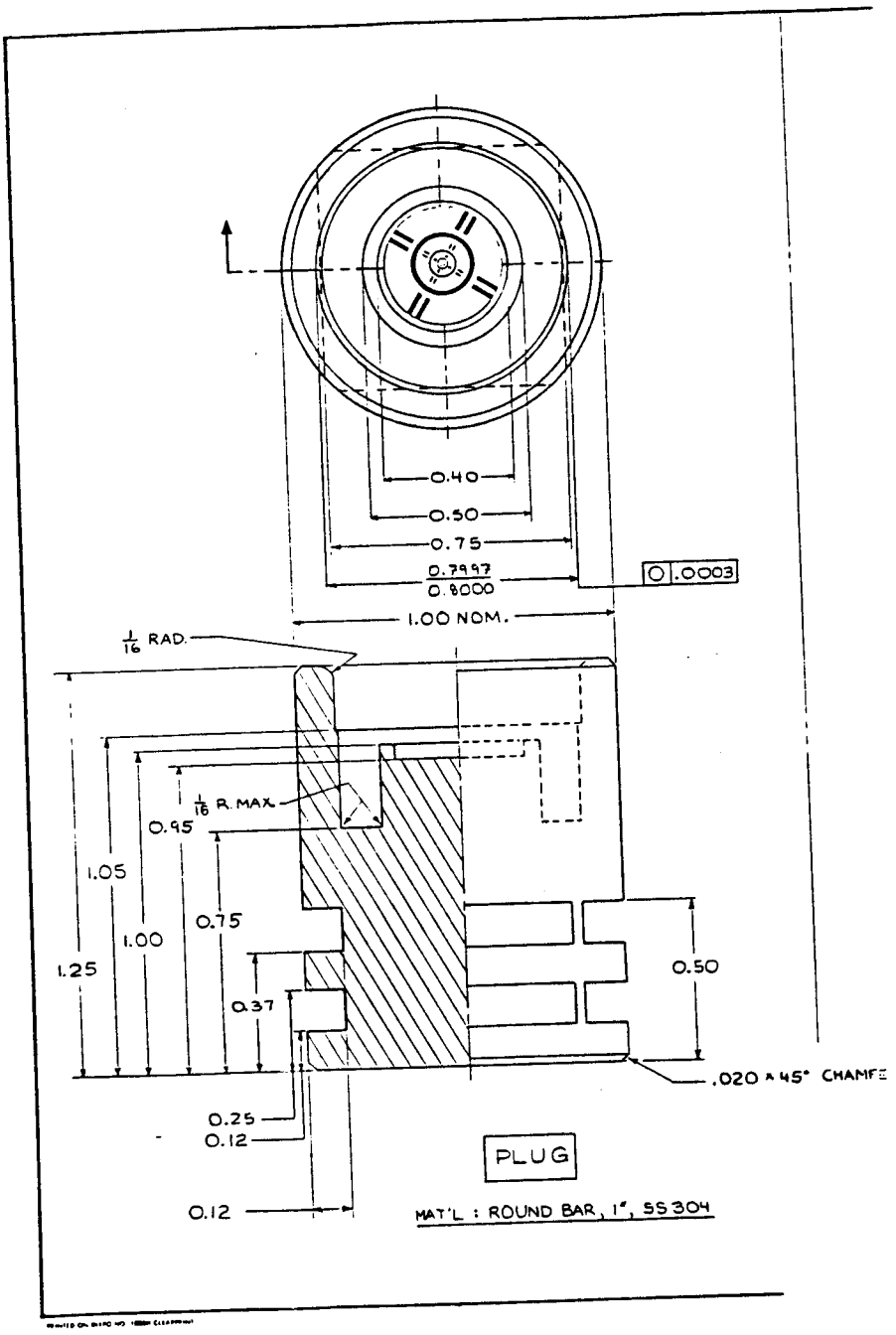

Figure 8.4.20 The reflector used at CERN.

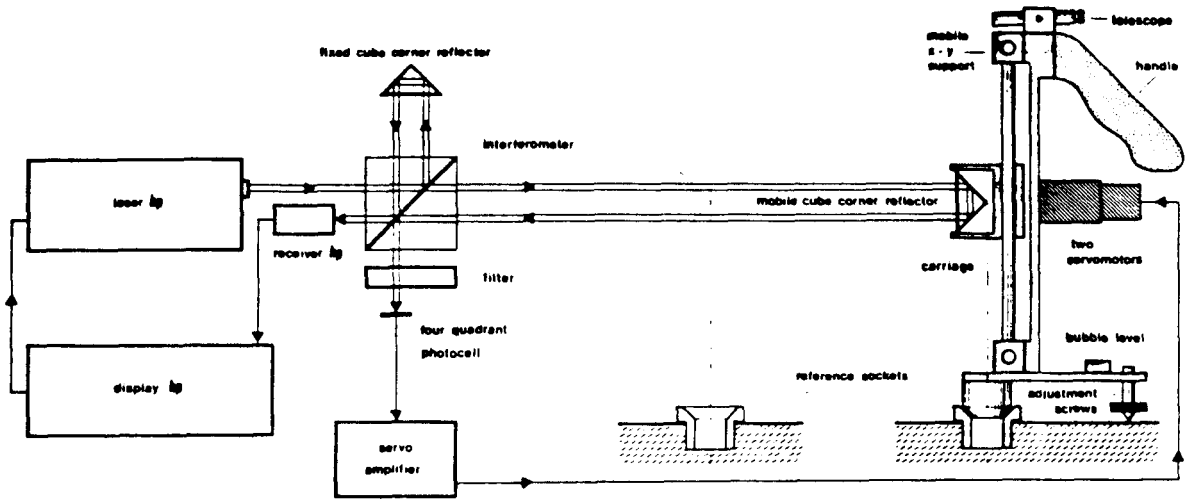

traverse points can be determined on the tripods. These heights must be known for the reduction of the sloped distances with a relative accuracy of ±0.1 mm. This is also the accuracy which is needed for the adjustment of the magnets.

8.4.4.2.2 Design of Bench Marks. Stainless steel rivets epoxied into the tunnel floor will be used.

8.4.4.2.3 Instruments Needed. For leveling in the tunnel the same instruments which are used to measure the surface elevation net, can be utilized. In the tunnel, it is not always possible to level exactly 'from the middle,' so that the lengths of backsight and foresight are not always exactly the same. In this case a level with a 'quasi-absolute horizon,' would make it possible to have unbalanced sight distances. The disadvantage of this instrument, the Ni002 of ZEISS/Jena, is that it is influenced by magnetic fields. Therefore it cannot replace the Wild N3 levels, and more classical methods will be applied to solve the unequal sight distance problem.

Also we must have other invar rods, because the rods used on the surface are too long. In the tunnel, 1 m and 2 m invar rods, which are identical in construction to the 3 m rods, are used.

8.5. ARC MAGNET ADJUSTMENT

8.5.1 Step 1 = Establishing the Pedestals

The aim of this step is to bring the pedestals to positions where they are bolted and grouted to the floor. After this step, the pedestals should be in place within an accuracy, relative to the traverse control points, of about ± 3 mm. This step relaxes the precision required by the construction survey. It also eases requirements on the tolerances of the pedestals, since fabrication tolerances play no role in the positioning. The vertex points between magnets are used for positioning.

8.5.1.1 Procedure In a horizontal tunnel this first step would be straight forward. The coordinates of each vertex point, which correspond to the position of the respective pedestal, could be marked on the floor and afterwards the pedestal mounted.

Figure 8.5.1 Orientation of pedestals with respect to coordinate system.

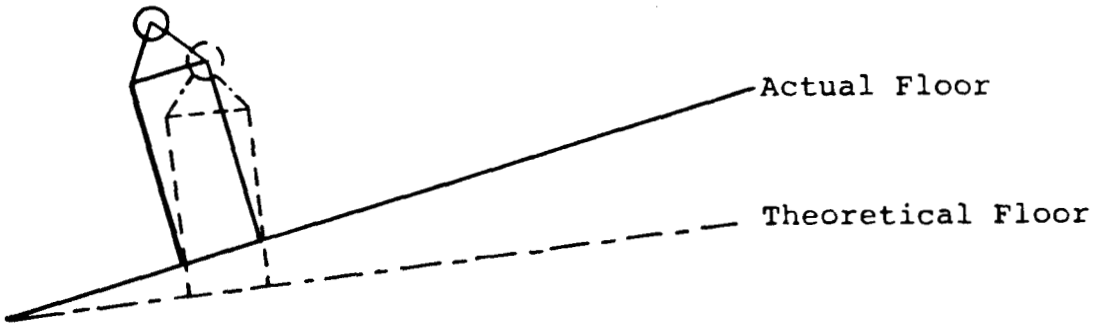

In this case the tunnel is sloped in Z-direction, while it is roughly horizontal in X-direction. Moreover, the pedestals will be perpendicular to the floor, and the magnets on top are rolled. It is therefore not sufficient to mark the ZX

coordinates of the vertex points on the floor, because this would not necessarily be the position where the pedestals are to be mounted (Fig. 8.5.1). In addition the Y coordinate must be known and several iterations must be made to obtain the correct position.

Figure 8.5.2 Positioning of the pedestals.

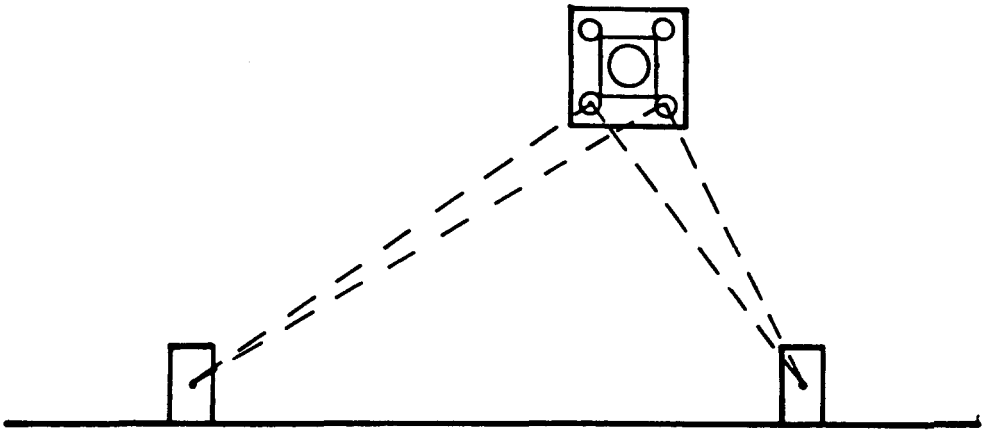

In a sloped tunnel a way to position the pedestals by using the vertex point itself must be found. First the pedestals will be positioned roughly to ± 6 mm. To do this, one could project the coordinates of the vertex point to the real pedestal foot position and determine this position by measuring two sets of horizontal directions from two neighbouring traverse points to each pedestal foot position (Fig. 8.5.2). The pedestal would then be placed, but not bolted to the floor, because of the uncertainties in the height and tilt of the floor. The determined points could be so far off that it would be impossible to bring the pedestal into the right position with only the adjustment screws.

Therefore, the bolts should only be screwed into the floor and the holes in the pedestal foot should be much wider than the diameter of the bolts to provide a wider adjustment range. Thus the pedestals will be standing on their bolts, but not grouted, when taken from the contractor.

To obtain tighter positional tolerances, there are three alternatives. All of them use a target characterizing the vertex point.

- Alternative A:

  After the rough positioning of the pedestals, the actual coordinates of the vertex points can be determined by measuring horizontal and vertical angles from the traverse points. The differences in the six degrees of freedom can be computed and with these values the pedestals can be adjusted. They will be brought to within ±5 mm of their correct position by tightening and loosening the nuts of the bolts which fix the foot of the pedestal; this adjustment step has to be done without using the precise adjustment mechanism. After this a new iteration is required by measuring the actual coordinates and adjusting now with the precise-adjusting mechanism to get an accuracy of ±3 mm.

- Alternative B:

  By using two theodolites set up on two neighbouring traverse control points and by pointing each telescope to the theoretical position of the respective vertex point, the intersection of the lines of sight describes the vertex point in space (Fig. 8.5.3). The procedure of adjusting the pedestals would be an iterative process because the intersection of the lines of sight is not visible. That means the operator of one theodolite must call out corrections for the adjusting person to make until the pedestal target is brought into the line of sight of the first theodolite. Then the operator of the second theodolite does the same. After several iterations they should obtain an accuracy of ±3 mm.

- Alternative C:

  An easier way to bring the pedestals to the correct position would be possible if we could make the theoretical position of the vertex point visible. This can be done by using two laser theodolites. Two theodolites combined with a laser attachment would be set up on traverse points as in alternative B. But now the intersection of the lines of sight would be visible. The adjustment of the pedestal can be done in one step without an iterative procedure.

Figure 8.5.3 An early interpretation of Alternative B for adjusting pedestals.

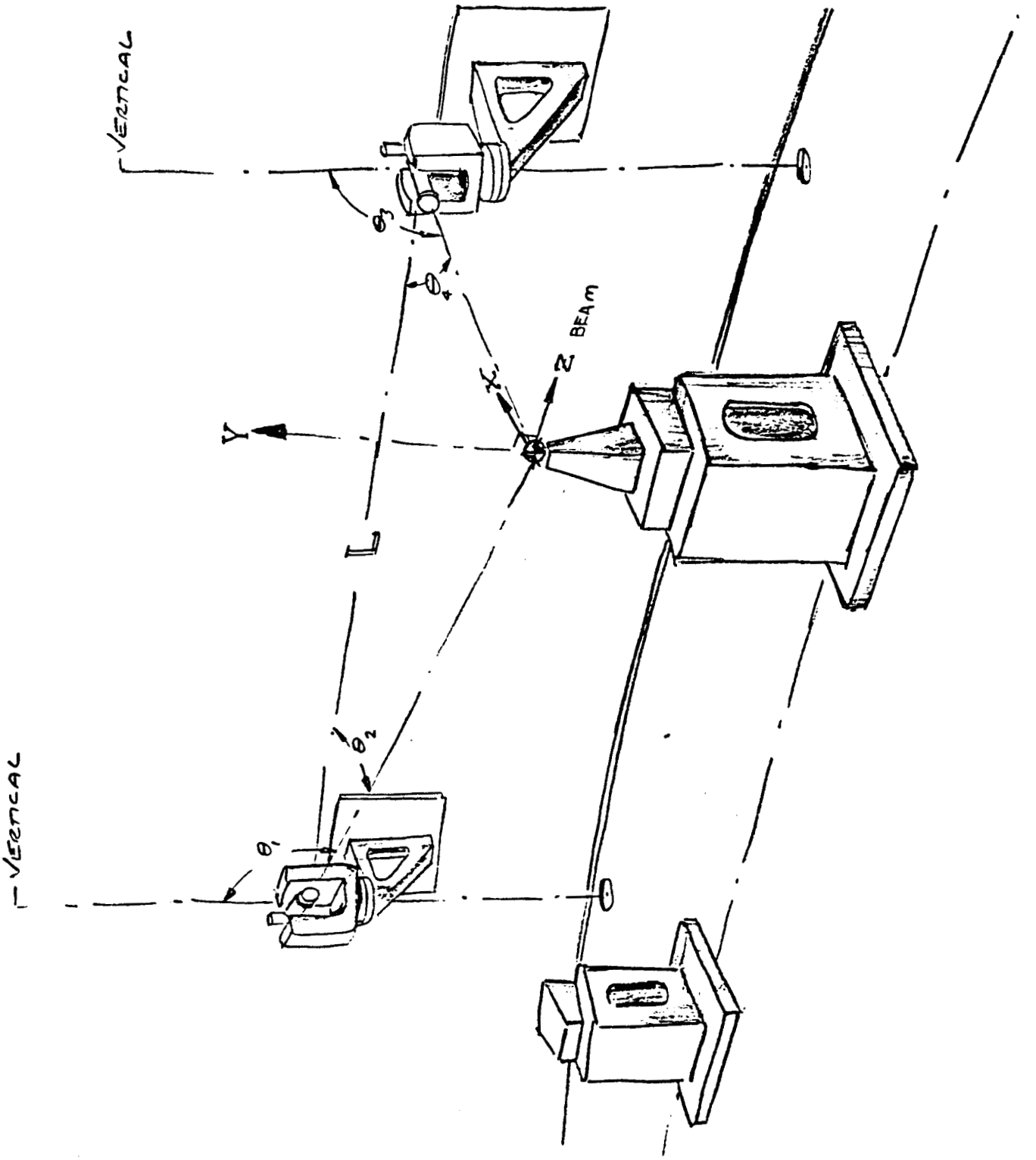

We would prefer the last alternative because of the following reasons:

- the positioning accuracy of ±3 mm can more easily be reached,
- it is only one step,
- adjustment of all three dimensions in one step,
- fewer computations are necessary,
- less time needed compared to alternative A,
- laser technique gives a saving of two operators.

8.5.1.2 Design of the Target

Design in progress.

8.5.1.3 Instruments Needed We need at least two theodolites with laser attachments. Two more would be desirable. This would allow us more flexibility, because we could then have two teams working in parallel. Furthermore, it would prevent us from having to stop our measurements if, for instance, a theodolite were to go down. The alignment laboratory does not have a theodolite which we could use to replace an E2.

For the adjustment of the pedestals we also need at least two inclinometers. Furthermore, we need targets representing the vertex point which are mounted on top of the adjustment mechanism of the pedestals, and use the support fixtures for the magnets.

8.5.2 Step 2 = Prealigning the Pedestals

The aim of this step is to align the pedestals to an accuracy of about ±0.5 mm relative to the traverse control points. This gives us an accuracy within an achromat of about ±0.8 mm.

8.5.2.1 Procedure To do this, similar methods as in step one will be used. To determine the actual coordinates Z, X, Y, of the targets on top of the

pedestals which represent the vertex point, we measure vertical and horizontal directions from the traverse points to the pedestal targets. Measurements made in accordance to a decided observation plan assuming an accuracy of ±0.5 mgon for a measured direction, results in point uncertainties within an achromat of less than ±0.5 mm. The error ellipses of this simulation for the vertex points of an achromat are shown in Fig. 8.5.4.

Then the actual positions of the targets can be corrected by the differences between the theoretical and the actual values.

From experience it is known that below the ±0.5 mm accuracy level, it is only possible to correct a position to about 20–40% of the displacement in one step. That means that two iterations might be needed to get the required accuracy.

The adjustment procedure with the precise adjustment mechanism of the pedestals will not rely on a control instrument like a transit or a theodolite, but on electronic dial gages. To keep from making corrections in the wrong direction or mixing up the adjustment screws and the respective adjustment values, proven methods will be adopted, e.g. the dial gages will be connected on-line to a computer which will verify the connection of each dial gage to the respective adjustment screw by using bar codes. Therefore the whole procedure can be controlled through a feedback loop.

8.5.2.2 Instruments Needed New instruments which we need for this step are PC-computers, electronic dial gages, interfaces, bar code equipment and custom software.

8.5.3 Step 3 = Smoothing the Magnets

The aim of this step is to get the required final accuracy. It can only be done after the magnets are mounted. The smoothing can be performed achromat by achromat, because the residuals will be so small that they will not exceed the accuracies defined for the connection of two achromats.

Figure 8.5.4 Error ellipses in alignment of pedestals.

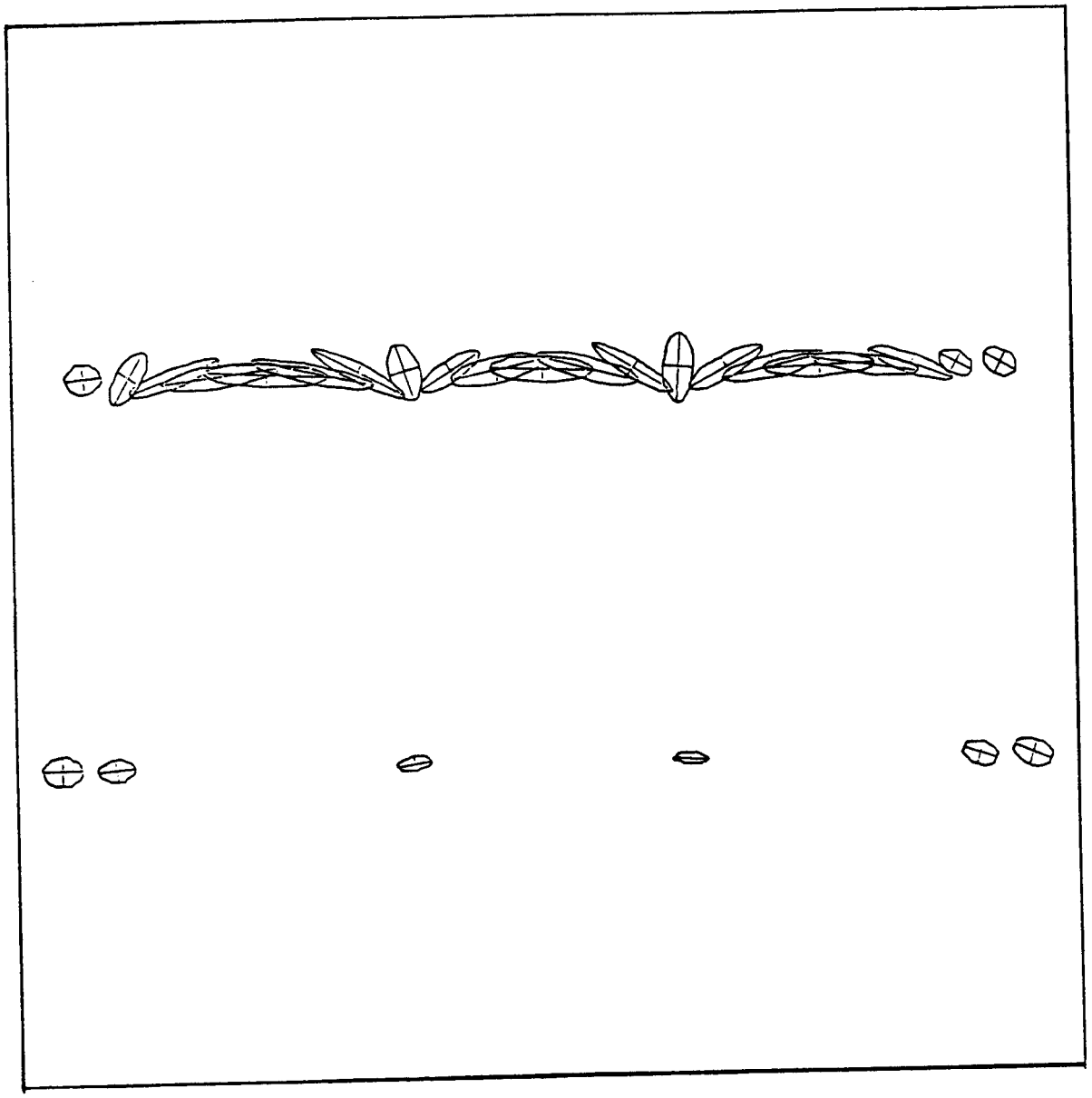

8.5.3.1 Procedure Let us assume that it will be possible to design a magnet-to-pedestal connection such that both magnet shoes rest on the same point. This connection mechanism would automatically give us the adjustment between the two neighbouring magnets. Then we have only to take care that the magnets are not positioned in sausage-link fashion, but in a smooth curve, i.e. that the sagittas of the zigzag line are not larger than the required accuracy.

To do this smoothing there are in principle two alternatives:

A. using methods such as in step 2,

B. using a method which works independently of gravity in the plane of an achromat (this coordinate system is described in section 8.1.2.2).

In both cases, we have to provide fixtures to adapt alignment tools and targets to the magnets or pedestals. If we assume the "one-point" support mentioned above, we need only one fixture for each pedestal. This fixture has to project the vertex point over the magnets and bus bars, because the vertex point itself is no longer accessible.

The differences for the design of the fixtures is that in alternative A the centering socket is to be mounted parallel to gravity and in case of alternative B perpendicular to the plane of the achromat.

The measuring procedures can be :

- Alternative Aa

  We could use in principle the same procedure as in step 2, but with an expanded observation plan, and replacement of the vertical angles by leveling. The main extension is that we have to set the theodolite above two vertex points to measure the directions and distances to the neighbouring vertex points.

- Alternative Ab

  The difference from alternative Aa is that we replace the direction measurement at the two vertex points by measuring offsets. The resulting error

Figure 8.5.5 Error ellipses for alternative Ab.

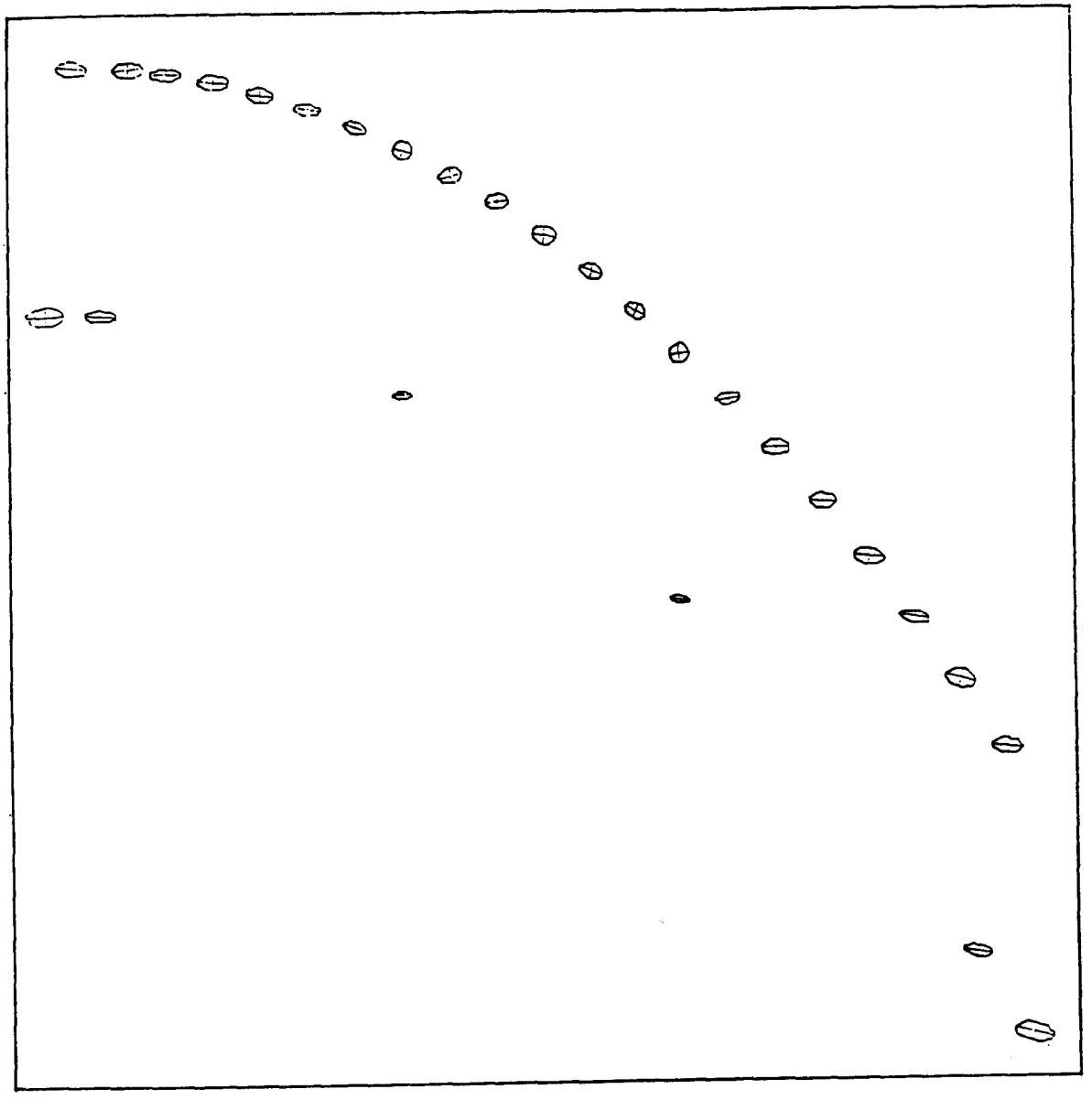

ellipses of an error propagation with such an observation plan is shown in Fig. 8.5.5.

- Alternative B

  The main difference from alternative A is that only offsets and distances and no directions will be observed. These measurements are done in the plane of the achromat. This observation plan results in error ellipses shown in Fig. 8.5.6.

We would prefer to use alternative B because it requires:

- much simpler calculations,
- simpler target fixtures,
- less time than the other alternatives

8.5.3.2 Design of the Offset-Measurement Equipment

The design of this device is still in progress.

Figure 8.5.6 Error ellipses for alternative B.

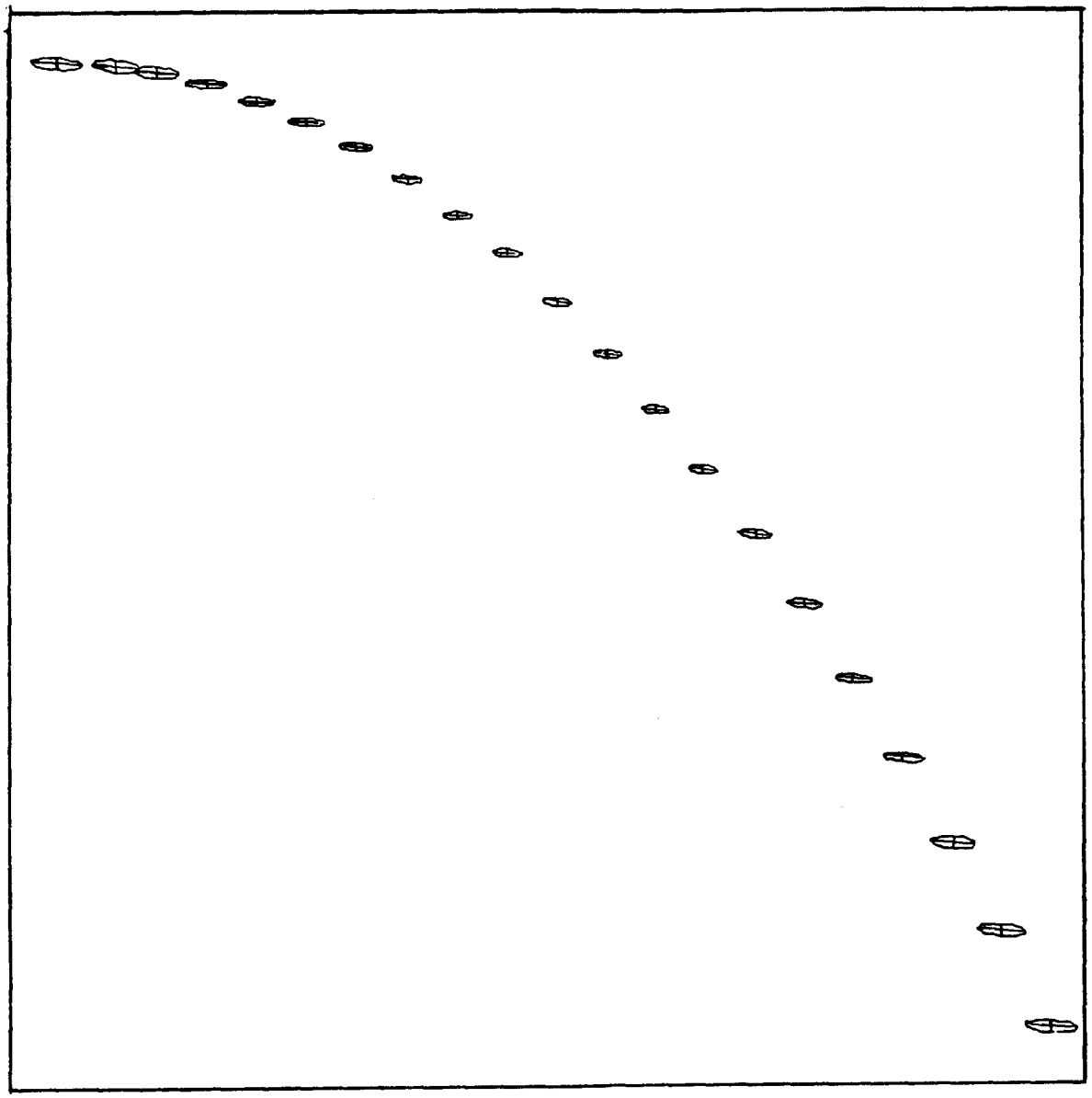

8.6. CALIBRATION

The relative precision required for installing the arc magnets of the collider is ±0.1 mm. Therefore, the distance measurements in the arc traverse must be made using the Distinvar. The standard deviation of Distinvar measurements is ±0.05 mm.

To obtain this accuracy the Distinvar must be calibrated, which means, it must be compared with a standard which has a much higher accuracy than the Distinvar itself. In this case a laser interferometer with a standard deviation of ±1 micron is used. To obtain ±1 micron the atmospheric conditions during the calibration procedure must be carefully monitored.

Figure 8.6.1 Interferometer set up for calibrations.

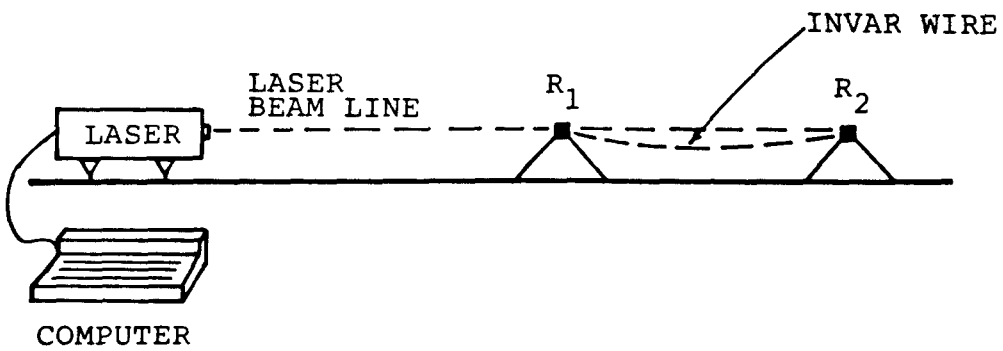

Figure 8.6.1 shows the principle of the calibration. First the distance between the laser and reflector R1 is measured with the interferometer. Similarly the distance between laser and reflector R2 is measured. The difference between these two measurements is the length of R1R2 . Then the line R1R2 is measured with the Distinvar. Finally the distances obtained, by the interferometer and the Distinvar are compared.

Figure 8.6.2 shows a modification of the system to calibrate the level rods. In this case two laser beams are used, one to measure the distance between laser and microscope, the other to measure the difference between neigbouring rod graduations. During the calibration procedure the rod rests on a support which can move it automatically. A feedback loop laser-microscope-computer-support controls the movements.

Figure 8.6.2 Using interferometer to calibrate the level rod.

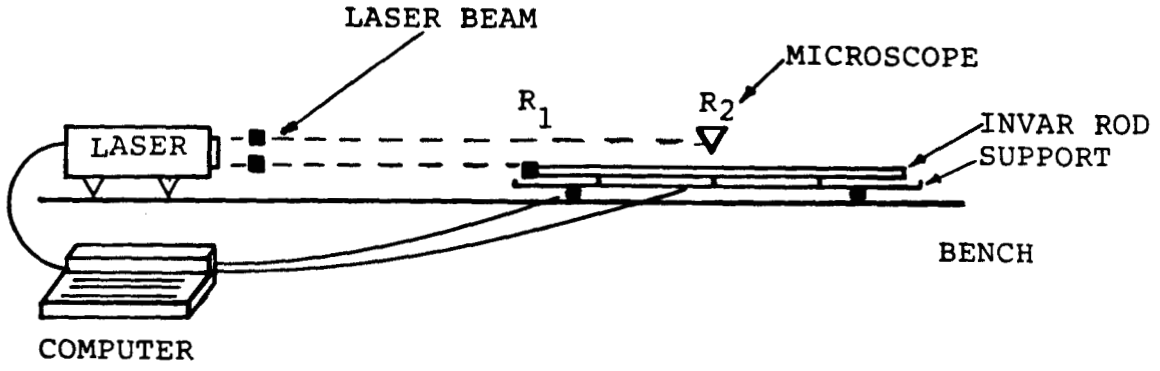

Figure 8.6.3 shows the variation of the rod graduations due to production limitations. The calibration was done at the Physikalisch-Technische Bundesanstalt in the Federal Republic of Germany. Most rods have a linear and osculating systematic error as shown in the example. For the SLC survey these variations must be taken into account to obtain the needed accuracies.

Figure 8.6.3 Data from calibration of Distinvar.

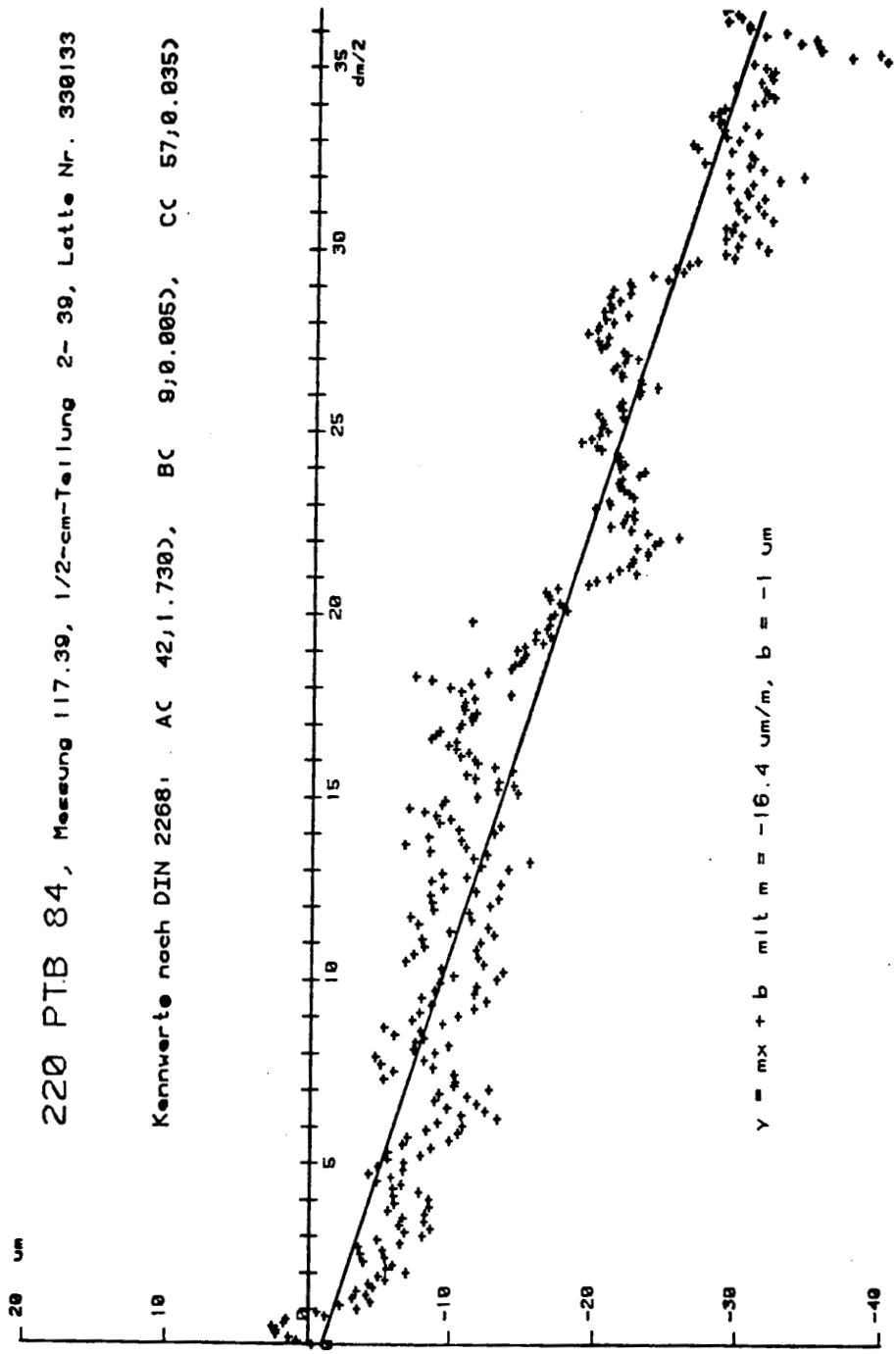

CHAPTER 9.
LUMINOSITY AND BACKGROUNDS

9. LUMINOSITY AND BACKGROUNDS

9.1 INTRODUCTION

The usefulness of the SLC as a tool for particle physics research depends ultimately on the integrated luminosity that can be provided on a reasonable time scale for the experiments. In the next section, we discuss the peak luminosity expected during the initial operation and some possibilities for improvements.

The success of the experimental program in exploiting the SLC will also depend on our success in minimizing background radiation. There are significant differences between the backgrounds expected at the SLC and those experienced at conventional storage rings. While the basic sources, beam-gas scattering and synchrotron radiation, are the same, the flux, the energy, and the duty cycle are unlike those of any previous machine. Some of the physics goals, including in particular those that require the use of small aperture precision vertex detectors, may have a significant impact on the machine design. This is discussed in Section 9.3 below.

9.2 LUMINOSITY

9.2.1 Definitions

The event rate for a process with cross section σ can be expressed as:

$$\text{Event Rate} = \mathcal{L}\sigma \quad .$$

This expression defines the luminosity $\mathcal{L}$, which is a function only of the properties of the two colliding beams and their relative orientation.

$\mathcal{L}$ is given by:

$$\mathcal{L} = \mathcal{L}_0 \, H(D) \tag{1}$$

where L_0 is the "undisrupted luminosity," and $H(D)$ is an enhancement factor due to the beam-beam pinch effect. The enhancement factor, H, is a function of the disruption parameter D. This is discussed in Section 9.2.3 below.

$\mathcal{L}_0$ can be approximated by

$$\mathcal{L}_0 = \frac{f N^+ N^-}{4\pi \sigma_x \sigma_y} \tag{2}$$

where: f = frequency of collisions,
N = number of particles per bunch,
σ = radius of gaussian beam distribution.

This expression, which is quite appropriate for describing conventional storage rings, is only a rough approximation in this case because it is based on the assumptions that the opposing bunches are gaussian and have the same dimensions (σ_x horizontally and σ_y vertically), and that the opposing bunches collide exactly head-on. A more accurate calculation of $\mathcal{L}_0$ in a linear collider requires a numerical overlap integral of the two actual beams in both space and time.

Simulation studies have shown that the two beams will generally be elliptical in transverse cross section at the IP, rather than perfectly round, and that the opposing ellipses will not necessarily be oriented the same way. This effect is a consequence of optical imperfections and misalignments in the arcs and final focus, which can, in principle, be compensated with corrector magnets. Furthermore, time-dependent perturbations will cause the beams to wander independently in space by small amounts. These imperfections will inevitably lead to some loss of integrated luminosity. The magnitude of this loss will depend on the effectiveness of the optical correction and steering systems.

9.2.2 Spot Size

The smaller the cross sectional area of the beams at the collision point, the higher will be the luminosity. In the ideal case of round gaussian beams, the radius is given by

$$\sigma^* = \sqrt{\epsilon\beta^* + (\delta\eta^*)^2} \tag{3}$$

where β and η are the standard geometrical and chromatic beam envelope functions, and the asterisk indicates the value at the IP. ϵ is the beam emittance and

$\delta = \Delta P/P$ is the momentum spread. Two optical designs are being built for the final focus: one based on superconducting quadrupoles, the other based on conventional iron quadrupoles. The first-order values for β^* for the two designs are 0.5 cm and 0.75 cm, corresponding to $\sigma^* = 1.2\,\mu$m and $1.5\,\mu$m, respectively. η^* is tuned to zero in both cases.

As discussed in Chapter 4, the beams are demagnified in the final focus system to the point where third and higher order aberrations become significant, even after the near-perfect correction for second-order chromatic aberrations. Thus, any estimate of the final spot size must include contributions from these higher order aberrations, and in practice the spot size is evaluated with ray-tracing computer simulations.

Other factors also influence the final spot size. Most significant are emittance growth in the arcs and the effects of field errors and misalignments of the various magnets. Emittance growth is caused by quantum fluctuations in the synchrotron radiation lost by the beams as they traverse the magnets. The magnitude of this effect depends strongly on the beam energy, and to a much weaker degree on the size of the beam envelope, which in turn depends on the momentum spread. Starting with a nominal value of 3×10^{-10} m rad at the end of the linac, the effective emittance at 50 GeV will grow to at least 4.2×10^{-10} m rad at the IP, slightly less in the vertical plane but more in the horizontal.

The potential effects of misalignments and field errors are impossible to describe adequately in a few paragraphs. However, simulation studies indicate that as long as the errors do not exceed the tolerances specified in Chapter 8, the resulting aberrations can be essentially eliminated, at least in principle, by proper tuning of trim and steering magnets.

9.2.3 The Pinch Effect

The electromagnetic beam-beam interaction, which has been the primary factor limiting the peak luminosity of e^+ e^- storage rings, promises to be a beneficial effect for the SLC. If the charge densities of the opposing bunches are high enough, they will experience a mutual focusing force as they pass through each other. This is best parametrized by the disruption variable, D, which can

be expressed as:

$$D = \frac{14.4\, N(\times 10^{10})\ \sigma_z\,(\mathrm{mm})}{\mathrm{E}\,(\mathrm{GeV})\ \sigma_x\,(\mu\mathrm{m})\ \sigma_y\,(\mu\mathrm{m})} \quad .$$

The resultant luminosity enhancement has been calculated by numerical simulations which follow the evolution of ensembles of macroparticles as they collide.[1] The enhancement factor is plotted in Figure 9.2.3.1 as a function of D. In this calculation, the beams were approximated by gaussian charge distributions among macroparticles moving on parallel trajectories into the collision point.

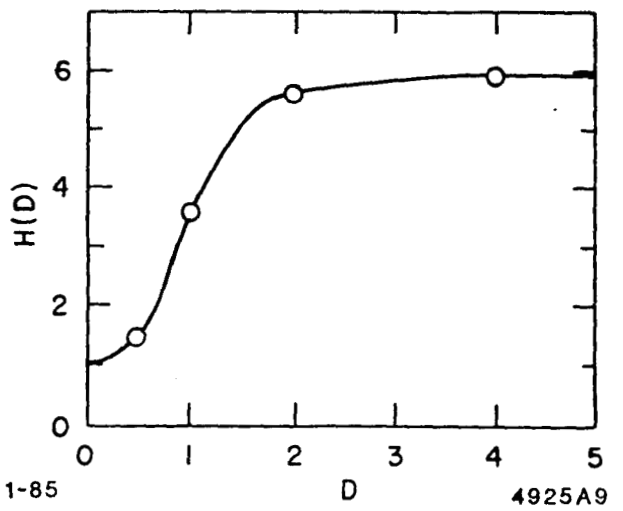

Figure 9.2.3.1

It should be noted that D is proportional to the bunch length, σ_z, and that for typical SLC specifications, the enhancement factor becomes significant only when σ_z is on the order of 1 mm or more. If the momenta of individual particles within a bunch are correlated with their z positions when the bunch enters an arc, such that the higher-momentum particles are near the head of

the bunch and the lower-momentum particles are near the rear, then the bunch will be compressed as it traverses the arc. This is because the higher-momentum particles follow a longer trajectory, giving the trailing particles time to catch up. It has been estimated[2] that with the original design specifications,[3] σ_z would have shrunk to $\sim$ 0.2 mm at the IP, effectively eliminating the enhancement effect. It has recently been pointed out, however, that the pinch effect can be restored by lengthening the bunches and reducing the momentum spread to ± 0.2 percent.[4] Both of these measures are feasible in the SLC and have been incorporated in the design.

9.2.4 Luminosity Expectations

The luminosity expected under various assumptions is summarized in Table 9.2.4.1 below. The column labeled "First Year" is based on estimates of likely conditions during the first year of operation. It is assumed, for example, that the "technical contingency" option of 120 pulses/sec operation will be invoked, and that conventional iron quadrupoles will be used in the final focus.

The second column lists the full nominal SLC design specifications. The differences between these and the earlier values listed in the SLC Design Report[3] are mainly due to emittance growth in the arcs and the effects of magnet misalignments. A useful measure of machine performance is the Z° production rate. Based on theoretical calculations, the total cross section for Z^0 production is expected to be about 30 nb at the peak. A luminosity of 6.0×10^{30} cm^{-2} sec^{-1} corresponds to about 15000 Z^0/day.

Table 9.2.4.1 Luminosity Specifications

	First Year	Nominal	Units
Beam Energy	50	50	E(GeV)
Repetition Rate	120[a]	180	$f(\text{sec}^{-1})$
Interaction Flux	5×10^{10}	7.2×10^{10}	$N^{\pm}(\text{e}^{\pm}/\text{bunch})$
Normalized Emittance (at RTL)	3×10^{-5}	3×10^{-5}	$\gamma\epsilon$(m rad)
Effective Emittance (at FF)	4.2×10^{-10}	4.2×10^{-10}	$\epsilon_{x,y}$(m rad)
Momentum Spread	± 0.2	± 0.2	$\frac{\Delta P}{P}$ (percent)
Bunch length (linac)	1.5	1.5	σ_x(mm)
Bunch length (IP)	1.0[b]	1.0[b]	σ_z(mm)
Final Demagnification	$\times 4$[c]	$\times 5$	
Spot Size (IP)	2.07	1.65	$\sigma_{x,y}$ (μm)
Disruption Parameter	0.34	0.76	D
Pinch Factor	1.14	2.2	H
Luminosity	6.4×10^{29}	6.0×10^{30}	$\text{cm}^{-2}\ \text{sec}^{-1}$

(a) Assumes technical contingency exercised initially.

(b) Assumes σ_z compression in arcs due to p/z correlation.

(c) Assumes conventional iron quadrupoles initially.

9.3 BACKGROUNDS This section is not yet ready for distribution.

REFERENCES

1. R. Hollebeek, Nucl. Inst. and Methods **184** (1981) 333; CN-39 (1981).

2. A. Chao and Y. Kamiya, CN-218 (1983).

3. *Stanford Linear Collider Conceptual Design Report*, SLAC, June 1983.

4. R. Stiening, SLC Parameters Committee meeting of 9 January 1985.

CHAPTER 10.
EXPERIMENTAL USE

This chapter is not yet ready for distribution.

CHAPTER 11.
CONVENTIONAL FACILITIES

11. CONVENTIONAL FACILITIES

11.1 SITE

The experimental hall will be situated on the western side of a steep sidehill at the eastern end of the SLAC site hidden from view of the nearby residences; its site preparation will require the excavation of a rather large volume of earth.

The project's site work includes provisions for earthquake protection and for the disposition of excavated material from the hall and beam housings. It also includes landscaping, roads, fencing, drainage systems, permanent and temporary construction yards, parking areas, and the construction of a large sight beam at the north tunnel access way. There will be an underground duct bank for 12 kV power and a sanitary sewer to serve the experimental hall. (Other utilities will be transported in beam housings.)

11.1.1 Earthwork

About 129 000 cu m of earth will be excavated from the site of the experimental hall of which 15 000 cu m will be replaced as backfill. The balance will be used for construction of shielding fills or shaped into stockpiles contoured to blend into the landscape. All new earthwork surfaces will receive erosion control treatment and landscaping.

11.1.2 Road

Only one permanent road, providing access to the experimental hall, will be required by this project. It will run from an intersection with the PEP loop road south of PEP's Region 2 buildings to the experimental hall and will be designed for heavy loads.

11.1.3 Fences

It will be necessary to include the experimental hall within SLAC's radiation security boundary. Therefore, a standard radiation fence will be constructed to enclose the hall and its access road. In addition, the fence across the Alpine access road will also be relocated to the south.

11.1.4 Yards and Parking

A yard will be provided at the experimental hall. It will have to remain clear at most times as it will be used primarily as a turnaround for vehicles. A contractor's construction yard will be provided, south of the collider hall access road. Small yards may prove to be necessary at drainage shafts.

11.1.5 Landscaping

The hall site, road and new land surfaces resulting from the construction will be suitably landscaped. Oak tree plantings to match the natural landscape will predominate.

11.1.6 Utilities

A concrete-encased duct bank for permanent 12.47 kV power and temporary 480 V construction power will be provided. This bank runs cross country from sources in the research yard to the hall. Construction power on temporary poles will be provided to drainage shafts, working tunnel portals and the construction yards. This overhead system will be removed as soon as permanent power distributed underground is functioning.

11.1.7 Sanitary Sewer

A sanitary sewer to serve the experimental hall will require an annexation to the Menlo Park Sanitary District. The new connection will run to the existing sewer along Sandhill Road.

11.2 TUNNELS (BEAM HOUSINGS)

From the point where the two arcs depart from the beam switchyard, the two limbs comprise runs of about 1432 m (north) and 1450 m (south) to the interaction point at the eastern side of the SLAC site (see Fig. 11.2.1). The north run will be entirely through mined tunnels to the interaction area. A portion of the south run adjacent to the Alpine Road entrance will be constructed by cut-and-cover methods. Alluvial deposits and poor ground water conditions make mined tunneling inadvisable, if not infeasible, in this area. The remainder will be mined tunnels deep underground.

The size and orientation of the ring layout are guided by the following considerations:

1. Maximum radii of arcs consistent with good beam quality.
2. Site-boundary limitations.
3. Need for a difference of 17.6 m in the lengths of the beam paths to the interaction point.
4. Terrain, particularly in regard to the experimental hall site.
5. Distance on each side of the interaction point necessary for final focusing.
6. Maintenance of 5 m of earth shielding in those areas where the beam is outside the SLAC radiation fence.

Lengths of beam runs and types of construction are shown on the profiles of the north arc (Fig. 11.2.2) and the south arc (Fig. 11.2.3).

The various types of beam housings are summarized as follows:

In existing structures	100 m
Cut-and-cover construction	135 m
Mined tunnel construction	2680 m
TOTAL	2915 m

It is intended that the beam housings be subcontracted separately from the hall. As presently conceived the tunnel is 10 ft high $\times$ 10 ft wide, horseshoe

shaped, having a concrete floor slab and shotcrete walls.

That portion of the work involving the connection of the SLC tunnels to the beam switchyard will be scheduled to minimize interference with SLAC's operations programs.

As a design policy it has been decided to mount most of the services associated with the beam components directly on the support elements of the prefabricated magnet-lattice assemblies, with connection features between assemblies. This will limit the amount of services to be supported by the structure of the tunnel itself to cooling-water piping, telephone conduits, etc. At intervals throughout the beam housings provision will be made for ac power and I&C panels so that field connections between tunnel-supported services and beam components will be held to a minimum. This should result in simplified tunnel construction and rapid component installation work.

Access to the beam housings will be made via two tunnels with portals adjacent to PEP IR's 4 and 12 descending at grades of 8% to meet the housings, as shown in Fig. 11.2.1. Their positions dictate that the aisles shall be at the inner sides of the housings.

Drainage water from the low points will be pumped up shafts at the north and south extremes of the arcs.

As there are considerable elevation differences in the housings, convection forces should ordinarily suffice to provide ventilation, with exhaust shafts at high points and intakes at the low. However, supply and exhaust fans will be provided to reduce heat problems. Ventilation control for fighting fires may be necessary.

Housings for underground beam dumps will be constructed as part of the tunnel work at points 100 m to 120 m north and south of the experimental hall. Space necessary for pumps and other mechanical equipment will be provided on a concrete pad north of the hall.

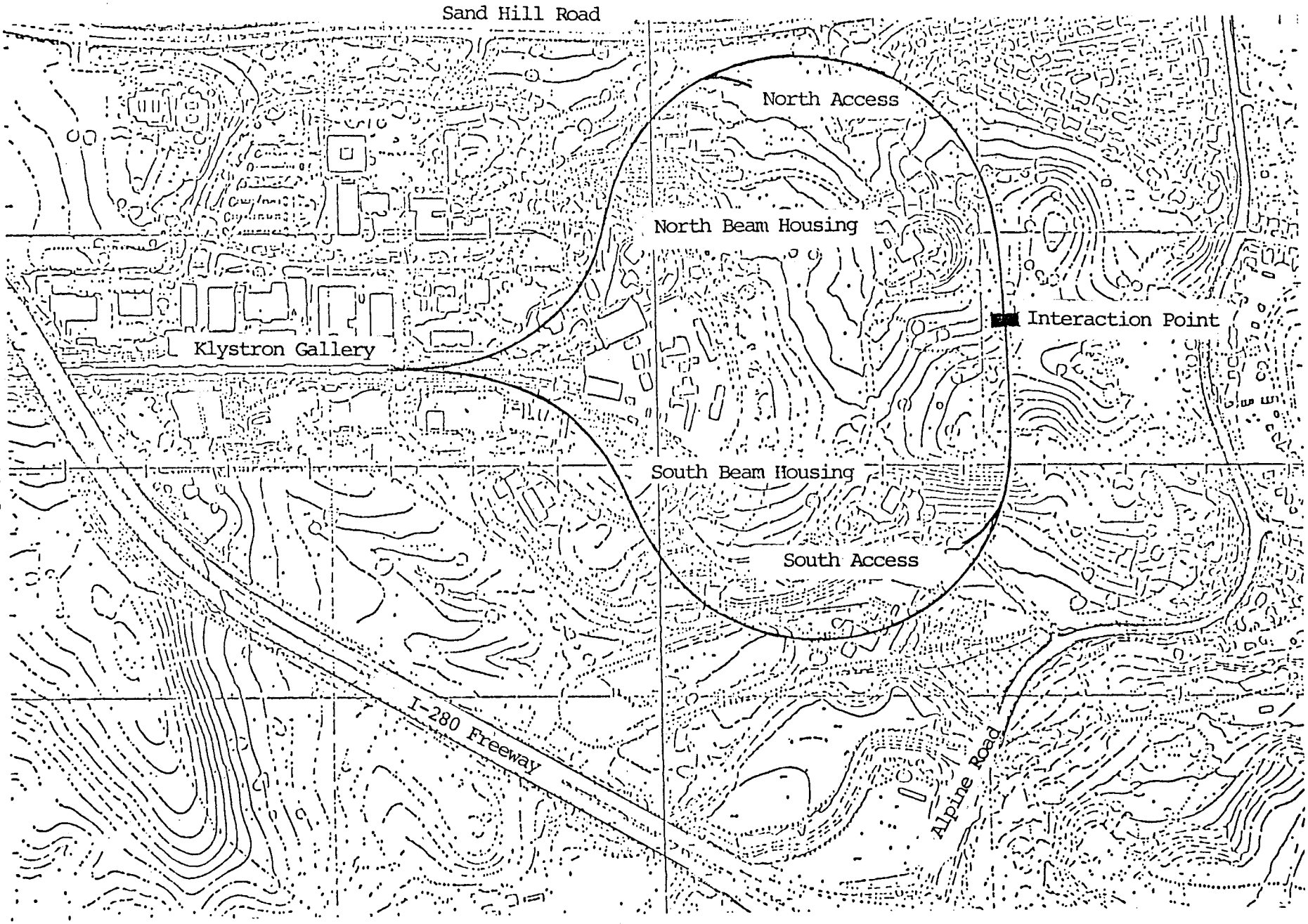

Figure 11.2.1 SLC Layout

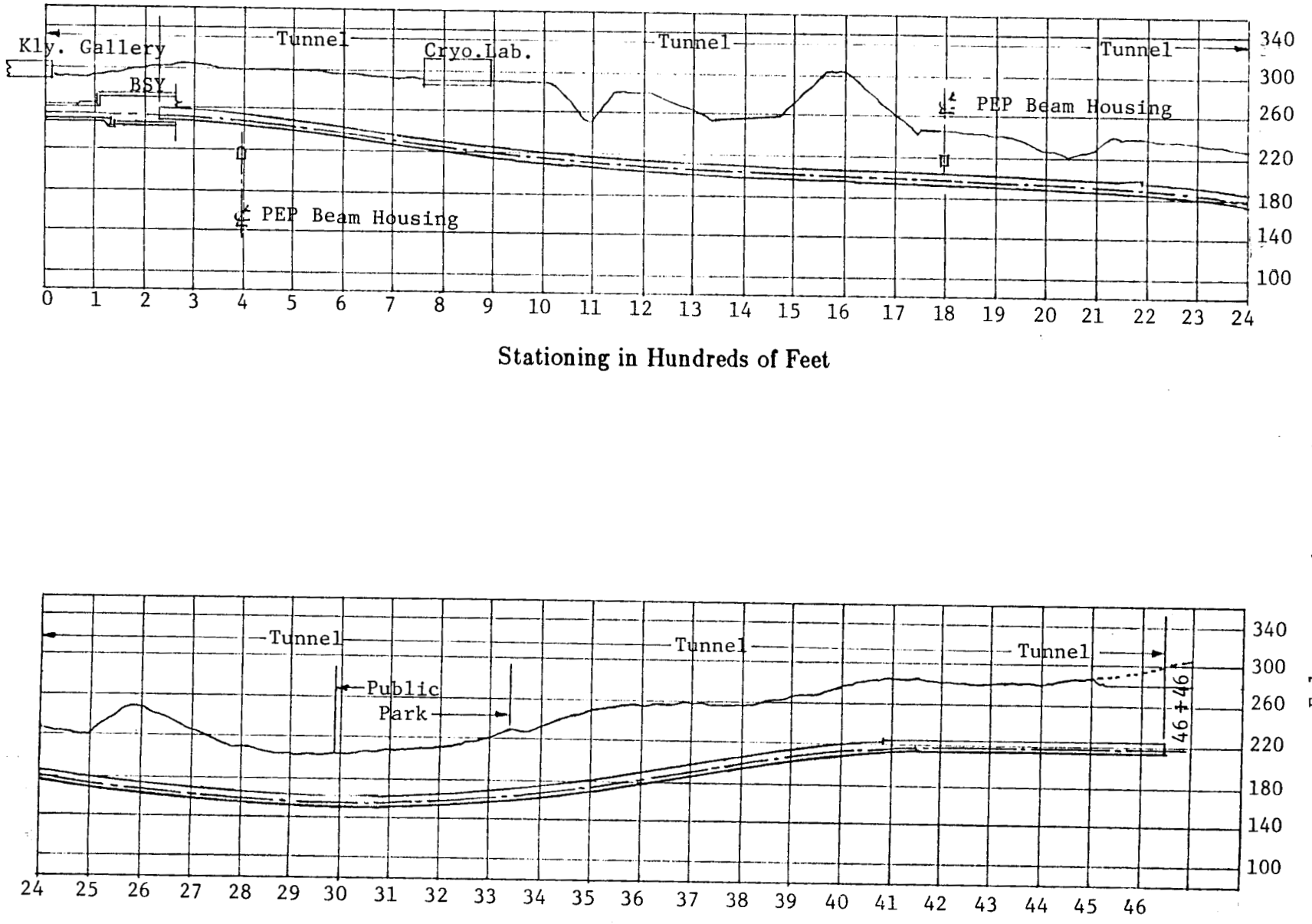

Figure 11.2.2 Profile of North Arc Tunnel

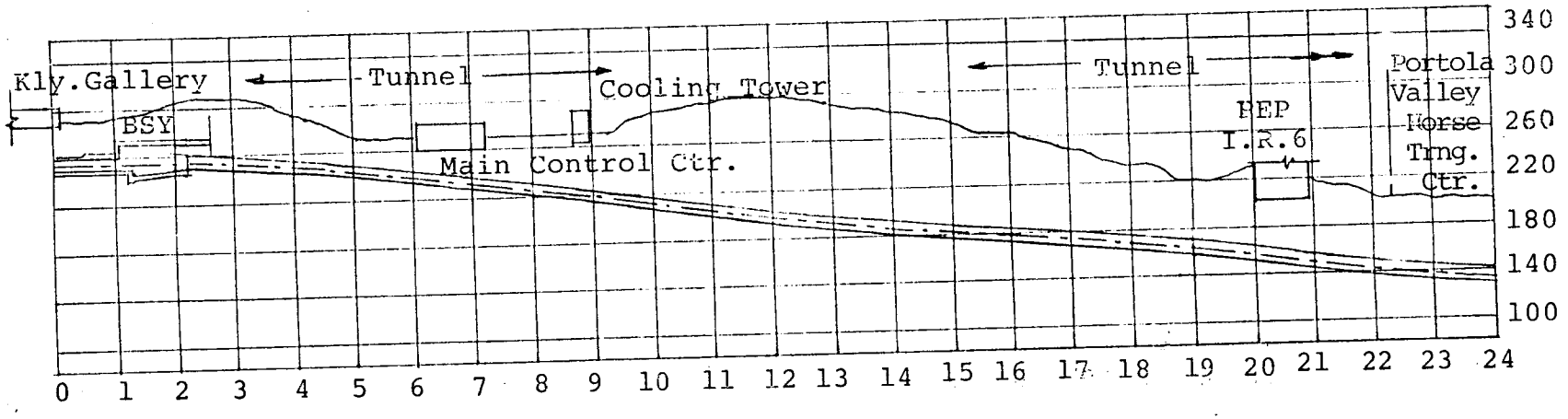

Stationing in Hundreds of Feet

Elevation in Feet

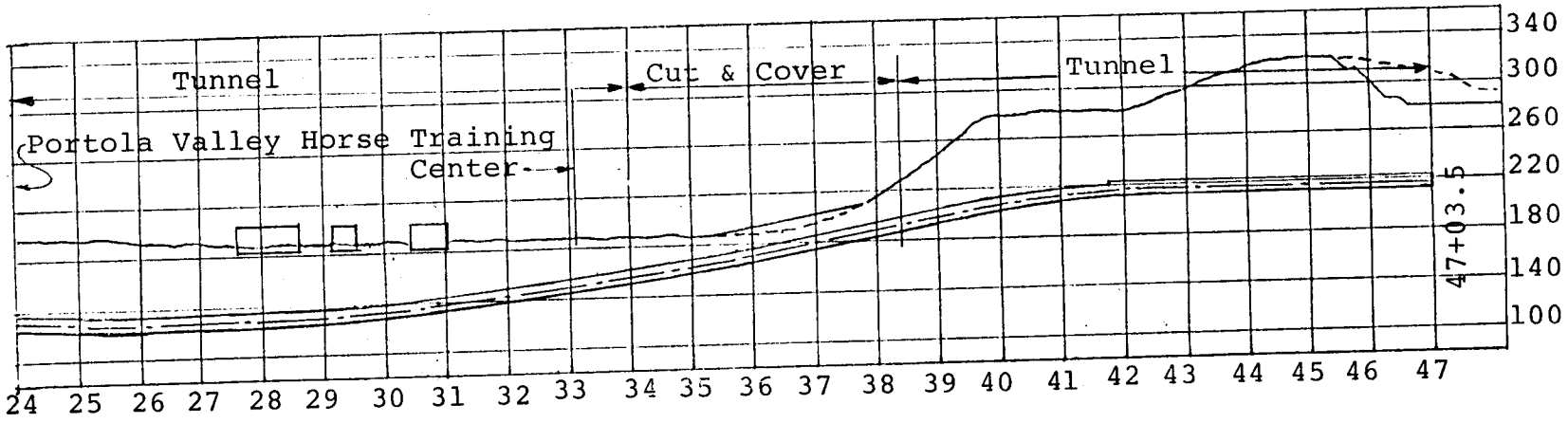

Figure 11.2.3 Profile of South Arc Tunnel

11.3 CONTROL ROOM

The SLC will operate as an extension of the existing SLAC Linac, and its functional integrity is vitally dependent on the operating characteristics of the entire length of the accelerator. Its control facilities must, therefore, be very closely linked with SLAC's Main Control Center. A new control room building with a floor area of 2500 sq ft has been added to the MCC building for the purpose. The entire area is devoted to control equipment and operating personnel space. Communications links with the experimental hall will be made via the collider's beam housings. Figure 11.3.1 shows the as-constructed control room.

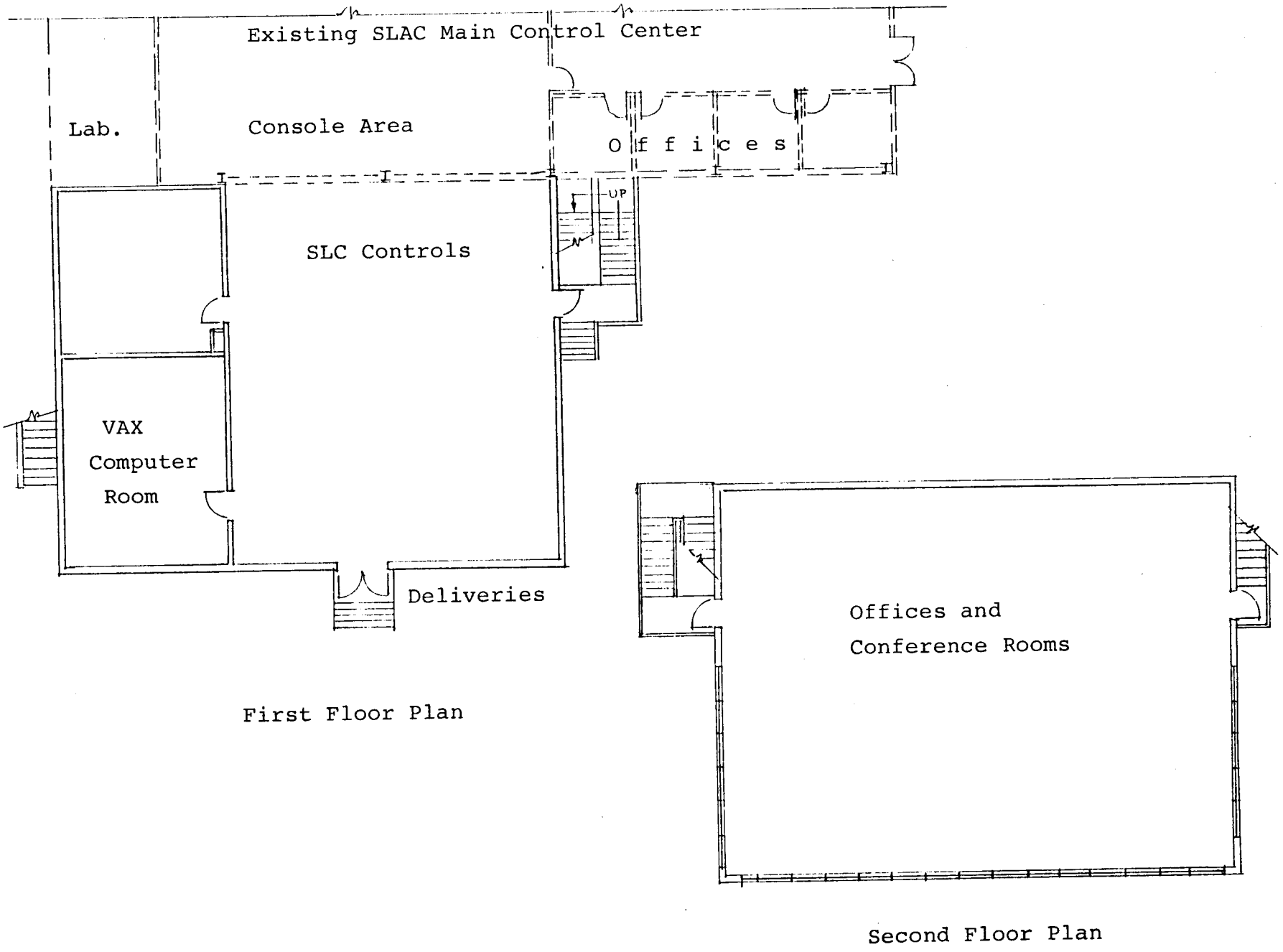

Figure 11.3.1 SLC Control Room

11.4 DAMPING RING VAULT

The two damping rings and their associated RF equipment are assembled in reinforced concrete underground vaults near the end of the linac's Sector 1. Sites immediately north and south of the roadway paralleling the klystron gallery were chosen to provide the simplest beam runs between the linac and the damping rings. Each vault has a floor area of 12 × 16 m with an equipment access shaft large enough to accommodate the magnets and other components. At present, two tunnels are provided to connect the accelerator housing with each vault. Figure 11.4.1 shows one of the damping ring vaults prior to ring installation. Each vault is shielded by earth overlying it. The access shafts are shielded by concrete blocks. Ready access to the vaults during linac operation is provided by a stairway located in the shafts. Forced ventilation is provided via the accelerator housing. Power and mechanical services are supplied from the klystron gallery.

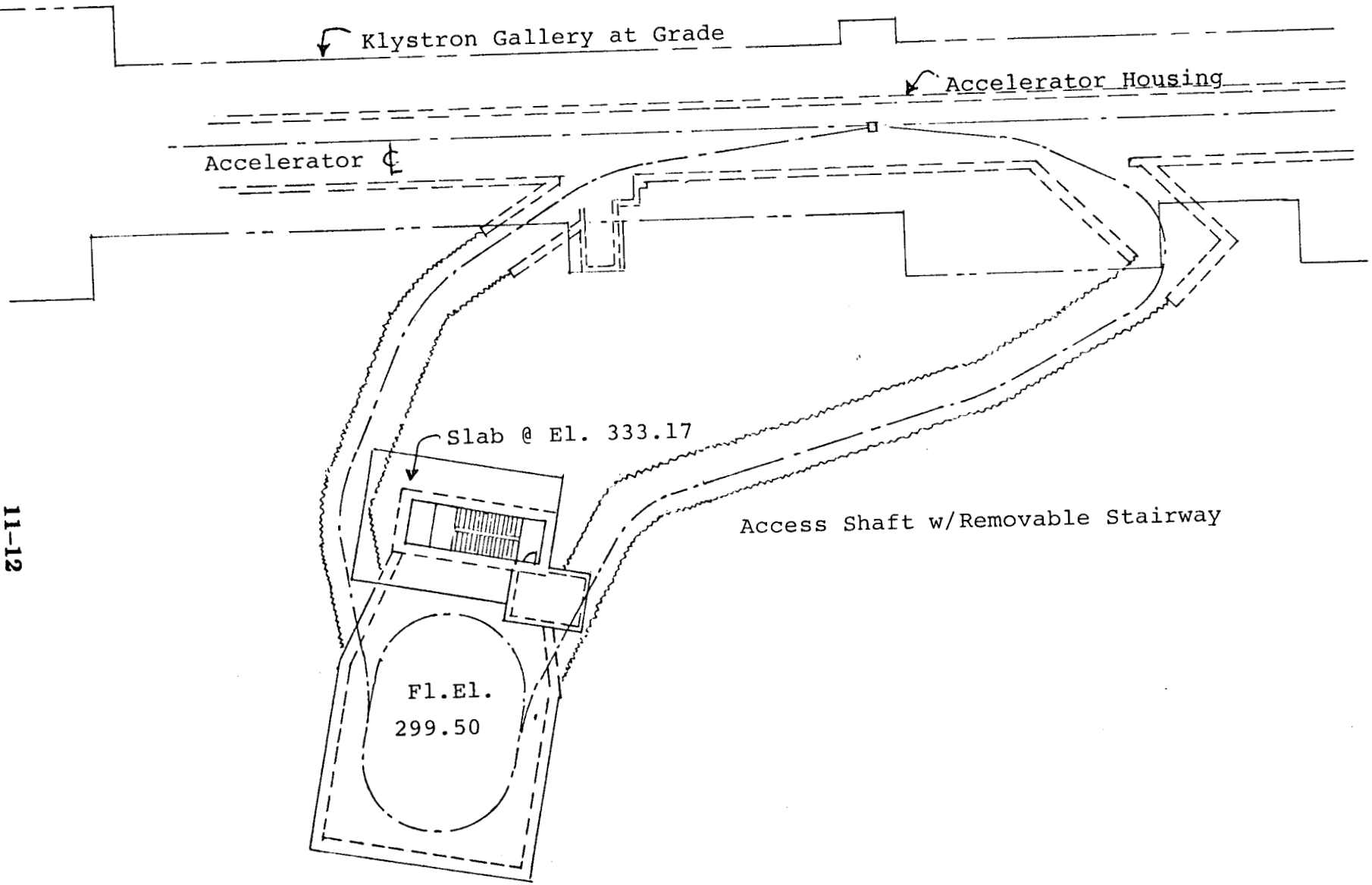

Figure 11.4.1 Damping Ring Vault (south)

11.5 COLLIDER EXPERIMENTAL HALL

11.5.1 General Principles

The experimental hall and the support and assembly building are shown in Figure 11.5.1. In arriving at this design, many different conceptual designs were analyzed and compared on the basis of costs, gain in beam utilization time, and flexibility. Consideration was given to one versus two vaults as well as ground level access versus deep pit construction. The deep pit, single interaction region, push-pull design was chosen primarily on cost considerations. The design has been executed in such a manner that, should the physics warrant it, the hall could be easily modified to include a second experimental vault.

The size and facilities of the experimental building allow the simultaneous construction, testing and maintenance of two large and complex detectors. While one detector is taking data in the interaction vault, the other detector can be constructed, be fully tested and kept operational in its assembly area. This includes keeping all electronic and cryogenic systems operational. This capability is obtained by having two separate and complete control rooms and having sufficient space for conventional and cryogenic utilities.

To minimize beam downtime, it is intended that a detector can be moved out of the interaction region vault in about a week, and that the other detector can be moved into the vault and made operational within an additional two to three weeks. This short downtime is obtained by bringing a detector to its fully operational state in its assembly area. It is then transported as a unit into the interaction region vault with most signal cables intact. It may be necessary to disconnect and reconnect major power, cooling, cryogenics, and vacuum lines.

11.5.2 Interaction Hall

Figure 11.5.2.1 shows a detailed layout of the interaction region hall. It consists of a steel frame building covering a pit 17 m deep having dimensions of 71 m in the east-west direction and 19 m in the north-south or beam line direction. The detector pit is designed with thin concrete walls supported by permanent solid anchors pretensioned to resist the expected static loads plus

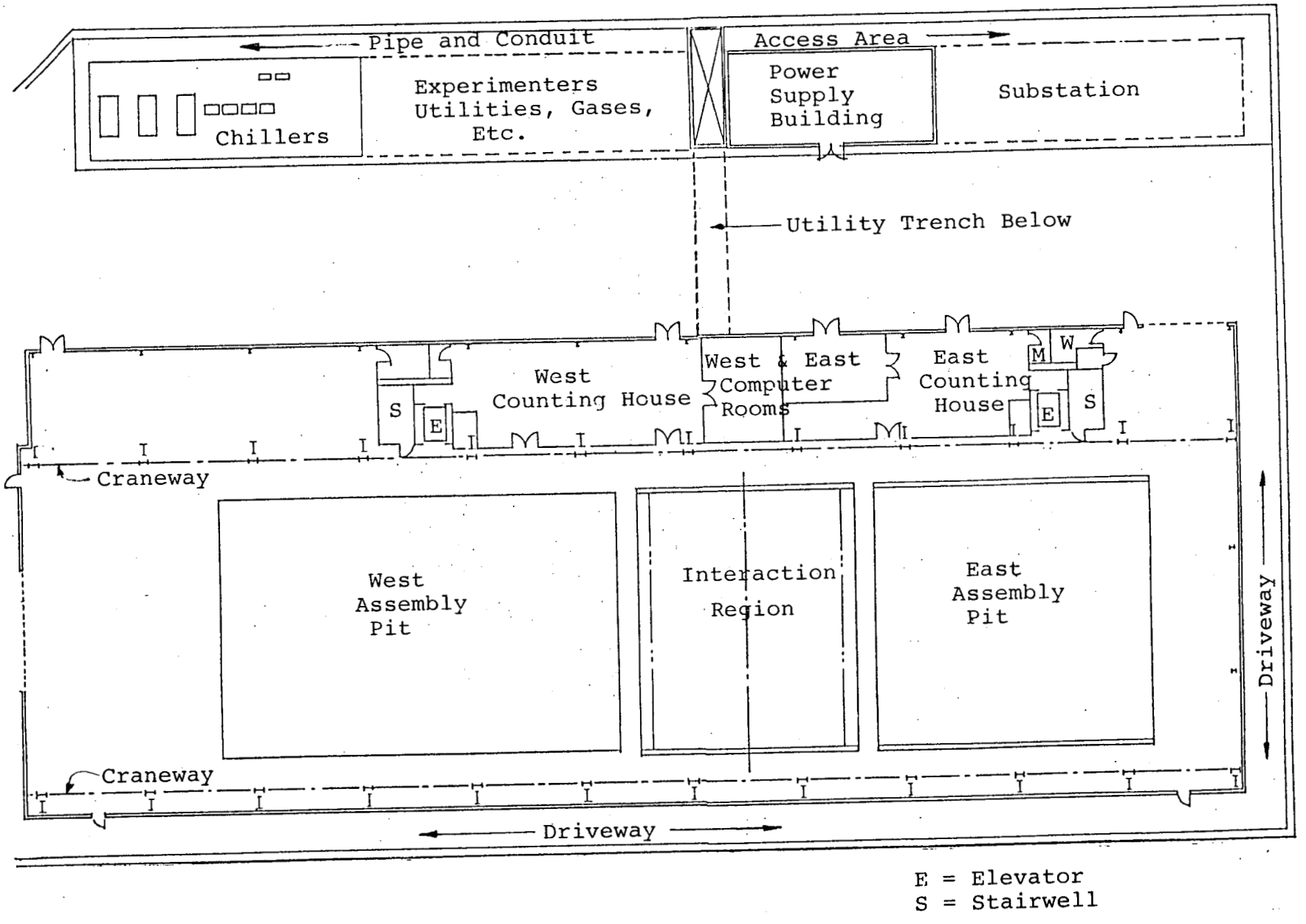

Figure 11.5.1.1 Experimental Support Facilities

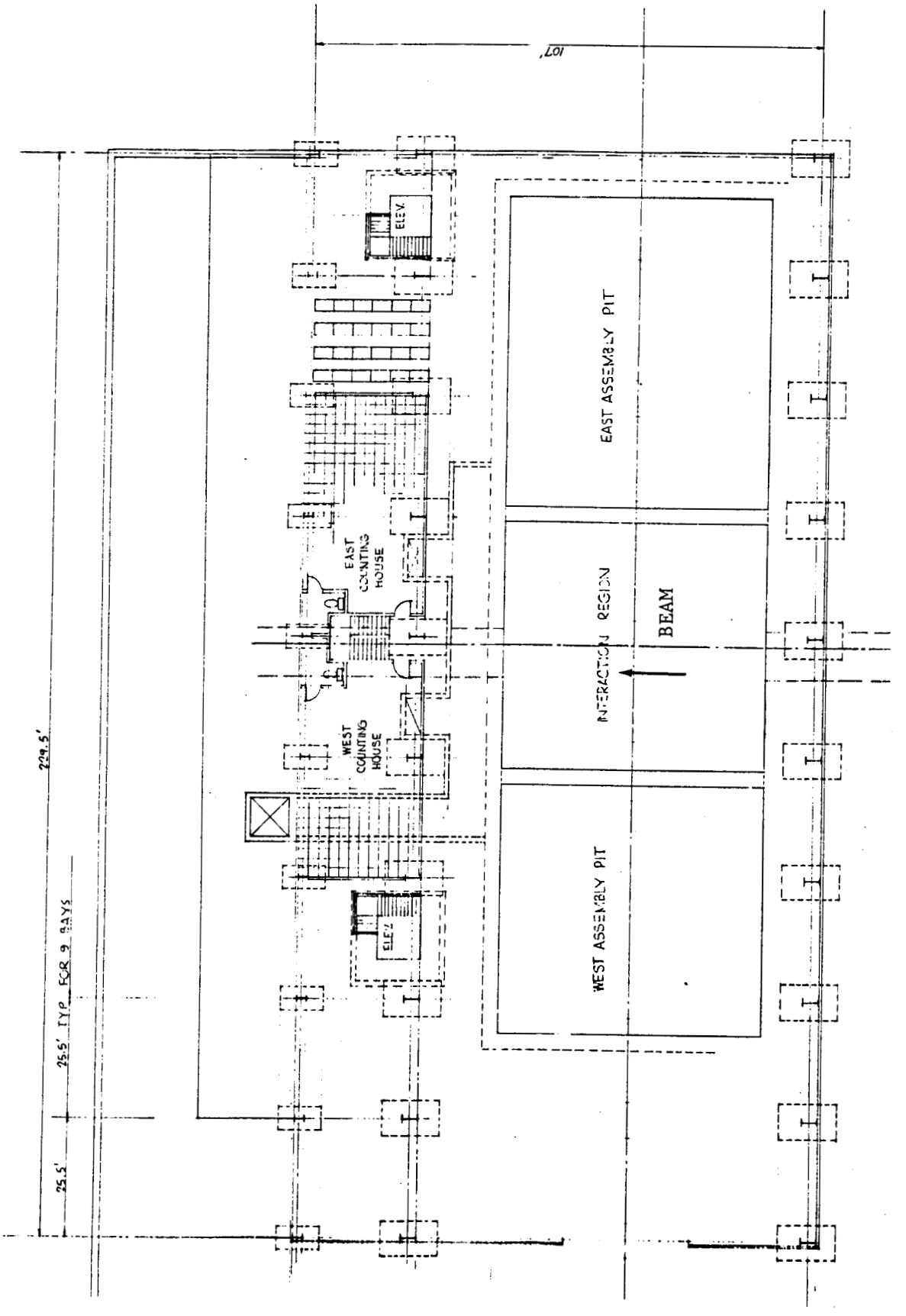

Figure 11.5.2.1 Floor Plan of SLC Interaction Hall

the seismic forces produced by a Richter 8 earthquake. The pit is divided into three separate areas by two shielding walls: the east assembly area having dimensions of 23 m $\times$ 19 m, and the experimental vault having dimensions of 16 m $\times$ 19 m including 2 m for the east and west shielding walls, and the west assembly area having dimensions of 32 m $\times$ 19 m. The floor of the pit is located 5.5 m below beam line, and is 0.6 m thick reinforced concrete.

Crane coverage of both assembly areas and the experimental vault is by a 100 ton crane at the upper level. In addition, there will be a high-speed 10-ton hook for smaller lifts. The design of the crane rails is such that a second crane of up to 50 ton capacity can be added in the future.

The three-floor steel frame building is shown if Figure 11.5.2.2. It contains two complete counting houses with independent computer facilities and lab space. Areas near the center of the building, on the second floor, directly above the tunnel, will be reserved for accelerator physics development work, and for instrumentation electronics for the final focus.

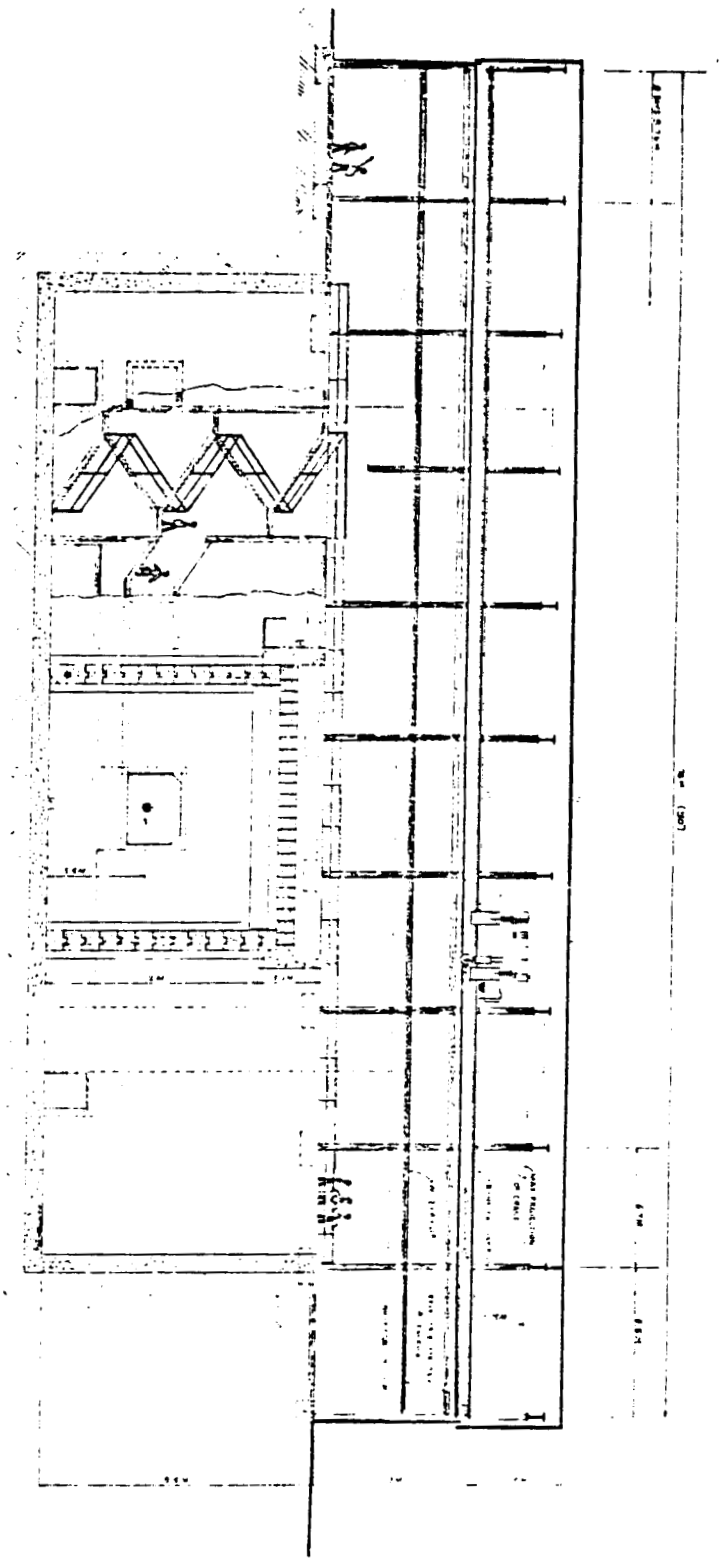

Figure 11.5.2.2 Vertical Cross Section of SLC Interaction Hall.

CHAPTER 12.

This chapter is not yet ready for distribution.

CHAPTER 13.

This chapter is not yet ready for distribution.

CHAPTER 14.
SUMMARY OF PARAMETERS

Parameters below are specified for operation at 50 GeV per beam.

14.1 General

Repetition Rate	120/180	sec^{-1}	(Initial/Nominal)
Beam Energy	50	GeV	
Energy Difference ($e^+ - e^-$)	$< 3\%$		
Momentum Spread ($\Delta E/E$)	$\pm 0.2\%$		
Invariant Emittance ($\gamma\epsilon$)	3×10^{-5}	rad m	

14.2 Electron Source

Flux at gun	1×10^{11}	e^-/bunch
Pulse width	2.5	nsec
Emittance at S1 ($\gamma\sigma_x\sigma_{x'}$)	3×10^{-4}	rad m
Buncher Frequency	178.5	MHz
Energy at BAS-1	200	MeV
Bunch Length	15	ps

14.3 Positron Source

Scavenger e^- Energy	33	GeV
Positron Yield @ target	2.5	e^+/e^-
Return Line Energy	200	MeV
Emittance ($\gamma\sigma_x\sigma_{x'}$)	0.01	rad m
$\Delta p/p$ @200 MeV	$\pm 5\%$	
Bunch length (σ_z)	± 7	ps

14.4 Damping Rings

Beam Energy	1.21	GeV	
Circumference	35.27	m	
Revolution Frequency	8.50	MHz	
RF Frequency	714	MHz	
Transverse Damping Time	3.1	msec	
e^+ Storage Time	16.7/11.11	msec	(Initial/Nominal)
e^- Storage Time	8.3/5.56	msec	(Initial/Nominal)
Emittance Out ($\gamma\epsilon$)	3×10^{-5}	rad m	
Bend Field	19.812	kG	
Bend Radius	2.0372	m	
Energy Loss/Turn	93.1	keV	
Power (Synch. Rad.)	12.68	kW	
Acceptance	4.2×10^{-6}	π rad m	
Betatron tune (x;y)	7.2; 3.2		

14.5 Linear Accelerator

Number of Klystrons	240	
Peak Voltage	315	kV
Peak Output Power	50	MW/klystron
ac Input Power	158	kVA/klystron
RF Frequency	2856	MHz
Modulator Pulse Width	6	μsec
RF Pulse Width	5	μsec
SLED II Pulse Width	0.8	μsec
Bunch Spacing	59.00	nsec
Accelerating Gradient	17	MeV/m

14.6 Arcs

Number of AG Magnets	940	
Effective Magnet Length	2.503	m
Bending Radius	279.378	m
Number of Magnets per cell	2	
Number of Magnets per Achromat	20	
Cell Length	5.192	m
Phase Shift per Cell	108°	
Magnet Current	3982	amps/pole
Field at 50 GeV	5.986	kG
Gradient at 50 GeV	7.014	kG/cm
Average Vacuum	1×10^{-4}	torr
Aperture	7	mm
dc Power	1.65	kW/magnet

14.7 Final Focus

Equivalent Emittance	4.3×10^{-10}	rad m	
Bunch Length	1.0	mm	
First Telescope			
Horizontal Demagnification	$\times 8.5$		
Vertical Demagnification	$\times 3.1$		
Intermediate Focus σ	$6.0\,\mu$m		
Chromatic Correction Section			
Hard-bend Field	12.5	kG	
Soft-bend Dipole			
Bend Angle	0.91	mrad	
Field	500	Gauss	
$E_{crit.}$	83	keV	

Final Telescope	Initial	Nominal	
Drift Length (L*)	9.25	7.25	ft
Quadrupoles	Conventional	Superconducting	
Clear Aperture	1.555	1.65	inches
Gradient	4.8	12.0	kG/cm
Demagnification	$\times 4$	$\times 5$	
β^*	0.75	0.50	cm
First Order Focus	1.5	1.2	μm
Vacuum	2×10^{-9}		torr

Extraction		
Momentum Pass	$\pm 3.0\%$	
Angular Acceptance at IP	± 2.2	mrad

CHAPTER 15.
PUBLICATIONS

15.1 BIBLIOGRAPHY

15.2 INTERNAL AATF NOTES

15.3 COLLIDER NOTES

15. PUBLICATIONS

15.1 BIBLIOGRAPHY

1. Conceptual Design Report 1982, SLAC-Report-229, June, 1980.
2. Proceedings of SLC Workshop, SLAC-Report-247, March, 1982.
3. PEP Design Handbook, SLAC (May, 1977).

15.2 INTERNAL AATF NOTES

AATF1	Feedback Compensation of Space Charge Forces in the Linac–Collider	R. Stiening	7/79
AATF2	Present Status of Linac–Collider Studies	R. Stiening	8/79
AATF3	Conceptual Design of a Linear Colliding Beam System to Reach 100 GeV in the Center-of-Mass	B. Richter	8/79
AATF4	Ideas on Linacs for Colliding Beams (I)	G. Loew	8/79
AATF5	Comments on a Single Pass Collider Ring Magnet	G. E. Fischer	8/79
AATF6	Phase Space Stability of the SLAC Linac	R. Stiening	9/79
AATF7	Remarks on Some Tolerances for the Linear Colliding Beam System	H. Wiedemann	9/79
AATF8	Some Remarks on the Parameters of a Damping Ring for the Linac Collider Project	H. Wiedemann	9/79
AATF9	Beam Emittance in a Fodo Structure for the Linac Collider	H. Wiedemann	9/79
AATF10		M. Allen	
AATF11	A Possible Scheme to Compress the Bunch Lengths for the Linac Beam Collider	H. Wiedemann	9/79
AATF12	Energy and Luminosity of the Collider	H. Wiedemann	9/79
AATF13	Steady State Distribution for Unbunched Beams Colliding in a Drift Space	S. Kheifets A. Chao	12/79
AATF14	A Beam–Beam Simulation for the SPC	R. Sah	2/80
AATF15	Energy Loss and Wall Heating for a Gaussian Bunch in a Cylindrical Pipe	P. Morton P. Wilson	11/79
AATF16			
AATF17	Misalignment Tolerances for the SLC Transport Ring	D. Ritson	2/80
AATF18	Some Comments on Ground Motion	G. Fischer	3/80

AATF19	"Beam–Strahlung" in the Single Pass Collider	R. Sah	3/80
AATF20	300 GeV from SLAC: Single–Bunch Accelerator Using Energy Storage Cavities	P. Wilson	4/80
AATF21	Beam Emittance Growth Caused by Transverse Deflecting Fields in a Linear Accelerator	A. Chao	4/80
AATF22	Beamstrahlung	J. Jaros	5/80
AATF23	Disruption Limits for Linear Colliders	R. Hollebeek	6/80
AATF24	The SLAC Linear Collider	B. Richter	6/80
AATF25			
AATF26			
AATF27			
AATF28	Polarized Electrons in the SLC	R. Stiening	8/80

15.3 COLLIDER NOTES

CN–1 to CN–10	Index of Collider Notes (CN)		
CN–11	Shielding for the Collider	J. Harris	1/18/80
CN–12	The Magic Beam Bump	R. Stiening	1/25/80
CN–13	Compressor–Parameter (Use for Budget Only)	H. Wiedemann	2/7/80
CN–14	Sampled Feedback in the Linac Collider	R. Stiening	2/11/80
CN–15	A Note on Shielding for the SPC	T. Jenkins	2/26/80
CN–16	Wake Functions for the SLAC Linac	P. Wilson K. Bane	2/28/80
CN–17	A Possible Trajectory Correction Scheme	A. W. Chao	2/28/80
CN–18	Energy Spectrum of Collider Beam After Collision	H. DeStaebler	2/28/80
CN–19	Effects of Momentum Dispersion in the Linear Accelerator	R. Stiening	3/4/80
CN–20	The Effects of Wake Fields in the Collider Arc Vacuum Pipe	R. Stiening	3/13/80
CN–21	Temperature Calculations for the Positron Target	H. DeStaebler	3/31/80
CN–22	Tapered Solenoid for SPC Positron Source	D. Sherden	5/7/80
CN–23	Calculations for Positron Target Test in ESA	H. DeStaebler	5/15/80
CN–24	More Calculations for Positron Target Test in ESA	H. DeStaebler	6/4/80
CN–25	Considerations with Respect to e^+ Emittance	S. Ecklund	9/11/80
CN–26	Head Tail in the Damping Ring	J. Le Duff	8/18/80
CN–27	Energy Acceptance of the Damping Ring	M. Allen	9/12/80
CN–28	Fundamental Scaling Relations for Accelerating Structures for Large Linear Colliders	W. Panofsky	10/6/80
CN–29	Effect of Transverse Wake Field on Polarization	A. W. Chao	10/28/80

CN–30	Investigation of S–Band RF Pickup with Stripline Positron Monitors	J.Clendenin H. Martin	11/4/80
CN–31	Residual Radioactivity in the Cooling Ring	T. Jenkins	11/10/80
CN–32	SLC Frequencies and Associated Problems	G. A. Loew	1/13/81
CN–33	SLC Emittances	G. A. Loew	1/28/81
CN–34	Optical Diagnostics for the Damping Ring	A. Sabersky	11/24/80
CN–35	Parasitic Mode Losses in the Damping Ring	P. B. Wilson	12/18/80
CN–36	Can We Shift an e^+ Bunch Half Way Around the Damping Ring?	H. Wiedemann	12/3/80
CN–37–R1	Beam Size and Beam Stay Clear (BSC) in the Damping Ring	H. Wiedemann	5/6/81
CN–38	Transient Energy and Phase Oscillations in the Damping Ring	P. Wilson T. Knight	12/23/80
CN–39	Exit Angles for the Disrupted Beam	R. Hollebeek	1/19/81
CN–40	Preliminary Tolerances for the Sector 1 Transport	R. Stiening	1/16/81
CN–41–R1	Location and Geometry of the Damping Ring	H. Wiedemann	5/5/81
CN–42	How Straight is the Linac and How Much Does it Vibrate	R. Stiening	1/21/81
CN–43	Results of a Tracking Program for Computing the Transient Energy and Phase Oscillations in the Damping Ring	P. Wilson T. Knight	2/3/81
CN–44	Additional Path Length Constraints	T. Fieguth	2/9/81
CN–45	Position Monitor Calibration and Offsets for Sector 1 Tests	R. Helm	2/18/81
CN–46	The Injection and Extraction Systems of the Damping Ring	J. M. Peterson	3/3/81
CN–47	Timing for Damping Ring Injection and Extraction	T. Fieguth	4/15/81
CN–48	Illustration of Timing Sequence for Damping Ring Operation (Never Published)	T. Fieguth	4/15/81
CN–49	Requirements for Resistive Coating on Ceramic Tubes in Kicker Magnets	J. M. Peterson	4/6/81

CN-50	Radiation Levels Inside the Vault Compressor/ Transport Tunnels from Beam Loss in the Accelerator Housing	T. Jenkins	4/3/81
CN-51	Radioactive Air and Ozone Concentrations in the Cooling Vault	T. Jenkins	4/30/81
CN-52	Radiation Transport Computer Programs Currently Available and in use at SLAC	T. Jenkins W. Nelson	4/9/81
CN-53	Some Observations on Some XK-5 Type Klystron Magnets	J. Cobb D. Jensen G. E. Fischer	4/23/81
CN-54	Timing Requirement in the Damping Ring	M. Allen	4/27/81
CN-55	Parameter of the Positron Beam Line from Damping Ring to Linac	H. Wiedemann	5/6/81
CN-56	Magnet Parameters for the Damping Ring	H. Wiedemann	5/6/81
CN-57	Parameters for the Positron Compressor	H. Wiedemann	5/7/81
CN-58	Parameters for the Damping Rings	H. Wiedemann	5/7/81
CN-59	SLC Linac Vertical Pulse Magnet Power Supply	B. T. Tomlin	5/12/81
CN-60	Specification for the Damping Ring Kicker Modulator High Voltage DC Power Supply	B. T. Tomlin	5/12/81
CN-61	The Collider Injector Vacuum System	C. Sinclair	8/7/81
CN-62	Touschek Effect and Multiple Coulomb Scattering in the Damping Ring	H. Wiedemann	5/12/81
CN-63	Compressor RF System Stability	R. Stiening	5/14/81
CN-64	Synchronizing the Master Oscillator to Power Line Frequency Using a Predictive Digital Filter	E. Grund	5/28/81
CN-65	Klystron Faults and SLC Performance	R. Stiening	5/15/81
CN-66	Time Required to Establish a Static Magnetic Field in Accelerator Pipe	J. Cobb T. Porter	5/19/81
CN-67-R1	Linac Magnet Specifications (Revisions)	R. Stiening	6/4/82
CN-68	Position Monitor Offsets—Corrections for Monitors Tilted with Respect to the Beam Axis	J.-L. Pellegrin	5/21/81

CN-69	Synchrotron Radiation in the Collider Arcs	T. Jenkins W. Nelson	6/3/81
CN-70	Available Electrical and Electrical Power Requirements for the Damping Ring	W. Davies-White	5/28/81
CN-71	Threshold for Turbulent Bunch Lengthening in the Damping Ring	P. Wilson	5/28/81
CN-72	Kicker Magnet and Pulser	F. Bulos	5/29/81
CN-73	QD Type Quadrupoles for Higher Gradients	W. Brunk	6/3/81
CN-74	Transient Energy Oscillations in the Damping Ring with an RF Phase Jump at Injection	P. Wilson T. Knight	6/12/81
CN-75	Cooling Water for Damping Ring	W. Davies-White	6/11/81
CN-76	Damping Ring Electronics I&C Summary	J. Kieffer T. Fieguth	6/15/81
CN-77	Damping Ring Electronics Rack Requirements	J. Kieffer	6/15/81
CN-78	Measurements on SLC Corrector Dipoles in Sector 1	J. Cobb	6/15/81
CN-79	Notes on Compressor I&C and Length of Injected Bunch	T. Fieguth	6/19/81
CN-80	Some Beam Positron Monitor Considerations for Damping Ring Complex	G. E. Fischer J.-L. Pellegrin	6/22/81
CN-81	Heat Loading Estimates for the Electronics Racks for the Damping Ring	J. Kieffer	6/26/81
CN-82	Basic Arc Lattice for the SLC	H. Wiedemann	6/25/81
CN-83	Luminosity in the SLC	H. Wiedemann	6/25/81
CN-84-R1	Eta Matching in the Collider Arcs	H. Wiedemann	6/26/81
CN-85-R1	Reverse Bend Section in the SLC-Arc	H. Wiedemann	7/7/81
CN-86	Minimum Klystron Power Required for Capture in the Damping Ring	P. Wilson T. Knight	6/30/81
CN-87	Can We Put the e^-e^- Beam Separation Kicker Magnet Inside the Linac Acceleration Section?	A. W. Chao	7/1/81
CN-88	SLC Wide Band Cable System	W. C. Struven	7/1/81
CN-89	Ion Effects in the Damping Ring	P. Morton	7/6/81

CN–90	A Modest Proposal for Linac Phase Stabilization	M. Breidenbach	7/8/81
CN–91	AC Power Requirement Estimates for the Damping Ring I&C Alcove Area	J. Kieffer	7/14/81
CN–92	Tests on Phase Stability in Sector 9	H. Hogg H. Schwarz	7/7/81
CN–93	A Quadrupole Design for Focusing in the Main Collider Arc	R. Early H. Shoaee	7/14/81
CN–94	Constraints on the η–Functions at the Collision Point in the SLC	H. Wiedemann	7/16/81
CN–95	A Possible Scheme for Phase Stabilization of the Linac	H. Schwarz J. Weaver	7/17/81
CN–96	Calibration of Measuring Coil for Machine Quad	D. Jensen J. K. Cobb	7/21/81
CN–97	Parameters of the Positron Beam Line from the Linac to the Damping Ring	H.Wiedemann	7/21/81
CN–98	Some More Orbit Correction Considerations for the Damping Ring	G. E. Fischer	7/24/81
CN–99	A Note on Shielding the Collider Interaction Halls/Counting Houses	T. Jenkins	8/4/81
CN–100	Circuit Installation Notes for the Major Magnet Buses	J. Kieffer	7/29/81
CN–101	Temperature Regulation of the Accelerator	K. Jobe	7/30/81
CN–102	Accelerator Disk-Loaded Waveguide Temperature Control Specification	R. Steining	7/31/81
CN–103	Dose Rates Inside the Cooling Vault from e^+ Beams in the Rings	T. Jenkins	8/19/81
CN–104	Radiation Resistance of Some Plastics and Insulating Materials	T. Jenkins R. McCall	8/4/81
CN–105	Beam Position Detection Along the Collider Arms	J.-L. Pellegrin	8/12/81
CN–106	Positron Compressor (Beam Dynamics)	H. Wiedemann	8/7/81
CN–107	Standardizing Linac Type QA Quadrupoles	R. Steining	8/6/81
CN–108–R1	Strength Measurements on SLC Corrector Magnets Type 1 and Type 2	J. Cobb D. Jensen	8/20/81

CN–109	Transport Matrix Through a Region with Superimposed Solenoidal and Accelerating Fields	A. W. Chao	8/13/81
CN–110	Dynamic Beam Loading Compensation and Energy Spectrum in the SLC	R. Stiening	8/17/81
CN–111	Test of the Radiation Damage to the Beam Detector Signal Cables	J.-L. Pellegrin	8/14/81
CN–112	Recent Observations of Rf Phase Stability in Sector 9	J. Fox H. Schwarz	8/20/81
CN–113	SLC Beam Positron Monitor Near the Interaction Point	D. I. Meyer	8/25/81
CN–114–R1	The Energy Dependence of the SLC Luminosity	R. Stiening	9/10/81
CN–115	Machine Quadrupoles for Sectors 0 and 1	J. K. Cobb	9/4/81
CN–116–R2	Beam Position Monitor Signal Processor (Modification)	J.-L. Pellegrin S. Williams G. Oxoby	12/82
CN–117	Bunchlength as a Function of the Compressor Voltage	H. Wiedemann	9/17/81
CN–118	SLC Naming Conventions	M.Breidenbach	9/21/81
CN–119	Timing Requirements and Proposed Tests for the Position Monitors' Cables	J.-L. Pellegrin	10/24/81
CN–120	Lasers for the Production of High–Energy Gamma Beams from Collider Electron Beams	C. Sinclair	10/14/81
CN–121	Effect of Ions in the Linac and the Arcs	A. W. Chao	10/5/81
CN–122	Damping Ring Beam Position Correcting System	G. E. Fischer	10/7/81
CN–123	More on Ions in the Damping Ring	A. W. Chao	10/9/81
CN–124	Effect of SLED Cavity Temperature Changes on Effective Accelerating Field	Z. D. Farkas G. Loew	10/12/81
CN–125	Specification for Septum Magnets S–1 and S–2 in SLC Damping Ring	G. Fischer J. Peterson	10/12/81
CN–126	Low Cost Electronics for Beam Position Monitoring on the Damping Ring and its Beam Lines	J.-C. Denard	10/81
CN–127	Quadrupole Beam Break-up	A. W. Chao	10/20/81
CN–128	Positron Target Materials Tests	S. Ecklund	10/20/81

CN–129	Requirements for Installation of a Liquid Level System	F. Linker	10/23/81
CN–130	Studies on SLC IR Shield	J. Harris T. Jenkins	11/4/81
CN–131	New Sextupoles Parameter for the Damping Ring	H. Wiedemann	11/18/81
CN–132	Linac Timing System Specifications	R. Stiening	11/19/81
CN–133	A Configuration for the VB–53 Vertical Bend Magnet	R. Early	12/1/81
CN–134	Pandira Calculations for the Damping Ring Bend Magnet	R. Early	12/1/81
CN–135	Energy Deposition and Thermal Heating in Materials Due to Low Emittance Electron Beams	S. Ecklund W. R. Nelson	12/8/81
CN–136–R1	Tune Variation in the Damping Ring	H. Wiedemann	1/5/82
CN–137–R1	Collider Damping Ring Distributed Ion Pump Cooling	J. Jurow D. Wright	1/7/82
CN–138	Accelerator Quad Calculations for SLC	R. Early H. Shoaee	12/19/81
CN–139	Change in the Design Tunes of the Damping Ring	H. Wiedemann	1/5/82
CN–140	More on Sextupoles for the Damping Ring	H. Wiedemann	1/5/82
CN–141	Effects of Misaligning LTR Optical Components and a Possible Correction Scheme	T. Fieguth	1/6/82
CN–142	Beam Breakup Due to Quadrupole Wake Fields for Sector 1	A. W. Chao R. Cooper	1/11/82
CN–143	Test of X6 Frequency Multiplier in Sector 9	H. Schwarz	1/11/82
CN–144	Pulse-to-Pulse Control of the Linac with the New Control System	M. Breidenbach R. Melen	1/11/82
CN–145	Effectiveness of the Outer Conductor of the E Bend Magnet	R. Early	1/14/82
CN–146	Propagation of Fiducial Timing Pulse on Main RF Drive Line	H. Hogg R. Koontz G. Leger	1/14/82
CN–147	Some Effects in the Compressor	A. Chao H. Wiedemann	1/18/82

CN–148	A Meek Proposal for Linac Phase Stabilization	J. Weaver	1/27/82
CN–149	A Humble Proposal for Linac Phase Stabilization	H. Hogg J. Weaver	2/2/82
CN–150	The SLC Linac Transport System for Sectors 2 through 30	R. Helm	1/28/82
CN–151–R1	Linac Quadrupole System Parameters—Sector 2 through 10	R. Stiening	3/25/82
CN–152	Damping Ring Electronics Installation Identification Nomenclature	K. Bailey	1/26/82
CN–153	Measurements Made on Six Type-3 SLC Corrector Dipoles	D. Jensen	1/19/82
CN–154	Energy Contribution of Sectors 0 and 1	G. Loew	2/4/82
CN–155	Accelerator Control Transition Committee—Report #1	R. Melen *et al.*	2/19/82
CN–156	A Constant Phase Line and Its Possible Application	Y. Zhao J. Weaver	3/12/82
CN–157	The Tao of RF Phasing and Monitoring Systems from A to Z	J. Weaver *et al.*	2/26/82
CN–158	Wide Angle Secondaries Produced by "Beamstrahlung" Interaction	D. B. Smith	2/5/82
CN–159	Linac Degaussing System	R. Stiening	2/16/82
CN–160		H. Hogg J. Weaver	
CN–161	Focusing Errors in the SLC Quadrupole Lattice	R. Stiening	2/24/82
CN–162	SLED I Energy Gain for Each Klystron in Sector 2	G. Nelson G. Gilbert	3/12/82
CN–163	New Instrumentation of the Accelerator Klystrons	K. Jobe	3/22/82
CN–164	Temperature Measurement for SLC	K. Jobe	3/17/82
CN–165	A Transport Data Set for the Linac–Ring Beam	M. Lee M. Woodley H. Wiedemann	3/29/82

CN–166	Damping Ring Kickers	F. Bulos B. Tomlin J. Weaver	3/22/82
CN–167	Tests on Quad Center Shifts with Heat or Magnetic Field Changes	B. Dozhier D. Jensen	3/31/82
CN–168	Pulse to Pulse Amplitude and Phase Jitter on Sector 9 RF Signals	H. Schwarz	3/25/82
CN–169	A Magic Data Set for the Damping Ring	M. Lee H. Wiedemann M. Woodley	4/1/82
CN–170	Temperature Measurements on the First Ten Sectors of the Linac	K. Jobe	3/31/82
CN–171–R1	Online Model Calculations for the Damping Ring and its Transport Systems	M. Lee M. Woodley J. C. Sheppard	4/8/82
CN–172–R2	Linac Quadrupole Connections	R. Stiening	7/23/82
CN–173	PAS II – A Beam Analysis System at Sector 10	V. Luth K. Brown	4/16/82
CN–174	Measurement and Optimization of the Prototype Permanent Magnet Quadrupole (PMQ)	J. Spencer	4/26/82
CN–175	Locking of Damping Ring Beam to Compressor	M. Allen	4/82
CN–176	Resistive Wall in the Damping Ring	A. Chao P. Morton	5/14/82
CN–177	Test Results of Sector 9 Phase Reference Line	H. Schwarz K. Jobe J. Judkins	5/5/82
CN–178	Emittance Calculations for Sector 1 Tests	J. C. Sheppard *et al.*	5/6/82
CN–179	Lattice Modeling for the Sector 1 Tests	J. C. Sheppard *et al.*	5/10/82
CN–180	Energy Spread Caused by the Longitudinal Dipole Wake	A. Chao P. Morton	5/28/82
CN–181	Specification for SLC Linac RF Phase and Amplitude Measurement	R. Stiening	5/14/82
CN–182	Temperature Stabilization of the SLAC Linac	K. Jobe	6/25/82

CN–183	The SLC IR Conceptual Design	L. Keller	6/21/82
CN–184	Damping Ring, LTR and RTL Device Identification	T. Fieguth W. Linebarger	6/25/82
CN–185	MUX System for the Damping Ring BPMs	J.-C. Denard G. Oxoby	6/31/82
CN–186	A Beam Phase Reference from a Stripline Monitor	M. Allen J. Fox J. Weaver	7/82
CN–187	SLC Parameters for Experimenters	R. Stiening L. Keller	7/82
CN–188	Pin Diode Attenuator	H. Schwarz Y. Zhao	7/82
CN–189	Effect of Strong Transverse Fields on Permanent Magnets	J. del Corral J. E. Spencer S. St. Lorant	7/19/82
CN–190	A Proposal to Increase the SLC Luminosity	A. Chao H. Wiedemann	7/23/82
CN–191	Alternate Gradient (AG) Magnet, Arc Magnetic Field Orientation	M. Anderson	7/26/82
CN–192	Lattice Modeling for Sector 2 through Sector 9	J. Sheppard R. Helm M. Lee	7/26/82
CN–193	Proposed Online Model Calculations for the Sector 10 Tests	M. Lee J. Sheppard R. Helm	7/82
CN–194	Hybrid Alternatives for the Collider Arc and Final Focus Magnets	H. Shoaee J. Spencer S. St. Lorant	7/30/82
CN–195	Final Focus Optics Near the Interaction Point	J. Matthews	8/10/82
CN–196	Effects of Synchrotron Radiation on Superconducting Magnets	J. Spencer W. R. Nelson	
CN–197	Beam Gas Bremsstrahlung in the SLC Final Focus	J. Matthews	8/13/82
CN–198	A Beam Profile Monitor for SLC Emittance Measurements	V. Luth *et al.*	9/13/82

CN–199	Summary of Cycle 82/2 Sector 1 Tests	J. Clendenin *et al.*	9/20/82
CN–200	Emittance Measurements for Sector 1 Tests	J. Clendenin *et al.*	10/18/82
CN–201	Radiation Damping in the SLC Arcs	A. Chao R. Helm	10/19/82
CN–202	Vacuum Requirements in the Collider Area	B. Richter	10/25/82
CN–203	Wide Angle Secondaries Produced by "Beamstrahlung" Interactions	D. B. Smith	11/1/82
CN–204	Possible Advantages of Using Superconducting Quadrupoles for the First Few Quadrupoles in the SLC Final Focus System	K. Brown F. Bulos	11/10/82
CN–205	Some Ideas for the SLC IR	R. Blumberg	11/12/82
CN–206	Measurement of Neutron Streaming in the RTL and LTR Tunnels	T. Jenkins	11/82
CN–207	Subharmonic Buncher Phase Jitter	E. Higgins	11/16/82
CN–208	Klystron RF Synchronization to Beam	E. Higgins	11/17/82
CN–209	Supplementary Note to CN–208 11/17/82	E. Higgins	11/18/82
CN–210	Online Beam Bump Calculations	J. Sheppard M. Lee	11/19/82
CN–211	Beam Spot Size and Tolerance	H. Wiedemann	12/15/82
CN–212	Estimate of Maximum Expected Rate of Vertical Movement of SLC Arc Tunnel Floor	F. Linker	12/17/82
CN–213	A Note on Some Tolerances in the Final Focus System	H. Wiedemann	12/22/82
CN–214	SLC Arms Position Monitors	J.-L. Pellegrin	1/83
CN–215	Linac and Collider Arcs Beam Position Monitor Electronics Resolution and Error	J.-C. Denard J.-L. Pellegrin	2/83
CN–216	Steering Effects in the SLC Main E Bend Magnet	R. Early	1/25/83
CN–217	Specifications and First Model Test Results of a Beam Position Monitor Analog-to-Digital Converter	G. Oxoby J.-L. Pellegrin	3/21/83

CN-218	Bunch Shape at IP and the Pinch Effect	A. Chao Y. Kamiya	3/28/83
CN-219	Radiation Backstreaming from the SLC Dumps	T. Jenkins	4/6/83
CN-220-R1	SLC Arc Lattice	H. Wiedemann	5/13/83
CN-221	A Note on Shielding the SLC Positron Source	T. Jenkins	4/21/83
CN-222	Ozone in the SLC Arcs	T. Jenkins	4/27/83
CN-222a	Ozone in the SLC Arcs	T. Jenkins	5/11/83
CN-223	Some Measurements of Ground Motion at SLAC	S. Whitaker	4/28/83
CN-224	Superconducting Quadrupoles for the FFS-I	S. St. Lorant E. Tillman	5/4/83
CN-225	SLED Temperature Stabilization by a Cooling Water Bypass	J. N. Weaver Z. Farkas	5/83
CN-226	Radioactive Air and Ozone in the Positron Source Tunnel	T. Jenkins G. Warren D. Busick	5/28/83
CN-227	Radioactive Air and Ozone in the SLC Dump Tunnel	T. Jenkins G. Warren D. Busick	5/28/83
CN-228	Sector 1 Beam Matrices	J. Sheppard	5/31/83
CN-229	L-101 Corrector/Monitor Test	J. Sheppard M. Lee	5/31/83
CN-230	Radiation Dose Rates Near the Collimators in the SLC Arcs	T. Jenkins	6/6/83
CN-231	Tolerances on SLC Final Quadrupoles	J. Murray J. Peterson	6/10/83
CN-232	Emittance Growth in the Collider Arcs Due to Transverse Wakefields	P. Wilson J. Peterson	12/83
CN-233	Klystron Voltage Pulse Timing Experiment	H. Hogg H. Deruyter H. Bernstein	6/21/83
CN-234-R1	First Order Comparison of Numerical Calculation and Two Different Turtle Input Schemes to Represent a SLC Defocusing Magnet	J. Jaeger	7/14/83

CN–235	Temperature Rise Calculations for the Beam Pipe in the SLC Arcs	W. R. Nelson T. M. Jenkins	7/7/83
CN–236	Recommendations for On-Site Vibration Standards	G. Fischer	6/16/83
CN–237	Effects of Superposition of Detector Solenoid and FFS Quadrupole Fields in SLC and Correction Methods	J. J. Murray	7/25/83
CN–238	System for Saving 6 MW of SLC RF System Line Power	Z. D. Farkas	7/27/83
CN–239	Modifications of the Design of the Final Transformer in the FFS to Accommodate Lower Gradients in the Final Quadrupole Triplet	J. J. Murray	7/29/83
CN–240	Simulation of Systematic Errors in the SLC Magnets	J. Jaeger	8/8/83
CN–241	Update on Beam Extraction	L. Keller	8/16/83
CN–242	Mask Locations in the SLC Final Focus Region	R. J. Cence	7/5/83
CN–243	Further Effects of Ions in the Arcs	J. R. Rees	8/17/83
CN–244	Preliminary Study of the Positions of Elements in LTR	G. Hall	8/12/83
CN–245	Occupancy of the SLC Arcs during Linac Operation	T. M. Jenkins	8/24/83
CN–246	Ground Motion—Frequency of Occurrence versus Amplitude of Disturbing Transient Events	K. L. Werner	9/12/83
CN–247	Optimum Operating Temperature for Accelerator Disk Loaded Waveguide—Test Results from Sector 2	M. Allen A. Millich H. Schwarz	9/23/83
CN–248	BPMO's Histos Plots	J. Clendenin S. Williams	8/23/83
CN–249	Phase and Amplitude Control System for Stanford Linear Accelerator	Sung Joo Yu	9/26/83
CN–250	Engineering Basis for Selection of Positron Source Material	B. Feerick	10/10/83
CN–251	New Magic Angle Bumps and Translation Bumps Magic Angle Bumps and New Examples of Both	J. Seeman	10/28/83
CN–252	Simulations of the Magnet Misalignments, Field Errors and Orbit Correction for the SLC North Arc	S. Kheifets *et al.*	11/83

CN–253	Positron Acceleration to 200 MeV	H. Leboutet	11/11/83
CN–254	An Attempt to Compare Two Arc Orbit Correction Schemes Analytically	A. Chao W. Weng	12/15/83
CN–255	Consequences for SLC of Using Full Beam Power in Shielding Design	T. M. Jenkins	12/5/83
CN–256	Beam-Dump Kicker Magnets	B. Tomlin F. Bulos A. Odian	12/12/83
CN–257	One Way to Save the Number of BPM Buttons in the Arcs that is Not Recommended	A. Chao S. Kheifets	12/83
CN–258	Quadrupole Wakefield Effects in Sectors 0 and 1	K. Bane	19/19/83
CN–259	Lowering the Beam in the SLC Arcs	J. J. Murray R. V. Servranckx	12/16/83
CN–260	Optical Transition Radiation from a Thin Carbon Foil—A Beam Profile Monitor for the SLC	E. W. Jenkins	11/1/83
CN–261	Forces on the Conductors of the Arc AG Magnet	W. T. Weng	12/28/83
CN–262	Temperature Rise in the Lambertsen Septum Magnet Associated with the Positron Target	W. R. Nelson T. M. Jenkins	1/10/84
CN–263	Effect of Magnet Alignment Jittering in the Damping Ring and RTL on Wake Fields in the Linac	A. Chao L. Rivkin	1/84
CN–264	Some Optics Alternatives for the FFS	J. Spencer	2/3/84
CN–265	Vibrational Modes of the Pedestal Support System for the SLC Arc Magnets	W. T. Weng A. Chao	4/84
CN–266	A Survey of Vibration Amplitudes Throughout the Linac	K. L. Werner	5/2/84
CN–267	Ground Motion—Some Relative Phase Measurements in the PEP Tunnel	G. Fischer K. Werner	5/9/84
CN–268	Positron Source: First 50 Nanoseconds (and Addendum)	K. Moffeit	5/22/84
CN–269	Model Test of Damping Ring	M. Lee	5/29/84
CN–270	Reference Klystron Output Phase Values for the First Ten Linac Sectors	A. Millich	6/8/84

CN–271	SLC Intergirder Quad Vibrations	K. McLagen	6/25/84
CN–272	Modification of the code BEAMCORR and Some Simulation Results of the Magnet and Achromat Misalignments for the SLC South Arc	H. Shoaee S. Kheifets	7/11/84
CN–273	SLC Nomenclature for Beamline Components	J. Paterson J. Silva	7/12/84
CN–274	North and South Damping Ring Nomenclature	W. Linebarger J. Silva	7/12/84
CN–275	Temperature Rise in Iron Beam Position Monitors	W. Nelson T. Jenkins	7/24/84
CN–276	Temperature Rise in Aluminum Beam Position Monitors	W. Nelson T. Jenkins	7/31/84
CN–277	The Positron Flux Concentrator—An Update	F. Bulos	8/29/84
CN–278	Energy Spread in SLC Linac with Landau Damping	J. Seeman	8/22/84